

**UPPER OCEAN PHYSICAL PROCESSES IN THE TROPICAL INDIAN OCEAN**

**(A monograph prepared under CSIR Emeritus Scientist Scheme)**

**by**

**L.V. Gangadhara Rao and P. Shree Ram**  
**National Institute of Oceanography**  
**Regional Centre, Visakhapatnam**

**April 2005**

## PREFACE AND ACKNOWLEDGEMENTS

This monograph is the outcome of an attempt by the authors to present a synthesis of the studies on physical processes in the Tropical Indian Ocean (TIO) in relation to air-sea interaction, monsoon/climate variability and biological productivity through a review of the published work so far and analysis of the latest available data sets. Various oceanic features and processes in the upper 1000 m of the TIO are described and discussed. An Oceanographic Atlas prepared for this purpose is appended to the monograph.

The monograph consists of six chapters. Chapter 1 entitled 'Introduction', gives the significant/special features of TIO, the names of various expeditions/experiments carried out in this region and the scope of the different aspects covered in the monograph. Chapter 2 deals with the features of surface parameters/fields. Chapter 3 describes the hydrographic features in the upper 1000 m. Chapter 4 gives a comprehensive account of upwelling processes in the TIO. Chapter 5 deals with internal waves. Summary of the results and a few suggestions for improving our understanding of the physical processes are included in Chapter 6 entitled 'Concluding Remarks'.

The work was carried out at the Regional Centre of National Institute of Oceanography (NIO), Visakhapatnam under Emeritus Scientist scheme sanctioned by the Council of Scientific and Industrial Research (CSIR), New Delhi for a period of 3 years (2002-05). The authors are thankful to CSIR for the financial support and to Dr. E. Desa, former Director, Dr. S.R. Shetye, Director, NIO and Dr. K.S.R. Murty, Scientist-in-Charge, NIO Regional Centre, Visakhapatnam for extending support and providing necessary facilities to carry out the work. Thanks are due to Dr. M.P. Tapaswi, NICMAS, NIO Library for helping in literature survey, Shri J. S. Sarupriya and Shri G.V. Reddy, NIO Data Centre for helping in data acquisition, Dr. S.S.C. Sheno, NIO, Goa for providing satellite tracked drifting buoys data and SOC climatology and to Dr. Y. Sadhram, NIO RC, Visakhapatnam for critically going through the manuscript of the monograph. The help rendered by Dr. T.V. Ramana Murty (NIO RCV) in the computation of MLD & MLHC and Dr. D. Shankar (NIO, Goa) in computing the Ekman drifts and Shri G.S. Michael (NIO, Goa) in generating the figures using GMT is gratefully acknowledged. Thanks are also due to Dr. Suryachandra A. Rao, Institute for Global Change Research, FRSGC, Yokohama, Japan for help in acquiring the NCEP/NCAR wind data and Reynolds SST data. During the course of this work, the authors had useful discussions on various aspects of the subject with scientists at NIO, NPOL, IISc, IITM, SAC, NRSA, Andhra University and Cochin University of Science and Technology, and wish to thank them all.

A few of the figures of the monograph are reproduced from some research papers and the concerned references and their authors are also acknowledged.

## CONTENTS

1. INTRODUCTION
  2. FEATURES OF SURFACE PARAMETERS / FIELDS
    - 2.1 SEA SURFACE WINDS
    - 2.2 SEA SURFACE TEMPERATURE
    - 2.3 SEA SURFACE SALINITY
    - 2.4 SURFACE HEAT FLUXES
    - 2.5 SURFACE CIRCULATION AND CURRENTS
    - 2.6 CHLOROPHYLL AND PRIMARY PRODUCTIVITY
  3. HYDROGRAPHIC FEATURES OF THE UPPER OCEAN
    - 3.1 THERMOHALINE FIELDS IN THE UPPER 1000 METRES
      - a) Temperature
      - b) Salinity
      - c) Density ( $\sigma_t$ )
    - 3.2 SURFACE LAYER
    - 3.3 CIRCULATION AND CURRENTS
    - 3.4 WATER MASSES
  4. UPWELLING
  5. INTERNAL WAVES
  6. CONCLUDING REMARKS
- REFERENCES
- ANNEXURE: OCEANOGRAPHIC ATLAS

## 1. INTRODUCTION

The oceans occupy about 63% of the surface area in the tropics (between 30° N and 30° S latitude). Indian Ocean is the third largest of the world's oceans and has a unique geographic setting. The Tropical Indian Ocean (TIO) is of particular significance to the oceanographers and meteorologists as it experiences the seasonally reversing monsoon winds and is land locked on its northern side unlike the Atlantic and Pacific oceans.

The Indian peninsula divides the northern part of TIO into two adjacent intracontinental seas: the Arabian Sea and the Bay of Bengal. Though located in the same latitudinal belt, they exhibit distinct oceanographic features. The Arabian Sea is connected to the warm and highly saline waters of the Persian Gulf and Red Sea, and experiences more evaporation than precipitation (except along the west coast of India during the southwest monsoon) for most of the time in a year, resulting in an upper layer of rather high saline waters. In contrast, the Bay of Bengal receives a large quantity of fresh water and sediment as river discharge and experiences more precipitation than evaporation for most of the year leading to an upper layer of less saline water. The surface waters in the Bay have such low salinity that the stratification in the upper layer is dominated by salinity gradients rather than temperature gradients. The sea surface temperature (SST) in the Bay is above 28° C and thus conducive to generation of large scale convection/precipitation for most part of the year, while in the Arabian Sea, west of about 70° E, SST is below this threshold value for most part of the year.

The circulation in the TIO differs markedly from that in the Atlantic and Pacific oceans. North of 10° S, the surface winds blow from the southwest during May to September (southwest monsoon) and from the northeast during November to February (northeast monsoon) and under their influence the circulation reverses twice during the year. During the northeast monsoon, the surface circulation resembles the general pattern in the Pacific and Atlantic oceans with westward flowing North Equatorial Current (NEC), South Equatorial Current (SEC) and an eastward flowing Equatorial Counter Current (ECC) in-between. But during the southwest monsoon, the flow north of the equator is reversed and combining with ECC, the whole eastward flow called Southwest Monsoon Current (SMC) is present. During the transition periods between the northeast monsoon and southwest monsoon, April-May and October-November, an eastward flowing current called Equatorial Jet (EJ) appears at the equator. An Equatorial Under-current (EUC) is found in the Indian Ocean, east of 60° E during the northeast monsoon period. It is weaker than that in the Pacific and Atlantic, and is not evident during the southwest monsoon.

An important oceanic phenomenon in the TIO is the Somali current system, which varies significantly with time. It is fed by the northern branch of SEC during the southwest monsoon and attains surface velocities as high as 3.7 m/sec and thus becomes one of the fastest currents found in the open ocean. Strong upwelling occurs along the Somali and Arabian coasts during this period which is very important in relation to the biological productivity and fishery resources.

The upper ocean processes play significant role in determining the SST and air-sea fluxes, which are vital for understanding the monsoon and climate variability in the TIO. SST is known to be an important parameter for organized convection/cloudiness over the tropical region, especially in the Bay of Bengal. The large scale cooling of Arabian Sea during summer and the spatio-temporal variation of warm pool in the TIO are linked to the monsoon variability. The surface parameters and the upper layers of TIO exhibit significant seasonal variation and the upper ocean physical processes influence the biological productivity also.

The Indian Ocean used to be the least known among the world ocean prior to 1960's. The International Indian Ocean Expedition (IIOE) conducted from 1962 to 1965 with participation of 20

countries and 40 research vessels led to the collection of a vast amount of oceanographic data and increased our knowledge immensely. Subsequent to IIOE, several field experiments designed for monsoon related and process oriented studies viz. ISMEX (1973), MONSOON (1977), MONEX (1979), INDEX (1979-80) MONTBLEX (1990), WOCE (1990-1997) Indian / Arabian Sea JGOFS (1992-1997), INDOEX (1998 and 1999), JASMINE (1999) and BOBMEX (1998 -1999) and ARMEX (2002 - 2003) under ICRP were conducted and a vast amount of data were collected. The Indian research vessels RV Gaveshani (commissioned in 1976) and ORV Sagar Kanya (commissioned in 1983) played significant role in the data collection under these programs. For the last few years, satellites with dedicated sensors for ocean parameters like SST, sea surface winds, waves, topography, and ocean colour are providing a wealth of data contributing to the study of ocean surface processes.

In view of the above, a study of the spatio-temporal variation of sea surface parameters / fields (surface winds, SST, SSS, circulation and currents, chlorophyll and primary productivity) and the hydrographic features/thermohaline fields including watermasses and circulation/currents in the upper 1000 m of TIO (Fig. 1) has been attempted using the latest available information/data sets and the results are summarised in this Monograph. Surface heat fluxes (including their role in Arabian Sea cooling), surface layer features (including warm pool variability), upwelling and internal waves are also discussed.

A series of diagrams showing the mean monthly variation of surface parameters and the hydrographic features/thermohaline fields of the upper ocean (upto 1000 metres depth) prepared for this study are presented in the Oceanographic Atlas appended to this Monograph. It is hoped that this Monograph would serve as a useful reference document for the students and researchers in Physical Oceanography.

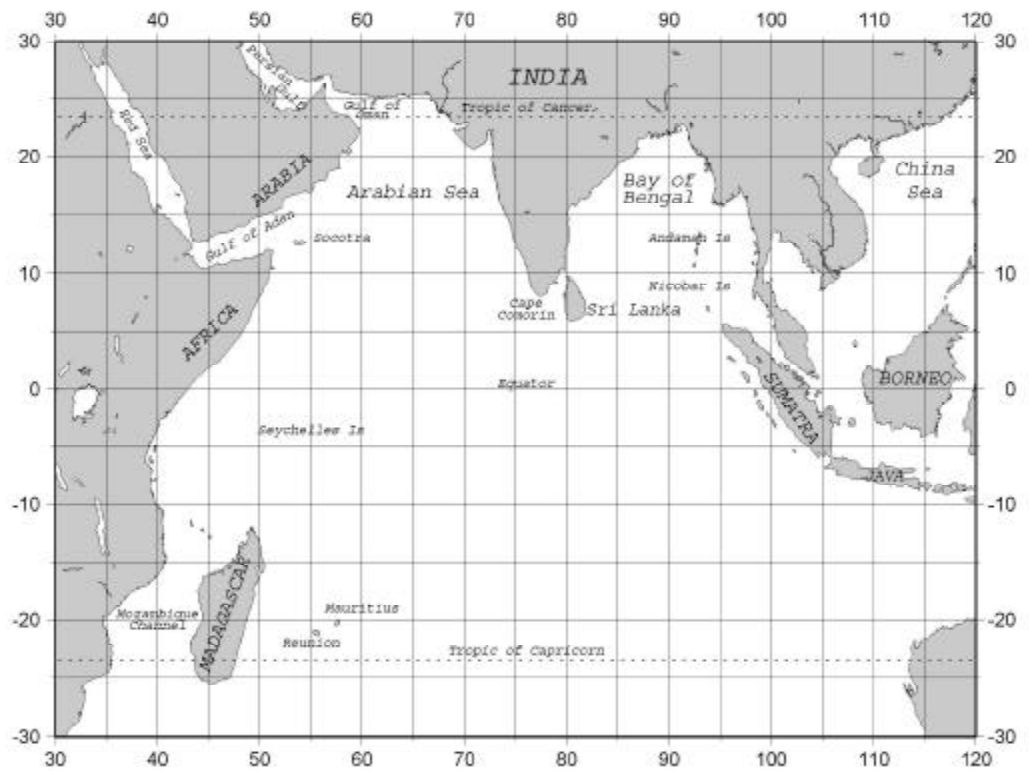


Fig. 1. The Tropical Indian Ocean

## 2. FEATURES OF SURFACE PARAMETERS / FIELDS

### 2.1 Sea Surface Winds

Sea surface wind (SSW) field determines the sea surface roughness and wave climate, and thereby plays significant role in the energy exchange at the air-sea interface. Surface winds drive the circulation of the upper ocean (Ekman layer - upto a depth of about 200 m). The vast land mass of the Asian continent with a winter high pressure (HP) centre and a summer low (LP) causes the seasonally reversing monsoon winds over the north Indian Ocean, which determine the climate of the region. During November to March, the winds blow from the northeast (northeast or winter monsoon), the situation resembles that over the Pacific Ocean and the Inter-tropical Convergence Zone (ITCZ) is located near 5 degree S. During May to September, the winds blow from the southwest (southwest or summer monsoon) replacing the northeast trade winds, the southeast trade winds turn into a southwest flow (after crossing the equator) and join the monsoonal flow. The ITCZ is absent. The summer monsoon is much stronger than the winter monsoon. It reaches its peak in July –August and fades away in September-October.

Kalnay et al. (1996) have generated the mean monthly surface winds for the global oceans on a  $2.5^\circ \times 2.5^\circ$  grid under the NCEP/NCAR 40-year Reanalysis project. Updates for the period 1948-2003 are downloaded from <ftp://ftp.cdc.noaa.gov/Datasets/ncep.reanalysis.derived/surface/> and the mean monthly surface wind vectors for the TIO have been generated. Charts showing the distribution of SSW from January through December are presented in Figures A01, A02 and A03. Salient features of the spatio-temporal variation of SSW are as follows:

During December-January, the northeast monsoon winds are strong with speed more than 4 m/s in the western Arabian Sea and in the central Bay of Bengal. The directions are more northerly in head of the Arabian Sea and the head of the Bay of Bengal, and more easterly in the Andaman Sea. The southwest monsoon winds are the strongest with speed more than 10 m/s in the western Arabian Sea (and more than 6 m/s in the central Bay of Bengal) during July. This produces strong Ekman transport away from the coasts of Somalia and Arabia resulting in intense upwelling. During April, wind directions change from southerly east of Sri Lanka to northerly over the coast of Burma turning in a big anticyclonic pattern centered on the Ten Degree Channel. During October, winds are variable and weak (speed less than 2 m/s) over the Bay.

Winds at the equator change direction, but are generally weak (speed < 2 m/s during March-April and November-December). The southeast trades are strong, compared to those other the oceans and extend from about  $5^\circ$  to  $20^\circ$  S with speed more than 6 m/s during July-August.

The atmospheric circulation over the Arabian Sea undergoes a complete reversal during a year. During the southwest monsoon season, southwest winds blow with speeds of about 20 knots over large areas in the Arabian Sea, often exceeding 30 knots off Somalia and Arabia (Wooster et al., 1967). On the other hand, the northeast monsoon is weakly developed and the associated northeast winds rarely exceed 15 knots.

### 2.2 Sea Surface Temperature

The physical property that can be measured with relative ease is the sea surface temperature (SST). It is the most important parameter for both meteorologists and oceanographers because of its significant role in the exchange of heat, moisture and gases across the air-sea interface. SST is indicative of ocean surface processes/features like upwelling, fronts, eddies and current boundaries. SST is primarily affected by the energy transfer processes at the air-sea boundary and advection in the oceanic surface layer.

Reynolds et al. (2002) have constructed an optimally interpolated weekly SST data set for 1982-1993 on a  $1^\circ \times 1^\circ$  grid over the globe. Updates of monthly mean SST data for the period 1982-2003 are downloaded from [ftp://ftp.ncep.noaa.gov/pub/cmb/sst/oimonth\\_v2/](ftp://ftp.ncep.noaa.gov/pub/cmb/sst/oimonth_v2/) and the mean monthly SSTs for the TIO has been generated. Charts showing the distribution of SST for January through December are presented in Figures A04, 05 and 06. Salient features of the spatio-temporal variation of SST are as follows.

The surface temperatures in TIO vary from less than  $20^\circ\text{C}$  (in the southern part during July – October) to more than  $30^\circ\text{C}$  (in the northern part during April – May). In the Persian Gulf and Red Sea the surface temperatures exceeding  $32^\circ\text{C}$  are found during July – August.

The distribution of isotherms is mainly zonal south of  $10^\circ\text{S}$ . At  $10^\circ\text{S}$  the SST varies from about  $29^\circ\text{C}$  (in March – April) to about  $26^\circ\text{C}$  (in August). At  $30^\circ\text{S}$  it varies by about  $5^\circ\text{C}$  ( $27\text{--}22^\circ\text{C}$ ) in the west and about  $2^\circ\text{C}$  ( $22\text{--}20^\circ\text{C}$ ) in the east.

In the region north of  $10^\circ\text{S}$  the SST is significantly influenced by the monsoon winds and the associated currents. During January-February, between  $10^\circ\text{S}$  and  $10^\circ\text{N}$ , SST increases from about  $28^\circ\text{C}$  in the west to more than  $29^\circ\text{C}$  in the eastern part. In February, the thermal equator runs from  $10^\circ\text{S}$  off the African coast to the equator near  $90^\circ\text{E}$ . During April-May, it moves towards  $10^\circ\text{N}$ . It descends southward and is located just south of the equator in July. The equatorial SST minimum found in the Pacific and Atlantic is absent in the Indian Ocean as there is no upwelling along the equator.

In both Arabian Sea and Bay of Bengal SST decreases northwards during January- February (from about  $28^\circ$  at  $10^\circ\text{N}$  to about  $24^\circ$  in the northern most parts). SST raises gradually as the sun moves polewards over the northern hemisphere with the Bay of Bengal warming faster than the Arabian Sea. A zonal band of high SST ( $>30^\circ\text{C}$ ) is present in the south-eastern Arabian sea including the Lakshadweep Sea during April. SST exceeds  $30^\circ\text{C}$  in most of the area from equator to  $15^\circ\text{N}$  by May. With the onset of summer monsoon in June, SST starts falling and continues to fall until August due to strong winds and advection of upwelled water from the Somali and Arabian coasts. While the decrease of SST in Bay of Bengal is only marginal ( $1^\circ\text{C}$ ), it is very prominent in the Arabian Sea and equatorial part with a distinct spatial gradient toward west (SST  $< 25^\circ\text{C}$  off the Somali coast). Once the southwest monsoon starts retreating in September, both the basins warm up until October. SST is more than  $29^\circ\text{C}$  in Bay of Bengal and is about  $28^\circ\text{C}$  in the Arabian Sea in October. Thereafter with the onset of northeast/winter monsoon in November, SST decreases in both the basins again till January. In the head of the Bay of Bengal significant reduction in SST is noticed from October to December ( $29^\circ - 26^\circ\text{C}$ ).

The SST is found to vary from more than  $28.5^\circ\text{C}$  in the southern and eastern Arabian Sea to less than  $18^\circ\text{C}$  off the coast of Somalia. A remarkable feature of the Arabian Sea is that SST in July is  $2^\circ\text{C}$  lower than in April, and in July, SST is almost as low as that in January. This typical behaviour for northern latitudes in summer is caused by extreme ocean-atmosphere interactions during the southwest monsoon (Halpern et al, 1998).

### **2.3 Sea Surface Salinity**

Salinity or the total amount of dissolved material in sea water is a fundamental property, which together with temperature determines the density and thereby influences the ocean dynamics. In the open ocean, changes in surface salinity depend mainly on the difference between evaporation and precipitation. Advection and mixing processes also affect the surface salinity. The average surface salinity distribution in oceans is basically zonal and shows a minimum just north of the

equator and a maximum in the subtropics at about 25° North and South of the equator. In the case of TIO, the Sea Surface Salinity (SSS) is highest in the Red Sea and Persian Gulf due to intense evaporation and lowest in the northern Bay of Bengal due to discharge of large quantity of fresh water from the rivers.

Monthly mean values of SSS for the TIO (on 1° × 1° grid) have been extracted from the World Ocean Atlas (2001): Objectively analysed temperature and salinity data, (available at [www.nodc.noaa.gov/oc5/WOA01/WOA01dat.html](http://www.nodc.noaa.gov/oc5/WOA01/WOA01dat.html)) and charts showing the distribution of mean monthly SSS for January through December are presented in Figures B154, B155 and B156. Salient features of spatio-temporal variation of SSS are as follows.

During January to June, the SSS is more than 36 psu in the Arabian Sea, north of 10 degrees N and west of 70 degrees E, and decreases towards SE, where as in the Bay of Bengal, the SSS increases from about 30 psu in the head of the Bay towards South upto about 34 psu at 5° N. The SSS distribution in January clearly shows the spreading of low salinity waters (Salinity less than 34 psu) into the southeastern Arabian Sea under the influence of northeast monsoon. During July to December, the SSS of more than 36 psu in the Arabian Sea (between 50° and 60° E) extends towards south upto equator, while in the Bay of Bengal the SSS increases significantly from less than 28 psu near the coast to about 34 psu at 10° N.

In the equatorial region, the SSS decreases from more than 35 psu in the western part to less than 34 psu in the east reflecting the influence of low salinity waters of the Indonesian through flow. South of 10° S, the SSS distribution is mainly zonal and increases towards south reaching maximum (of more than 35.5 psu) around 30° S reflecting the P-E minimum in this region.

## **2.4 Surface Heat Fluxes**

Oceans play an important role in the global climate system. They absorb most of the incoming shortwave radiation entering the earth's atmosphere and redistribute heat energy within the oceanic environment by both horizontal and vertical movements. This energy is then further transported back into the atmosphere in the form of latent and sensible heat fluxes and long wave radiation, which are the main sources of energy for the atmospheric circulation. Latent heat flux results from evaporation at the ocean surface. As water changes from liquid to vapour, the ocean loses energy in the form of latent heat of vaporization and the atmosphere gains heat when the vapour condenses. Since water vapour pressure depends on temperature, SST is an important parameter in determining the latent heat flux. The sensible heat flux is a function of the temperature difference between the ocean surface and the atmosphere immediately above. Both the latent heat flux and the sensible heat flux are controlled by the characteristics of atmospheric boundary layer (water vapour content, wind speed and atmospheric stability). The net heat flux at the ocean surface results from the balance between incoming short wave and long wave radiation, the heat loss by outgoing long wave radiation and through evaporation (latent heat), and to some extent by the surface turbulent fluxes of sensible heat.

The TIO is an important region where active air-sea interaction processes such as monsoons take place. Hence a study of surface heat fluxes in this region assumes special significance. Mean monthly values of sensible heat flux, latent heat flux and net surface heat flux over one degree square for the TIO are extracted from the SOC air-sea flux climatology (Josey et al., 1996) and the distributions of these fluxes for January through December are presented in Figures A13 to A15, A16 to A18 and A19 to A21 respectively. The salient features of the spatio-temporal variation of the fluxes are as follows.

**Latent heat flux** represents the heat lost through evaporation at the sea surface. The evaporation is highest in the subtropics and slightly less in the tropics. It varies from east to west across the ocean also. It is high ( $< -140 \text{ W/m}^2$ ) in the Arabian Sea during December - January; in the central Arabian Sea during June-July; in the northern Bay of Bengal during December, April and June; along the southern boundary of Bay of Bengal during June; in the southern subtropical Indian Ocean ( $10^\circ \text{ S}$  to  $25^\circ \text{ S}$ ) during May-August and in the south-eastern Indian Ocean during April and September – January.

From a study of air-sea fluxes based on NCEP/NCAR reanalysis data set for 1989, Shenoi et al. (1999<sub>a</sub>) reported high latent heat flux over the northwestern Arabian Sea and the Bay of Bengal and low latent heat flux over the southeastern Arabian Sea (because of weak winds) during the northeast monsoon; and high latent flux in the southeastern Arabian Sea (including the Lakshadweep Sea) in April. This broadly agrees with the features found in the present study (Figs. A13 to A15).

**Sensible heat flux** represents the heat leaving the sea surface by conduction. It mostly varies between 0 and  $-15 \text{ W/m}^2$  indicating that, in general, SST is more than air temperature in the TIO, except in the region off Somalia and Arabia (associated with low SSTs) during summer monsoon (June to September). It is less than  $-10 \text{ W/m}^2$  in the northern Arabian Sea during December – January; in the eastern Bay of Bengal during June; in the southern sub-tropical Indian Ocean (south of  $10^\circ \text{ S}$ ) during May-September; and in the south-eastern Indian Ocean during October-December and April (Figs. A16 to A18).

**Net surface heat flux** represents the net heat gain or loss at the ocean surface. It varies between  $+160$  and  $-160 \text{ W/m}^2$  in the TIO. It is more than  $100 \text{ W/m}^2$  in the northwestern and western Indian Ocean (north of  $10^\circ \text{ S}$ ) and in the Bay of Bengal during March-April; in the Arabian Sea and northern Bay of Bengal during July-August; off the Somalia and Arabia coasts and in the western Indian Ocean during September-October. It is less than  $-40 \text{ W/m}^2$  in the northern Arabian Sea during December-January; in the northern Bay of Bengal during December and in the southern subtropical Indian Ocean (south of  $10^\circ \text{ S}$ ) during May-August.

From a study of surface energy fluxes computed from COADS, Rao et al. (1989) reported in the southern tropical Indian Ocean, heat gain during austral summer and heat loss during austral winter; in the Arabian Sea, north of  $10^\circ \text{ S}$ , heat loss during height of both monsoons and heat gain during the transition periods between the monsoons; and in the Bay of Bengal and over most of the equatorial Indian Ocean, heat gain throughout the majority of the year. These observations agree with the features found in the present study, except for the heat gain seen during the height of summer monsoon (July-August) in the Arabian Sea, and the heat loss seen during the height of winter monsoon (December) in the northern Bay of Bengal.

Rao and Sivakumar (2000) inferred that during boreal winter, under the influence of dry and cold northeasterly winds, the net surface heat flux cools the northern Indian Ocean, in greater measure in the northwestern Arabian Sea and northwestern Bay of Bengal. During the pre-summer monsoon season (the spring transition), under the influence of both light wind and clear sky conditions, the net surface heat flux warms the surface in the region north of  $20^\circ \text{ S}$ , with increasing amplitude toward the north. Maximum heating occurs over the northern Arabian Sea and northern Bay of Bengal. During the summer monsoon season, the net surface heat flux produces a dramatic cooling over the entire TIO with an exception of a band off Arabia where SST is cooler because of coastal upwelling. The cooling is also pronounced over the southwestern TIO, central Arabian Sea and eastern Bay of Bengal. During the post-summer monsoon season, the net surface heat flux warms the entire Arabian Sea, with a maxima in the southwestern region where insolation is high and evaporation is low because of the presence of cold upwelled waters at the surface. The net surface heat flux also causes a mild warming in the region south of  $20^\circ \text{ S}$  and a mild cooling in the rest of the TIO (Figs. A19 to A21).

### **Arabian Sea Cooling:**

a) Summer cooling:

Arabian Sea is probably the only region in the world ocean which cools during summer (Hareeshkumar and Basil Mathew, 1997). The cooling of the Arabian Sea is mainly caused by the surface heat exchange processes and lateral and vertical advection. During the Indo-Soviet Monsoon Experiment (ISMEX-73), Ramesh Babu et al. (1976) observed significant fall (of about  $1^{\circ}\text{C}$ ) in the temperature of the surface waters in the eastern Arabian Sea (along  $71.5^{\circ}\text{E}$ ) from May to July. In a review of summer cooling of the Arabian Sea, Sastry and Ramesh Babu (1985) concluded that the entrainment of cold waters into the surface layer and the subsequent turbulent mixing play a dominant role in decreasing SST in the east central Arabian Sea. In the western Arabian Sea, upwelling and spreading of cold upwelled waters off Somalia and Arabia are the major processes for lowering of the SST. Duing and Leetma (1980) suggested that coastal upwelling plays a major role in the summer cooling of the Arabian Sea. A study of SST variability between May and August (Hareeshkumar and Mathew, 1997) revealed that the regions of maximum cooling are the coastal regions off Somalia ( $>5^{\circ}\text{C}$ ), Arabia ( $>4^{\circ}\text{C}$ ) and southwest coast of India ( $>3^{\circ}\text{C}$ ).

b) Winter cooling:

The northern Arabian Sea (especially north of  $10^{\circ}\text{N}$ ) experiences a net heat loss from October to December. The cool dry continental air brought into the northern Arabian Sea by the prevailing northeast trade winds enhances evaporation (Prasannakumar and Prasad, 1996). A combination of enhanced evaporation and the reduction in the solar radiation (from October to January) results in significant decrease of SST and presence of cold surface waters ( $25^{\circ}\text{C}$ ) in the northern Arabian Sea during winter (January-February). Luis and Kawamura (2002) reported SST cooling in the Gulf of Oman during winter monsoon 1993, from AVHRR data and discussed its mechanism. Cold SST evolves in the Gulf during an intense outbreak of winter time winds. The turbulence generated by these winds in the surface atmospheric boundary layer depletes large heat from the sea surface and causes  $1\text{-}2^{\circ}\text{C}$  SST cooling during January-March. The alongshore component of the wind stress promotes Ekman dynamics and further enhances SST cooling along the periphery of the Gulf. A study of 4 year mean SST pattern off the west coast of India using AVHRR data by Luis and Kawamura (2003) showed a strong cooling north of  $15^{\circ}\text{N}$  and cold surface waters ( $25^{\circ}\text{C}$ ) along the Gujarat shelf due to surface heat depletion during winter monsoon (December-March).

### **2.5 Surface Circulation and Currents**

The surface circulation of the oceans is related, in general, to the wind systems of the lower atmosphere because it is primarily due to the wind stress. The wind driven circulation is confined to the upper few hundreds of metres and is mainly horizontal. The rotation of the earth gives rise to the Coriolis force, which results in the wind driven currents in the upper wind mixed layer in the open sea moving in a direction to the right of the wind in the northern hemisphere and to the left in the southern hemisphere (Ekman Drift).

Surface circulation in the TIO is unique. Because of its response to the seasonally reversing monsoon winds, it differs in the northern and equatorial parts from that in the Atlantic and Pacific. In view of this, the major currents in this region also undergo seasonal variations. The major surface currents in the TIO are shown schematically in Fig. 2. During the winter (northeast) monsoon, the

surface currents resemble the general circulation patterns in the Pacific and Atlantic: the South Equatorial Current (SEC) and the North Equatorial Current/North Monsoon Current (NEC/NMC) with the Equatorial Counter Current (ECC) in between, and the associated boundary currents, namely the East India Coastal Current (EICC), West India Coastal Current (WICC), Somali Current (SC), East African Coastal Current (EACC) and East Madagascar Current (EMC). During the summer (southwest) monsoon, the surface currents differ from the Atlantic and Pacific: the eastward Southwest Monsoon Current (SMC) replaces the westward NMC and a northward flowing Somali Current (SC) replaces the southward flow along the coast of Somalia (Shenoi et al. 1999<sub>a</sub>). At the equator an eastward Equatorial Jet (EJ) appears during the transition periods, April-May and November-December (Wyrski, 1973<sub>a</sub>).

Just as the open ocean currents, the boundary currents in this region also undergo seasonal reversals (Shetye and Gouveia, 1998). The WICC flows poleward during winter (November-February) and equatorward during summer (June to September). The EICC flows poleward during February-April and equatorward during November-December. During the southwest monsoon, a weak poleward EICC appears in the south and an equatorward EICC appears in the north.

In the Arabian Sea, the coastal circulation becomes clockwise during the southwest monsoon and counter clockwise during the northeast monsoon. The strongest currents are found off the Somali coast during the summer monsoon. In the Bay of Bengal, there is a clockwise circulation, which in the south converges with NEC/NMC during the northeast monsoon. In the month of August, a counter clockwise circulation covers the Bay of Bengal between the Andaman Islands and the east coast of India.

In the equatorial region, during the northeast monsoon, the westward-flowing NEC/NMC is seen from 8° N to the equator; the eastward flowing ECC from the equator to 8° S and the westward-flowing SEC from 8° S to between 15° and 20° S. During the southwest monsoon, the flow north of the equator reverses to the east and combines with SMC. The westward-flowing SEC continues south of 7° S, but is stronger during the northeast monsoon.

In the southern tropical Indian Ocean, the main feature is the subtropical anticyclonic gyre characterized by counter clockwise circulation with its northern limit around 8° to 10° S, which merges with SEC. The circulation in the western part is complex due the presence of Madagascar and Mozambique Channel, and seasonal variations are quite marked.

The mean monthly surface Ekman currents estimated from NCEP/NCAR reanalysis surface winds (over 2° square for the period 1948-2003) for January through December are presented in Figures A07 to A09. The Ekman drift is not computed within 1.5° of the equator. The mean monthly current vectors derived from satellite tracked drifting buoys data (over 2° square for the period 1976-2002) for January through December (provided by S.S.C. Shenoi, NIO, Goa) are shown in Figures A10 to A12. The dynamic topography and geostrophic currents at the surface with reference to 1000 m depth level derived from objectively analysed temperature and salinity fields (World Ocean Atlas, 2001) for January through December are presented in Figures B469 to B471. The geostrophic currents are not computed within 1.5° of the equator.

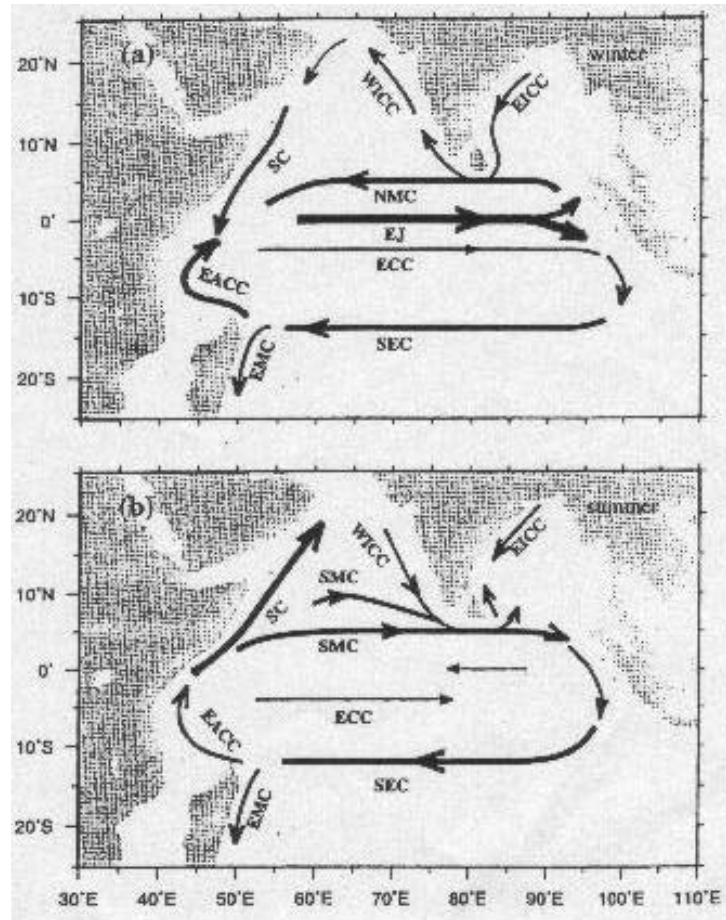


Fig. 2. Schematic diagram of major surface currents in the TIO during (a) the north east (winter) monsoon and (b) the southwest (summer) monsoon. The Equatorial Jet (EJ), though shown in the schematic for winter actually appears during the transition periods, April-May and November-December. The thickness represents the relative magnitude of the current.  
(Adapted from Shenoi et al., 1999<sub>a</sub>)

The current vectors derived from the drifters represent the total near-surface flow comprising the geostrophic currents, the Ekman currents and the Stoke drift. Salient features of the surface circulation and currents in the TIO derived from the drifter data are as follows

- The surface circulation exhibits significant mesoscale variability.
- The speed of surface current, in general, is less than 50 cm/s. Very few vectors exceed 100 cm/s.
- Two primary gyres, a southern gyre rotating clockwise and a northern gyre rotating anticlockwise, extend across the basin. The southern gyre appears as a permanent feature of the surface circulation with the SEC as its southern boundary. The northern gyre is seen during January to March on the northern side of equator.
- The eastward EJ that appeared during April-May and in November widened in the east and branched near 90° E, with the major branch turning southward along the west coast of Sumatra and the other branch turning northward. The southward branch ultimately feeds the SEC and the northward branch contributes to the coastal current along the eastern rim of the Bay of Bengal.

- The flow is westward in the central Arabian Sea during December. The SC turns towards northeast, north of 5° N, in March, well before the winds reverse. The onset of southwest monsoon winds (in May) replace the westward NMC with the eastward SMC.
- The EMC is seen throughout the year.

The above features, in general, agree with those reported by Molinari et al. (1990) and Shenoi et al. (1999<sub>a</sub>).

A comparison of the drifter trajectories with the dynamic topography/geostrophic currents and the Ekman currents leads to the following conclusions:

- The role of geostrophic currents in representing the surface currents varies both geographically and seasonally.
- The Ekman drift is weaker where there is a good match between the observed surface drifts and the geostrophic currents.
- The geostrophic flows dominate in the case of SEC and ECC.
- The Ekman drifts are stronger during July-August and dominate in the SC.
- The anti-cyclonic gyre in the dynamic height field in the Bay of Bengal during January-March is also seen in the buoy derived vectors.

A summary of major surface currents observed in the TIO is presented in Table 1.

**Table 1. Major surface currents in the Tropical Indian Ocean**

<i>Name of Current</i>	<i>Description</i>
South Equatorial Current (SEC)	A westward flow between 8° S and 16° S extending from 95° E to 50° E. Exists throughout the year, but stronger during the northeast monsoon season.
East Madagascar Current (EMC)	A southward flow fed by SEC, along the east coast of Madagascar. Exists throughout the year.
East Africa Coastal Current (EACC)	A northward flow fed by SEC, along the east coast of Africa. Exists throughout the year.
Equatorial Counter Current (ECC) Also known as South Equatorial Counter Current (SECC)	An eastward flow that appears south of the equator (between 3° S and 5° S). Absent during August
Equatorial Jet (EJ) Also known as Wyrtki Jet	An intense eastward current that appears at the equator twice a year (during April-May and November).
Northeast Monsoon Current (NMC) Also known as North Equatorial Current (NMC)	A westward flow that appears north of the equator, with its axis around 5°. Exists during December-April.

Southwest Monsoon Current (SMC) Also known as Indian Monsoon Current (IMC) Somali Current (SC)	An eastward flow that appears north of the equator, with its axis around 5° N. Develops in June associated with the southwest monsoon winds and persists till October  Flows southward along the coast of Somalia during December-February and northward during March-September. Very strong during the southwest monsoon.
West India Coastal Current (WICC)	The current along the west coast of India, flows poleward during November-March and equatorward during April-September.
East Indian Coastal Current (EICC)	The current along the east coast of India, flows poleward during February-April and equatorward during November-December. During the southwest monsoon a weak poleward flow develops in the south (south of 15° N) and an equatorward flow develops in the north.

## 2.6 Chlorophyll and Primary Production

Light and nutrients are the major factors for determining the primary productivity in the ocean. Light penetration in the ocean determines the depth of the photosynthetic zone whereas the nutrients – particularly nitrogen and phosphorous, indicate the fertility of water to promote productivity. Phytoplankton or the planktonic algae give the production at the primary stages of the food chain (Qasim, 1977). The chlorophyll-a (Chl-a) concentration is an indicator of the phytoplankton biomass in the sea and is responsible for the photosynthesis.

Chl-a concentration and primary productivity have been measured during several cruises in the Indian Ocean and most of these data are available in the Indian Oceanographic Data Centre at NIO, Goa . Using NIO BIO data base for the period 1951-97 (2002), maps showing the distribution of surface Chl-a concentration – seasonal average for Feb. -May, June-Sept., and Oct.-Jan. and annual average, are prepared and shown in Fig. A22 of the Atlas. Maps showing the distribution of surface Chl-a concentration derived from SeaWiFS data for the period 1998-2001, seasonal average for the above periods and annual average, are also prepared and presented in Fig. A23 of the Atlas. The features in these maps broadly reflect those seen in the maps prepared from NIO BIO data base. A brief review of the studies on transparency, Chl-a concentration and primary productivity in the TIO is given below.

Light penetration in the sea largely depends on surface irradiance and the type of watermass in a region, which determine the photic zone. Earlier reports on the light penetration in the Indian Ocean are mostly based on Secchi disk readings. Low transparency is found in the northern Arabian Sea, along west coast of India and African coast, where photic zone ranges between 40 and 60 m (Qasim, 1977). In the northern part of the Bay of Bengal and along the east coast of India also transparency is low probably because of the large influx of turbid riverine water into the Bay. The depth of euphotic zone varies between 80 and 100 m in the open ocean, except in the eastern part of the southern tropical Indian Ocean where the values are higher.

From Secchi disk observations in the western Bay of Bengal, Rao (1957) found that in November and December, the western drift of the northeast monsoon transports the turbid deltaic waters along the east coast of India and hence the transparency of the water gets considerably reduced. From February to April, there is a reversal of currents and the water gets characterized by high transparency. This water is oceanic in nature and is poor in its plankton content. Upwelling regions south of Java were characterized by low transparencies. The general distribution of

extinction coefficients was closely related to that of the plankton biomass. Relatively high values of attenuation coefficient were found in the high salinity water in the western Indian Ocean. Varkey and Kesavadas (1976) found high values of attenuation coefficient in the northern Arabian Sea due to high standing stock of plankton and the terrigenous suspended matter near the coast line and at the mouth of estuaries. Jerlov, while studying the scattering properties of the Indian Ocean observed high particle concentration in the fertile divergence zone in the boundary between the SEC and the ECC at 8° to 9° S (Qasim, 1977).

Qasim (1978) studied quantitative distribution of Chl-a in the Indian Ocean from the data collected during the IIOE. Average values of surface chlorophyll for the Arabian Sea and Bay of Bengal were 0.244 and 0.224 mg m<sup>3</sup> respectively. In the western Indian Ocean, the regions of maximum chlorophyll concentration are along the coastal waters of Saudi Arabia, Somalia and South Africa. In the north-eastern Indian Ocean, maximum concentrations are found in the regions close to West Bengal, Bangladesh, Burma and in the Strait of Malacca. The coasts of Saudi Arabia and Somalia have been identified as the regions of intense upwelling during the southwest monsoon, and maximum primary production has been found to be largely confined to these regions. The average Chl-a in the column 0-50 m of the Arabian Sea works out to be 13.81 mg m<sup>2</sup> and for the Bay of Bengal 8.37 mg m<sup>2</sup>. In the northern Bay of Bengal much of the Chl-a is largely confined to the surface.

Sarupria and Bhargava (1998) studied seasonal distribution of Chl-a in the different sectors of the EEZ of India based on the data for the period 1962-1988. Average Chl-a for the euphotic zone was maximum, namely 18.0 mg m<sup>2</sup> in the Arabian Sea sector during premonsoon (Feb.-May), followed by 14.8 mg m<sup>2</sup> for the Bay of Bengal sector during southwest monsoon and 14.5 mg m<sup>2</sup> for the Lakshadweep Sea during premonsoon.

Physical processes such as wind driven coastal upwelling, coastal runoff during the monsoons and convective overturning of surface waters due to winter cooling bring 0in nutrients into the euphotic zone and enhance primary productivity of the northern Indian Ocean (Madhupratap and Parulaker, 1993). The Arabian Sea is one of the most biologically productive ocean regions mainly due to the upwelling of nutrients during the summer (southwest monsoon). During winter sea surface cooling drives convection processes that lead to the injection of nutrients up into the surface waters of the northeastern Arabian Sea and this mechanism of nutrient supply has a dominant control on the winter productivity (Madhupratap et al. 1996).

A substantial area of the Arabian Sea is highly productive during southwest monsoon. Phytoplankton biomass generally shows high values with Chl-a ranging between 0.4 and 5 mg m<sup>-3</sup> and primary productivity varying from 1.3 to 1.8 g C m<sup>-2</sup> day<sup>-1</sup>. Extensive areas of high production (>50 mg C m<sup>-2</sup> day<sup>-1</sup>) are located along the east coast of Arabia, off Pakistan and northwest India. Interestingly, the high rate of production is maintained in this area even after southwest monsoon as the surface currents are weak, allowing time for biological production / succession to develop (Verlecar and Parulaker, 2001). In the eastern Arabian Sea, extensive areas of high fertility with Chl-a concentration of 30 mg m<sup>-3</sup> and surface production rate as high as 232 mg C m<sup>-3</sup> day<sup>-1</sup> have been observed during upwelling period of southwest monsoon. Fairly high production is sustained till October-November.

A recent report on productivity in the eastern and central Arabian Sea based on measurements carried out during the inter-monsoon, winter monsoon and summer monsoon seasons of 1994-1995 under JGOFS programme, have shown Chl-a in the surface waters to range from 0.03 to 0.45 mg m<sup>-3</sup> in offshore and from 0.03 to 1.34 mg m<sup>-3</sup> in the coastal waters, while the column values ranged from 8 to 44 mg m<sup>-2</sup> in offshore and 10 to 88 mg m<sup>-2</sup> in the coastal waters. The surface primary productivity during this period ranged from 0.7 to 35.8 mg C m<sup>-3</sup> day<sup>-1</sup> for offshore and 1.1 to 49.9

mg C m<sup>-3</sup> day<sup>-1</sup> for coastal waters, while the column values varied from 0.19 to 0.77 g C m<sup>-2</sup> day<sup>-1</sup> for offshore and 0.2 to 1.76 g C m<sup>-2</sup> day<sup>-1</sup> for coastal waters (Bhattathiri et al., 1996). The phytoplankton biomass and productivity are higher in coastal regions due to upwelling associated with southwest monsoon. The lowest Chl-a and primary productivity were reported for April-May 1995 with surface Chl-a being less than 0.05 mg m<sup>-3</sup> and column values less than 17 mg m<sup>-2</sup>, both for coastal and offshore waters. Prasanna Kumar et al. (2001) reported fairly high biological production (up to 1700 mg C m<sup>-2</sup> day<sup>-1</sup>) in the central Arabian Sea, along 64° E, during the summer monsoons of 1995 and 1996 and attributed the same to upward Ekman pumping and lateral advection.

Satellite imageries indicated sharp increase in surface Chl-a all over the Arabian Sea when upwelling attains the peak (July-August). During winter (December) Chl-a biomass is fairly high in northern areas. Namita et al., (2000) reported a large bloom of phytoplankton pigment north of 20° N in February 1997 from ADEOS/OCTS data. Surface cooling and convection resulting from reduced solar radiation and increased evaporation make the northern region productive in winter (Prasanna Kumar et al., 2000). Luis and Kawamura (2004) reported that the primary production rate integrated for photic layer and surface Chl-a estimated from the CZCS, both averaged for the entire western India shelf, increases from winter to summer monsoon from 24 to 70 g C m<sup>-2</sup> month and from 9 to 24 mg m<sup>-2</sup>, respectively.

The Bay of Bengal waters are considered to be less productive compared to the Arabian Sea. While nutrient input from many major rivers is large, the narrow shelf, heavy cloud cover and reduced light penetration limit the production rate. Average surface primary productivity rate for southwest monsoon (August-September) range from 51 to 113 mg C m<sup>-3</sup> day<sup>-1</sup> and surface Chl-a from 0.34 to 2 mg m<sup>-3</sup>. Production is quite high off Sri Lanka and there is an extensive area of high production in the eastern tropical Indian Ocean with high peak off Java, where there is an intense upwelling. The surface production and biomass along the coastal waters of east coast of India and eastern Indian Ocean during northeast monsoon is fairly high due to heavy rains during this period (October-November) which bring large quantities of nutrients into the coastal waters.

During southwest monsoon, regions north and south of equator have the lowest primary productivity ranging from 1 to 2 mg C m<sup>-3</sup> day<sup>-1</sup> and surface Chl-a between 0.05 and 0.1 mg m<sup>-3</sup>. The regions of low productivity further expand during northeast monsoon and in the central Indian Ocean there are low values of 0.05 mg m<sup>-3</sup> Chl-a. Low productivity has been observed in the Lakshadweep Sea, with Chl-a < 0.1 mg m<sup>-3</sup> and primary productivity < 1 to 5 mg C m<sup>-3</sup> day<sup>-1</sup>, while in the Andaman Sea the values were, Chl-a < 0.1 mg m<sup>-3</sup> during northeast monsoon period. In the open waters of the Bay of Bengal occasional patches of high production due to wind generated nutrient pulsing into euphotic zone from storm surge activity are reported. In the narrow band of upwelling along the equator alternating with narrow zones of sinking, distribution of biomass has a banded pattern in the Indian Ocean. Higher phytoplankton production rates are observed in August-September (0.4 to 1.4 g C m<sup>-2</sup> day<sup>-1</sup>) near equatorial waters due to divergence, which decreased (0.1 to 0.2 g C m<sup>-2</sup> day<sup>-1</sup>) in the area of convergence. Central Indian Ocean yields very low Chl-a of 0.05 mg m<sup>-3</sup> during northeast monsoon as a result of strong thermal stratification in these waters. Chl-a and productivity in subtropical regions and also around Mauritius island remain low.

### 3. HYDROGRAPHIC FEATURES OF THE UPPER OCEAN

#### 3.1 THERMOHALINE FIELDS IN THE UPPER 1000 METRES

##### a) Temperature

In the tropical regions of the Indian Ocean, a warm top layer of nearly constant temperature often called the mixed layer is present (Rama Sastry, 1961). Below this mixed layer, there is a layer known as the thermocline within which the temperature decreases rapidly with depth. The upper thermocline, which may be in part seasonal, contains the maximum temperature gradient and is followed by the lower/main oceanic thermocline. The maximum temperature gradient is situated just below the mixed layer in tropical regions. In the sub-surface water below the thermocline, the temperature decreases gradually and very slowly with depth. The features of mixed layer depth (MLD) and the mixed layer heat content (MLHC) in the TIO are reviewed in Section 3.2: Surface Layer.

The depth to the top of the thermocline generally coincides with the bottom of the surface mixed layer, whose depth may be taken as the depth at which the temperature is  $1^{\circ}\text{C}$  lower than at the surface. The  $20^{\circ}\text{C}$  is usually situated in the middle of the upper thermocline, which separates the warm surface water from the cooler water of the main oceanic thermocline. Consequently the topography of the  $20^{\circ}\text{C}$  isotherm has strong relation to circulation (Wyrki, 1971). The depth of the  $13^{\circ}\text{C}$  isotherm may be considered as the depth of the base of the thermocline (Sarma et al., 1999).

Prasad and Bahulayan (1996) and Radhakrishnan et al. (1997) studied the thermocline climatology of the Arabian Sea and western equatorial Indian Ocean using different data sets. The depth at which the vertical temperature gradient exceeds  $0.04^{\circ}\text{C/m}$  was found to be the best criterion for estimating the depth to the top of the thermocline. The base of the thermocline is taken as the depth at which the temperature gradient is less than  $0.4^{\circ}\text{C}$  over a 10 m depth interval (which may nearly coincide with the depth of  $13^{\circ}\text{C}$  isotherm). The features of the depth of thermocline top and that of thermocline base closely follow those of MLD. During the pre-monsoon period (March-May) the entire Arabian Sea is characterized by a shallow thermocline (30-40 m) due to strong surface heating. With the commencement of the summer monsoon, the thermocline shoals in the coastal regions as a result of upwelling, and deepens (120 m) in the central Arabian Sea as a result of combined effect of downwelling and increased vertical mixing. As the winter set in, the thermocline deepens (70 m) in the coastal regions as a result of downwelling. Weak gradients occur in the northern Arabian Sea and the thermocline thickness is less than 40 m throughout the year. Larger variability in thermocline gradient is found during July-September throughout the Arabian Sea. There is decrease in gradient in the equatorial Arabian Sea from January to June, probably due to the equatorial undercurrent which causes spreading of isotherms in the thermocline. During January-February, the thermocline thickness is less in a band between  $0-10^{\circ}\text{S}$  and at the northwestern boundary of the Arabian Sea. During the southwest monsoon season, the thermocline is found to be thin south of  $12^{\circ}\text{S}$ , off the coast of Somalia, Arabia and off the west coast of India.

In the north equatorial Indian Ocean the depth of occurrence of thermocline, in general, decreases towards the equator in accordance with the meridional depth variation of thermocline in the Atlantic as reported by Defant (1961). This feature is prominent in the western part of the north equatorial Indian Ocean where the decrease is from about 100 m north of  $6^{\circ}\text{N}$  to less than 50 m at the equator. But in the eastern part the depth of thermocline is found to increase towards the equator from about 50 m off the east coast of Sri Lanka to about 100 m at the equator during the northeast monsoon (Rao and Jayaraman, 1968<sub>a</sub>).

In the Bay of Bengal the thermocline is usually 50 m and occasionally goes down to 120 m depth. During February-March, the depth of occurrence of thermocline varied between 75 m and 120 m in the western Bay and between 50 m and 100 m in the eastern Bay. The thermocline developed well with high thermal gradients in the middle part of central and southern Bay (Rao and Jayaraman, 1968b). At 100 m depth, during the pre-summer season a warm water cell is seen centered at 14° N, 85° E with a core temperature of 28° C. Two cold water cells are noticed towards the west (18° C) and north (17° C) of the warm water cell. During the summer monsoon, a broad cold water (20° C) band oriented in a southwest-northeast direction in the central Bay characterizes the temperature distribution at this depth. During the post-summer season, a warm pocket (25° C) is located at 12° N, 83° E. During the winter monsoon, penetration of warm (27° C) waters from the southeastern Bay towards the central Bay is seen. An examination of the typical meridional and zonal distribution of temperature in the Bay of Bengal shows that the thermocline is strong south of 5° N during the winter monsoon. During the summer monsoon, the thermocline deepens gradually northward from 8° - 12° N and shoals gradually between 12° and 18° N (along 89° E). Between 86° and 90° E a well defined thermocline spreading between 50 and 300 m is seen (Varkey et al., 1996).

In the equatorial region during the pre-onset period an eastward depression in the isotherm topography of the thermocline was observed in association with the easterly jet (Rao et al., 1993a). Sarma et al. (1993) reported a weak thermocline spreading around 100 m depth between 3° N and 1° S in the western Indian Ocean during southwest monsoon (July-August) in association with an eastward flow. Suryanarayana et al. (1987) found considerable spreading of isotherms within the thermocline (in the upper 200 m) around 3° S along 51° E during August 1985. Ramesh Babu et al. (2001) reported that the thermocline in trough shape with maximum deepening around 11° - 12° S along 79° E section during January 1997 and attributed this to an anticlockwise circulation across this section. At 200 m depth, during northern winter the temperature distribution is characterized by a narrow band of cold water (13° - 13.5° C) along 5° - 7° S and a broad band of warm water (19-20° C) along 20° S. During northern summer, waters of nearly uniform temperature (13° - 13.5° C) dominate the southern Arabian Sea, Bay of Bengal and the equatorial Indian Ocean up to as far south as 5° S (Murty and Murty, 2001).

Mean monthly temperature distribution at 9 depth levels and vertical distribution along 11 meridional and 10 zonal sections (presented in Figures B001 to B153) broadly reflect the above features.

## **b) Salinity**

The vertical distribution of salinity is complex compared to that of temperature. This is because the density which determines the stability of the water body depends more on temperature than on salinity in the open ocean, except in the polar seas. Hence it is possible to have either high or low salinity in the top warmer waters. In the equatorial and tropical regions of the oceans there is a uniform layer of salinity from the surface upto a few tens of metres depth due to mixing by wind and waves. Below this layer, salinity first increases upto 100 to 200 m and then decreases with depth reaching a minimum around 800 - 1200 m. The zone or layer where salinity changes rapidly with depth is called the halocline (Reddy, 2001).

In the northern Arabian Sea the surface salinity is high (>36.0 psu) through out the year due to increased evaporation and low humidity (Hareeshkumar and Basil Mathew, 1997). There is a subsurface salinity maximum in the upper 200 m corresponding to Arabian Sea high salinity (ASHSW) water. Its value varies from >36.7 psu around 20 m depth in the northern Arabian Sea to about 35.3 psu around 100 m depth in the south. A salinity maximum associated with the core of Persian Gulf water is found with value varying from 36.8 psu at about 200 m in the Gulf of Oman to

about 35.0 psu at around 400 m in the south. Another salinity maximum associated with the core of Red Sea water (RSW) is found with value varying from 35.6 psu in the north to about 35.1 psu near the equator. A salinity minimum is often found at a depth of 400 m in those areas of southern Arabian Sea which have both ASHSW and RSW. An important feature of the vertical salinity structure in the Arabian Sea is the transient multiple subsurface maxima separated by pockets of low saline water. A subsurface salinity minimum is found at about 150 m depth and its aerial extent is highest during November-January. The factors leading to its formation appears to be (i) transport of low salinity water by the northeast monsoon coastal current along the west coast of India and subsequent increase in the surface salinity of the water due to evaporation in the north Arabian Sea and (ii) poleward coastal undercurrent along the west coast of India during the southwest monsoon (Shenoi et al., 1993).

An influx of fresh water of about  $28.1 \times 10^3 \text{ m}^3 \text{ s}^{-1}$  flows in to the Bay of Bengal annually and about 50% of this comes during the summer monsoon months (Varkey et al. 1996). During the summer monsoon, low saline water (~29.0 psu) spreads into the interior of the Bay in a southwesterly direction from the head of the Bay and the northern Andaman Sea. At 100 m depth during the pre-summer monsoon the salinity distribution is characterized by a low salinity cell with a core valued of 36.6 psu. During the summer monsoon a tongue of high salinity with a core valued of 35.2 psu protrudes in to the central Bay. Sastry et al. (1985) and Murty et al. (1992<sub>a</sub>) identified this high salinity water as being due to the penetration of ASHSW in to the central Bay from the southwestern Bay at subsurface depths (75-100 m). Murty et al. (1992<sub>b</sub>) recorded a uniform value of salinity (34.9 psu) at 100 m depth in the northwestern Bay during September 1983. The ASHSW is not found in the southern Bay during the pre-monsoon period. At 200 m depth, during the pre-summer monsoon salinity variation is marginal (34.90 – 35.05 psu). During the summer monsoon season, salinities all over the Bay are over 35.0 psu indicating the stronger intuition of Indian Equatorial Intermediate Water. During the winter monsoon, a large cell of low salinity (34.90 psu) occupies the central Bay. At 500 m depth during the summer monsoon the salinity distribution is characterized by zonally oriented isohalines with relatively high salinities (> 35.06 psu) in the central Bay and southern Bay and low salinities (< 35.06 psu) north of 16° N. The penetration of subsurface high salinity layer is maximal during summer and post-summer periods. The whole Bay of Bengal is occupied by this high saline water during summer and winter. At 1000 m depth during the pre-summer monsoon a cell of low salinity (34.94 psu) appears in the central Bay. During the summer season, lower salinities (34.92 psu) in the northwestern Bay and higher salinities (34.98 psu) off the southern east coast of India are seen. During the post-summer season, salinities are much less compared to the summer season with the lowest salinities (34.88 psu) near the Nicobar Islands. During the winter monsoon, along the 91° E meridional section two pockets of low salinity centered at 8° N and 15° 30' N are seen in the upper 50 m. The salinity of the northern pocket is comparatively low (31.4 psu) due to the influence of fresh water influx from the Irrawady river. The depth of the halocline is 100 m at 15° 30' N where as it is about 75 m between 7° 30' N and 9° 30' N. The intermediate high salinity water exhibits large depth and thickness variations from south to north. Along 50° N zonal section surface salinity decreases from 33.8 psu in the west to 31.6 psu in the east. In the upper 100 m, in the western part of the section relatively high salinities are observed in association with the northward flow. During the summer monsoon along 89° E meridional section low salinity (< 33.8 psu) waters are seen north of 12° 30' N with salinity decreasing northward to 32.6 psu. Two cells of high salinities (35.0 – 35.2 psu) identified as the result of penetration of ASHSW are located around 50 m at 12° N and around 40 m at 14° N. The intermediate high salinity layer is seen with its core value of more than 35.1 psu at 8° N. At depth greater than 500 m, relatively low salinity waters are seen north of 12° N. Along 13° N zonal section, high surface salinities (33.6 psu) are seen off the Madras coast. Low salinities (32.4 psu) are observed at 91° 30' E because of the influx of the fresh water from the Irrawady river. The halocline is located at about 75 m. High salinity cells appear at depths of about 90 m due to penetration of high salinity water mass. The intermediate high salinity layer is divided into large cells occupying the western and

eastern regions. The meridional distribution of salinity along 95° E in the Andaman Sea during the winter monsoon shows low surface salinities (32.0 psu) owing to the runoff from the Irrawady river. The thickness of the Intermediate High Salinity water is about 350 m and the core salinity is slightly less in the northern Andaman Sea.

Salinity in general increases with depth to give a salinity maximum at the top of thermocline within the equatorial waters. This subsurface salinity maximum is generally found in the north equatorial Indian Ocean during the northeast monsoon (Rao and Jayaraman, 1968<sub>a</sub>). Suryanarayana et al. (1987) reported the presence of subsurface salinity maximum with salinity greater than 35.1 psu between 500 m and 900 m at 2° to 4° N in the western equatorial Indian Ocean during August 1985 and attributed this to the penetration of Red Sea Water. Near 10° S, the hydrological structures of northern and southern parts of the Indian Ocean are separated by a hydrological front marked by a salinity minimum found to a depth of about 500 m (Tchernia, 1980). During January 1997, Ramesh Babu et al. (2001) found the presence of low salinity waters (< 34.70 psu) occupying the upper 100 m between 9° and 14° S along 79° E section brought in from the east by the south equatorial current. They located a subsurface salinity maximum around 250 m depth. They reported the presence of a very strong halocline within the upper 20 m around 70° E along 10° S section and attributed this to the surface dilution by heavy precipitation associated with the Inter Tropical Convergence Zone.

Mean monthly salinity distribution at 9 depth levels and vertical distribution along 11 meridional and 10 zonal sections (presented in Figures B154 to B306) broadly reflect the above features.

### **c) Density (Sigma-t)**

In general, surface water density in tropical oceans decreases either by increase of temperature or by decrease of salinity (through precipitation) and increases either by decrease of temperature or by increase of salinity (through evaporation). In the northern Indian Ocean, at the head of the Bay of Bengal the density is low (< 20.0 s<sub>t</sub>) because of low salinity resulting from heavy monsoon rains and large influx of fresh water from the rivers, while in the northern Arabian Sea, the density is relatively high (> 23.0 s<sub>t</sub>) because of high salinity resulting from evaporation and advection of waters from Persian Gulf and Red Sea.

In the equatorial and tropical regions, there is a thin layer of low and uniform density near the surface. Just beneath this, there is a layer of rapid increase in density with depth called the pycnocline and below this, density increase increases slowly towards the deeper layers. In the north Indian Ocean the depth of pycnocline exhibits spatial and seasonal variations. In the north equatorial part during the northeast monsoon period along the equator (east of 76° 40' E) and from equator to 3° N in the eastern part the pycnocline is sharply developed with steep density gradients and starts (along with thermocline) at 95 to 100 m depth (Rao and Jayaraman, 1968<sub>a</sub>). North of 3° N the pycnocline gradually rises towards the surface and of the east coast of Sri Lanka (along 83° E) it is seen at 50 m depth. Along the equator there is shallowing of pycnocline towards west (from about 95 to 100 m depth in the eastern part to about 30 m depth in the western part). During the transition period between winter and summer in the western Bay of Bengal (west of 90° E), the depth of pycnocline slightly increases towards south and varies from 75 m to 100 m. In the eastern Bay and the Andaman Sea, it normally starts at comparatively lower depth (Rao and Jayaraman, 1968<sub>b</sub>).

The low salinity of surface waters of the Bay of Bengal causes them in all seasons to be isolated from the deep waters by a sharp pycnocline between 50 and 100 m (Tchernia, 1980). The surface salinity variations within and between seasons are controlled by insolation, evaporative cooling and influx of saline and fresh water (Varkey et al. 1996). During the pre-summer monsoon

season low density ( $< 20.5 \sigma_t$ ) waters occupy the east central Bay near the Andaman Islands and relatively dense ( $21.0 \sigma_t$ ) waters are found along the coast and offshore areas. During the summer monsoon, the lowest density ( $< 13 \sigma_t$ ) waters are seen in the north western Bay and the distribution pattern of density in this area resembles that of the salinity. Density increases gradually towards the south and tongue of low density water spreads southwestwardly in the central Bay. South of  $12^\circ$  N density increases to  $22.0 \sigma_t$  in the southern Bay where relatively saline waters are found. During the post-summer monsoon season, surface density varies between  $20.0 \sigma_t$  and  $22.0 \sigma_t$  and a flow of dense waters, characterized by high salinity, from the southwestern Bay is seen upto  $8^\circ$  N. During the winter monsoon, density of the surface waters is less than  $21.8 \sigma_t$ . Two cells of very low density are found off the central east coast of India and northwest of the Andaman Islands, where fresh water discharges from the Krishna and Irrawady rivers respectively enter the Bay. A large tongue of high density water, protruding northwards, appearing in the central part of the Bay between  $5^\circ$  N and  $15^\circ$  N and separates the two cells of low density water. Spreading of low density water from the Andaman Sea towards the Bay of Bengal through the Ten Degree channel is evident. During the south west monsoon a tongue of high density water with its axis oriented in a SW-NE direction is noticed in the central Bay at depths of 50 m and 100m (Murty et al., 1992<sub>a</sub>). At 100 m depth during the pre-summer monsoon season a large cell of low density water with core value of  $22.0 \sigma_t$  is seen between  $12^\circ$  N and  $17^\circ$  N. During the summer monsoon season, a broad band of high density water ( $> 24.5 \sigma_t$ ) is seen in the central Bay. During the post-summer monsoon season, density varies between  $24.0 \sigma_t$  and  $25.0 \sigma_t$  in the southern Bay of Bengal. During the winter monsoon season density varies between  $24.96 \sigma_t$  and  $21.8 \sigma_t$  (Varkey et al. 1996). During the pre-monsoon season and summer monsoon season the low density cells observed at 100 m depth persists at 200 m depth also. In the western Bay the distribution is characterized by alternate cells of low ( $26.0 \sigma_t$ ) and high ( $26.4 \sigma_t$ ) density waters. During the post-summer monsoon season density varies between  $25.8 \sigma_t$  and  $26.4 \sigma_t$ . During the winter monsoon season density is low in the north western Bay and relatively high off the central east coast of India and the coast of Burma. At 500 m depth two cells of high density appear in the northern and western Bay during the pre-summer monsoon season. High density waters are noticed in small cells during summer monsoon season also.

Mean monthly density ( $\sigma_t$ ) distribution at 9 depth levels and vertical distribution along 11 meridional and 10 zonal sections (presented in Figures B307 to B459) broadly reflect the above features.

### 3.2 SURFACE LAYER

#### **Mixed Layer Depth:**

Turbulence generated in the ocean by wind, convective cooling, breaking waves, current shear and other physical processes create a surface layer characterized by uniform to near uniform density, active vertical mixing and high dissipation (Wijesekera and Gregg, 1996). The depth of this mixing layer is ultimately determined by a balance between the destabilizing effects of mechanical mixing and the stabilizing effects of surface buoyancy flux (Brainerd and Gregg, 1995). In the low and middle latitudes during winter SST is low and mixed layer depth (MLD) is more, while in summer SST rises and a “seasonal” thermocline often develops in the upper zone.

Estimates of mixed layer depth are important to a variety of investigations including upper ocean productivity, air-sea exchange processes and long term climate change (Thomson and Fine, 2003). In the absence of direct turbulent dissipation measurements mixed layer depth (MLD) is commonly derived from oceanic profile data using threshold difference method. The depth at which density ( $\sigma_t$ ) is more than  $0.2 \text{ kg/m}^3$  from the surface value is defined as MLD in this study. Using this criteria mean monthly MLD ( $1^\circ \times 1^\circ$  grid) for the TIO has been generated from the mean

density ( $\sigma_t$ ) profiles (derived from objectively analysed temperature and salinity profiles data of WOA, 2001) and the charts showing the distribution of MLD for January through December are prepared (Figs. B460, B461 and B462 in the Atlas). Salient features of the spatio-temporal variation of MLD are as follows.

The depth of mixed layer varies between 10 m and 140 m in the TIO. MLD is lowest (< 20 m) in the Bay of Bengal and Arabian Sea during northern spring (April) and in a cell at 10°S-65°E in January. Significant deepening of the mixed layer (50-75 m) in the central Arabian Sea during the onset phase of summer monsoon is reported by Basil Mathew et al. (2003) from observations. Highest MLDs (>90 m) are found in the central Arabian sea during the peak summer monsoon (July – August) due to strong wind driven vertical mixing. MLDs are higher (>70 m) during the winter monsoon (January-February) in the central and northern Arabian Sea due to convective vertical mixing. In the northern most extremity of Arabian Sea the mixed layer is particularly deep (>100 m) during January and February. In the equatorial zone, MLDs generally vary from 20-30 m in April to 50-60 m in July. A region of high MLDs (>70 m) is located in the southeastern part (around 15°S-100°E) during September. Between 20° S and 30°S, MLDs are highest (>100 m) during southern winter (August-September) and lowest (<40 m) during southern summer (December - January). These features in general agree with those reported in earlier studies (Rao et al., 1989, Prasad and Bahulayan, 1996) based on temperature difference criteria using different data sets.

### **Mixed Layer Heat Content:**

The heat content of the water column within the mixed layer depth of the ocean is very important for the synoptic weather disturbances (Gnanaseelan et al., 2003). MLD and its heat content (MLHC) were found to be more correlated to buoyancy flux and net heat flux in the central western equatorial Indian Ocean during pre-onset and onset phases of summer monsoon (Joseph et al, 1996).

Using the monthly mean temperature data over 1°x1° grid for standard depths ( 0, 10, 20, 30, 40, 50, 75, 100, 125 and 150 m) for the TIO extracted from WOA, 2001 and the mean monthly MLDs (estimated from the density difference criteria, as explained in the above section), Mixed Layer Heat Content (MLHC) has been computed from the equation:

$$MLHC = \rho C_p \int_0^D \bar{T} dz$$

where  $\rho$  is density of sea water,

$C_p$  is specific heat of sea water at constant pressure,

$T$  is the mean temperature of the layer thickness,  $dz$

$D$  is the depth upto which integration is carried out (i.e., MLD).

Charts showing the distribution of MLHC for January through December are prepared (Figs. B463, B464 and B465 in the Atlas). Salient features of the spatio-temporal variation of MLHC are as follows:

Heat content of the mixed layer varies between 10 and 110 ( $\times 10^8$  J/m<sup>2</sup>) in the TIO. MLHC generally followed the pattern of MLD variation. MLHC is low (< 40) in the region north of 10° S during March-May. It is high (> 70) in the northern and western Arabian Sea during January-February and highest (> 80) in the south central Arabian Sea during July-August. It is lowest (< 20) in the northern Bay of Bengal during August-September. In the equatorial Indian Ocean (along 5° S) MLHC is lowest (< 20) during December-January and highest (> 50) in the eastern part during August. In the southern part (10° S - 30° S) MLHC is highest (> 90) during July-September and lowest (< 30) during December-January.

### **Indian Ocean Warm Pool:**

The minimum SST required for active convection is 28° C (Gadgil et al., 1984). A large region of tropical ocean with SST >28° C called Warm Pool (Joseph, 1990) lies in the western Pacific and the eastern and central Indian Ocean. The area of Indian Ocean Warm Pool (IOWP) change three fold during a year from a minimum of  $8 \times 10^6$  km<sup>2</sup> during September to a maximum of  $24 \times 10^6$  km<sup>2</sup> during April. The warming phase of IOWP begins in February, when the pool begins to spread on both sides of the equator. The northern boundary of the pool merges with the coast line in the Bay of Bengal during April and in the Arabian Sea in May. The summer monsoonal cooling begins during June in the western equatorial Indian Ocean and during July in the Arabian Sea, and continues through September. In the Bay of Bengal the SST does not fall below 28° C during summer. All these features reported by Vinayachandran and Shetye (1991) are reflected in the charts showing the distribution of mean monthly SST in the Atlas. These charts show that the Warm Pool in the Bay of Bengal recedes during November – December. A study by Murty et al. (1998) based on the NOAA/AVHRR SST data of 1992 revealed the persistence of Warm Pool (SST =28° C) in the Bay of Bengal for March through October.

The maximum depth of 28° C isotherm in the Indian Ocean is 100 m during May-June. The maximum volume of IOWP is  $9 \times 10^5$  km<sup>3</sup> which is three times its minimum value. An important feature of IOWP is the large seasonal variation in the surface area covered by the pool. The dramatic changes that occur to the Warm Pool during April and May prior to the onset of the summer monsoon rains over India are particularly noteworthy/significant. The factors that control the variability of IOWP include the fluxes of heat and momentum and ocean currents, whose spatial and temporal variation is complex and difficult to observe. An obvious conclusion is that the IOWP is a region of net annual heat gain by the ocean.

### **Arabian Sea Mini Warm Pool:**

During the pre-summer monsoon (February-May) the near surface waters in the Arabian Sea progressively warm up and a mini warm pool with a core temperature greater than 30° C is manifested in the southeastern region (Rao and Sivakumar, 1999). This SST high (Temperature >29° C) develops off the southwest India in the Lakshadweep Sea in March well before the thermal equator moves into the area, and continues to retain its identity until the onset of monsoon (Shenoi et al., 1999<sub>b</sub>). During most of the years the monsoon onset vortices have occurred only over the mini warm pool, suggesting that the SST high helps in producing conditions favourable for the genesis of the monsoon onset vortex.

Shenoi et al., (1999<sub>b</sub>) explained the mechanism of formation of the SST high as follows. During winter the equatorward East India Coastal Current (EICC) forced by the downwelling coastal Kelvin waves in the Bay of Bengal, turns around Sri Lanka and on reaching the west coast of the Indian subcontinent flows as a poleward West India coastal Current (WICC) and carry low salinity waters from the Bay of Bengal to the Lakshadweep Sea. As the Kelvin waves propagate poleward along the west coast of India, they radiate downwelling Rossby waves that produce a high in the sea level off southwest India. The downwelling and the low salinity surface layer provide a breeding ground for the formation of a SST high in January and by March with increase in solar insolation and stable surface layer, the SST high is evident in the Lakshadweep Sea. Toward the end of April the thermal equator runs over this high further enhancing its temperature. By the end of May the SST high becomes the core of the warm pool over the Arabian Sea and there by the warmest spot in the region. The mean monthly SST distribution for March, April and May presented in the Atlas broadly reflect these features.

Sanilkumar et al. (2004<sub>a</sub>) in a recent study based on observations found the existence of a mini warm pool with temperature more than 30.25° C along 9° N between 68° and 75.5° E during May 2000. Existence of a clockwise gyre during May and the possibility of recirculation of low salinity waters in the study region are also inferred.

### **The Barrier Layer**

An oceanic mixed layer is defined as the region of the upper ocean affected by the surface mixing processes (and normally corresponds to the layer over which the density is uniform). Traditionally it has been assumed that the depth over which the temperature is uniform (isothermal layer depth) can be used as an indication of the depth of the mixed layer (Tomczak and Godfrey, 1994) and MLD has been determined accordingly from the temperature information alone. Availability of better data base including information on salinity facilitated verification of this assumption. In the tropics the difference between isothermal and isopycnal layer depth is found to be often positive indicating density change within the isothermal layer. The density change is caused by salinity stratification/halocline and in these regions the halocline is the true indicator of MLD. The layer between the halocline and the thermocline is referred to as the Barrier Layer (BL), because of its effect on the mixed layer heat budget.

A BL is present in the Bay of Bengal through most of the year due to advection of low salinity water diluted from monsoon river runoff. The fresh water influx into the Bay of Bengal maintains a BL, which has a thickness of 25 m during the summer monsoon (Sprintall and Tomczak, 1992). From time series of hydrographic observations conducted in the northern Bay of Bengal at 20° N, 89° E during August-September 1990 (MONTBLEX), Murty et al. (1996) found that the mixed layer based on a temperature criterion is deeper than that using density. Vinayachandran et al. (2002) observed the formation of a BL in the Bay of Bengal during summer monsoon (BOBMEX) from time series measurements of temperature and salinity profiles in the upper ocean at 17.5° N, 89° E from 27 July to 6 August 1999. Initially the upper layer that is homogeneous in both temperature and salinity was about 30 m deep. Subsequently, the arrival of a fresh water plume (from river discharge and rainfall) caused MLD to decrease to about 10 m and salinity in the surface layer by about 4 psu. The plume led to the formation of a new halocline and hence a BL (of about 15 m thick) within the upper 30 m of the water column. The ensuing ocean-atmosphere interaction was restricted to the new thinner mixed layer. The cooling that was restricted to the mixed layer led to an inversion in temperature (0.5 C) just below the mixed layer.

From time series measurements of temperature and salinity profiles conducted in the southeastern Arabian Sea during 27 March-7 April and 23 May-7 June 2003 as part of ARMEX, Shenoi et al. (2004) found that a 20 m thick BL exists during March-April owing to a surface layer of low salinity waters advected earlier during December-January from the Bay of Bengal. The BL is annihilated during April-May by upwelling and inflow of high salinity waters from the north and by mixing due to stronger winds, which deepen the mixed layer.

### **Temperature Inversion**

Surface layer temperature inversion occurs in the southeastern Arabian Sea (SEAS) during winter. Pankajakshan and Gosh. (1992) from an analysis of BT data collected during cruises of RV Gaveshani and ORV Sagar Kanya (1976-83), found that the inversion in this area is a stable seasonal feature and the occurrence is limited to the coastal waters. The thickness of inversion layer varies from 10 to 80 m and the temperature difference from 0.0 to 1.2° C. The causative factor for the inversion is identified to be the winter time surface advection of cold less saline Bay of Bengal water over the warm saline Arabian Sea water along the west coast of India.

A study from XBT and surface salinity data collected in the Lakshadweep Sea (LS) during May 2002-April 2003 (Shankar et al. 2004) showed that temperature inversions occur off the southwest coast of India in early December with the arrival of low salinity waters from the Bay of Bengal. The low salinity waters and the inversions propagate westward along with the downwelling Rossby waves that constitute the Lakshadweep sea level high; inversions occur in the western LS ( $\sim 73^\circ$  E) about 40 days after they occur near the coast in the eastern LS ( $75.5^\circ$  E). They disappear in April when the TCZ moves over SEAS and the warm pool engulfs the region. Ocean dynamics and air-sea fluxes are together responsible for the formation and westward propagation of the inversions.

Temperature inversion occurring in the surface layer of the Bay of Bengal was studied by Pankajakshan et al. (2002) using the hydrographic data archived in the Indian National Oceanographic Data Centre (INODC) and the results are as follows:

Spatially organized temperature inversion occurs in the coastal waters of the western and northeastern Bay during winter (November-February). Although the inversion in the northeastern Bay is sustained until February (with remnants seen even in March), in the western Bay it becomes less organized in January and almost disappears by February. Inversion is confined to the fresh water induced seasonal halocline of the surface layer. Inversions of large temperature difference ( $1.6^\circ - 2.4^\circ$  C) and thin layer thickness (10-20m) are located adjacent to major fresh water inputs from the Ganges, Brahmaputra, Irrawaddy, Krishna and Godavari rivers. Inter-annual variability of the inversion is significantly high and is caused by inter-annual variability of fresh water flux and surface cooling in the northern Bay. Fresh water flux leads the occurrence process in association with surface heat flux and advection. In the western Bay, the EICC brings less saline and cold water from the head of the Bay to the southwest Bay, where it advects over warm saline water, promoting temperature inversion in this region in association with surface heat loss. For inversion occurring in the northeastern Bay (where the surface water gains heat from atmosphere), surface advection of the less saline cold water from the head of the Bay and Irrawaddy basin is found to be the major causative factor.

### 3.3 CIRCULATION AND CURRENTS

The ocean circulation is in part due to changes in density (resulting from change of temperature or of salinity) caused by climatic changes and in part due to the wind stress. The wind driven circulation is confined to the upper few hundreds of metres and therefore is primarily a horizontal circulation in contrast to the thermohaline circulation. The ocean currents are result of the combined effects of the thermohaline motions and of the wind driven ones. The former extends to the deeper waters while the later prevail in the upper layers.

A brief account of the surface circulation and currents in the TIO is presented in Section 2.5. Broad features of the major current systems that extend to subsurface layers, namely the Somali Current (SC), the Equatorial Jet (EJ), the Equatorial Undercurrent (EUC), etc. are given below.

**Somali Current** is one of the fastest currents found in the open ocean. It is a western boundary current with speeds comparable to those of the Florida Current, and has a transport of about 65 Sv, most of it in the upper 200 m. It originates in the southern hemisphere and flows across the equator towards north during summer. It is first established as response to the wind reversal along the African coast. Winds strengthen abruptly in late May or early June and drive the flow across the equator. The flow turns offshore near  $3^\circ$  N and a coastal upwelling regime develops between  $3^\circ$  N and  $10^\circ$  N. A two gyre structure forms with the prime eddy, Great Whirl (with clockwise rotation) off the northern Somalia coast and the Southern Gyre off the southern Somalia coast. From a study of surface circulation during the summer monsoon of 1988 based on Geosat altimeter data,

Subrahmanyam et al. (1996) identified the prime eddy (Great Whirl) centered at 9.5° N, 53.5° E off northern Somalia and the Southern Gyre centered at 3° N, 51.5° E off southern Somalia during August. Associated with the formation of these two gyres, wedges of cold water resulting from upwelling appear off the coast of Somalia between 4° N and 10° N. The velocity of the current increases from south to north, about 2.0 m/s near the equator to about 3.5 m/s at 8° N. Its speed decreases to less than 0.5 m/s at 200 m depth. During the winter, the Somali Current flows southward and is limited to the region south of 10° N. It first occurs in early December, south of 5° N and expands rapidly to 10° N in January with speeds of 0.7 to 1.0 m/s (Tomczak and Godfrey, 1994).

**Equatorial Jet:** A narrow high speed surface jet flows along the equator from west to east across the entire Indian Ocean during the transition periods between the two monsoon seasons (Wyrtki, 1973<sub>a</sub>). The EJ appears during April, May with velocities of 0.7 m/s or more. Away from the equator the current speed falls off to less than 0.2 m/s at 3° S or 3° N. It appears again in October (before the onset of the northeast monsoon) with a eastward flow in a 600 km wide band along the equator and reaches its peak in November with velocities of 1.0 to 1.3 m/s (Tomczak and Godfrey, 1994). The presence of EJ is well documented through the drifting buoy trajectories, ship drifts and hydrographic observations.

**Equatorial Undercurrent (EUC)** system in the Indian Ocean is recognized as a seasonal phenomenon (Swallow, 1967). It is a strong (~ 1.0 m/s), narrow (~ 1° wide) current flowing eastward usually found in the regions of strong thermocline/pycnocline below the upper mixed layer. The core of this current lies close ( $\pm 1^\circ$ ) to the equator and has a vertical thickness of about 100 m. It is found in the thermocline, east of 60° E during the northeast monsoon period. Rao and Jayaraman, (1968<sub>a</sub>) inferred the presence of EUC between 50 m and 150 m within 2° S of the equator at 61° - 63° E during January-February 1963. The EUC was observed in the western Indian Ocean during the southwest monsoon (Bruce, 1973) with a core around 75 m depth. Knox (1974) found the evidence of the EUC near Addu Atoll in the Maldives during February-March 1972 from the current and temperature profiles to 300 m depth. The EUC in the Indian Ocean has a tendency to be asymmetric, being stronger to the south than to the north of the equator. It exhibits pronounced seasonal variations forced by the seasonal changes in wind (monsoons) over the ocean (Taft and Knauss, 1967).

**North Equatorial Current (NEC) or Northeast Monsoon Current (NMC)** is a major current flowing towards west between 10° N and the equator during the winter. It originates near Malay Peninsula and flows as a narrow current with a velocity of about 30 cm/s upto Sri Lanka. Towards west of southern Sri Lanka between 60° E and 75°E its velocity increases to about 50-80 cm/s. Its westward transport is about  $5 \times 10^6$  m<sup>3</sup>/s. The NEC waters accumulate at the western boundary of the ocean near the Somali coast and move towards south upto about 4° - 5° S, and then turn easterly and flow as ECC.

**South Equatorial Current (SEC)** is the most powerful perennial current system of the southern TIO. It forms the northern boundary of the anti-cyclonic gyre in the south Indian Ocean. It flows from east to west north of 20° S and its northern boundary lies between 6° S and 10° S depending upon the season. During southern winter (July-August), the SEC is found between 20° S and 6° S, and attains maximum velocity of about 50 cm/s on its northern side. The current is strengthened by the flow of water into the Indian Ocean from the Pacific Ocean, north of Australia. The volume of water transported by this current is estimated to be maximum ( $54 \times 10^6$  m<sup>3</sup>/s) during July-August and minimum ( $40 \times 10^6$  m<sup>3</sup>/s) during January-February (Reddy, 2001). Near the northern tip of Madagascar, the northern part of SEC bifurcates into two branches; the main branch flows towards the African Coast and becomes **EACC**, while the other flows southward as **EMC**. The EMC is a relatively weak boundary current flowing along the east coast of Madagascar with little variation

during the year. The EACC is a broadly northward flowing boundary current along the coast of southern hemispheric Africa and forms an extension of SEC.

**Equatorial Counter Current (ECC)** lies immediately north of SEC. It flows towards east throughout the year, being more prominent and located between the equator and 10° S during the northeast monsoon season. It merges with eastward flowing SMC during the southwest monsoon season. In the first half of the northeast monsoon (November-January), its origin is the southward flowing current along the east African coast. During the second half of the northeast monsoon (February-March), its origin is the westward flowing NEC, which takes a southward turn in the southern Arabian Sea. The velocity of the ECC is more (70 to 80 cm/s) towards west and less towards east (Reddy, 2001).

### **Arabian Sea Circulation**

The circulation in the Arabian Sea undergoes seasonal reversal due to forcing by the reversing monsoon winds. Apart from the winds, the currents from certain areas are influenced by the slope of the sea surface induced by changes in sea surface temperature or salinity or by some pre-existing current having set towards or away from the coast.

The Arabian Sea experiences the most dramatic changes in the circulation concomitant with the evolution of the southwest monsoon. During the southwest monsoon, the circulation in the Arabian Sea is clockwise. The Southwest Monsoon Current (SMC) is fully developed during July and August. It decreases in intensity during September and by October, current direction and intensity become variable over most of the Arabian Sea. From an analysis of ship drift data, Cutler and Swallow (1984) found the presence of SMC flowing towards east in the Arabian Sea. Based on the hydrographic data, Duing (1970) and ship drift data, Wyrтки (1973) inferred an overall movement of water in the Arabian Sea from west to east during the southwest monsoon. The surface current in the central Arabian Sea during the southwest monsoon is found to be directed towards northeast with a strength of about 0.8 m/s (Bauer et al. 1992). Due to the strong cross equatorial flow, the Somali Jet over the east African region, the circulation in the western and the southern parts of the Arabian Sea is much more energetic during the southwest monsoon, compared to that in the northeast monsoon (Schott, 1983). A dynamic high, characterized by higher dynamic heights appear and persists in the south central Arabian Sea from July through September, while lower dynamic heights occur along the coasts of Somalia and Arabia, where coastal upwelling is the strongest signal during southwest monsoon. The surface geostrophic flow during May-October is observed to be towards east (Shetye et al. 1994). It is stronger during the later half of the period when the flow has a northward component in the western part of the sea and a southward flow in the eastern part. The pattern of circulation at 200 m depth is observed to be complicated with cellular structures. During the second half of the southwest monsoon, the presence of a poleward undercurrent is indicated.

Shetye and Shenoi (1988) studied surface currents along the coast of Oman and the west coast of India utilizing ship drift data. They found that the currents along the coast of Oman are driven by winds in a northeastward direction during the southwest monsoon. Along the west coast of India a shallow equatorward current is noticed. Along the eastern boundary of the Arabian Sea, during the southwest monsoon, the longshore component of the wind stress is generally equatorward and its magnitude is maximum near the southern end. The coastal circulation along the eastern boundary of the Arabian Sea is similar to a wind driven eastern boundary current (Shetye et al., 1990). The equatorward surface current (WICC) is about 150 km wide, 75-100 m deep and its transport increases from  $< 1 \times 10^6 \text{ m}^3/\text{s}$  in the north to  $4 \times 10^6 \text{ m}^3/\text{s}$  near the southern end. A northward undercurrent is found close to the continental slope.

During the northeast monsoon period over most parts of the Arabian Sea, currents are directed towards west or northwest. During the winter a well developed poleward coastal current along the west coast of India (WICC) is a prominent feature of the circulation in the Arabian Sea. This poleward coastal current is mainly fed by the branching of the NEC and carries the low salinity waters of the Bay of Bengal origin. It forms some time in November in the south and transports the warm waters of the equatorial region towards north (Shenoi et al., 1992). It is found to be well established upto the coast of Saurashtra by December. During January the current stretches all the way from the southern tip of the coast of India to the coast of Pakistan. It is quite a strong current (with transport of about  $7 \times 10^6 \text{ m}^3/\text{s}$ ) moving poleward along the west coast of India against weak winds (Shetye et al., 1994). It is found to be driven by a pressure gradient which forms along this coast during this season due to either thermohaline forcing or due to the arrival of Kelvin waves from the Bay of Bengal. Another characteristic feature of this poleward coastal current is the presence of an equatorward flowing undercurrent at 300 m depth. This coastal current reverses its direction towards the equator during the southwest monsoon with a prevailing poleward undercurrent at 200 m depth (Muraleedharan et al., 1995).

During the northeast monsoon period over most parts of the Arabian Sea the currents are directed towards west or northwest. The reversal of currents in the Arabian Sea is observed to be complete by November (Varadachari and Sharma, 1967). In the open Arabian Sea the overall movement of water during this season is from east to west (Wyrski, 1973). In the central Arabian Sea during December the flow is to the southwest with maximum currents of 0.7 m/s (Bauer et al., 1992). During MASAI (Monsoon Arabian Sea Investigation), the currents north of  $20^\circ \text{ N}$  showed cyclonic rotation during the period 20 December 1986-18 January 1987 at the height of the northeast monsoon (Morrison and Olson, 1992). In the region between  $20^\circ \text{ N}$  and  $10^\circ \text{ N}$  the flow in the central basin is generally to the southwest due to the influence of the northeast monsoon winds.

#### **Lakshadweep High and Low:**

The circulation in the south Arabian Sea during winter is influenced by formation and propagation of mesoscale eddies. Using hydrography and altimeter data, Bruce et al. (1994) presented the evidence of a large (500-800 km diameter) anti-cyclonic eddy in the upper 300-400 m, namely Laccadive High (LH) in the southeastern Arabian Sea (centered at  $10^\circ \text{ N}$ ,  $70^\circ \text{ E}$ ) during early winter. It moves westward across the southern Arabian Sea and dissipates in the mid basin during the inter monsoon period. A cyclonic eddy, Laccadive Low (LL) forms during early summer at the same location and propagates westward across the southern Arabian Sea a few months after genesis. The times of formation of WICC, northward phase in early winter and the southward phase in early summer, coincide with that of LH and LL. Shankar and Shetye (1997) suggested that the formation of the LH and LL are a consequence of westward propagating Rossby waves radiated by Kelvin waves propagating poleward along the western margin of the Indian subcontinent.

#### **Arabian Sea High:**

A large anti-cyclonic eddy, Southern Arabian Sea High (SAH) appears in the southern Arabian Sea during the northeast monsoon (Prasad and Ikeda, 2001). The SAH forms west of the LH, first appears in January and grows rapidly insitu to a well developed anti-cyclonic eddy extending across the southern Arabian Sea by March, with its centre at  $\sim 5^\circ \text{ N}$ ,  $65^\circ \text{ E}$ . The SAH is bounded by a strong eastward current to the north and a weak southward flow between  $65^\circ$  and  $70^\circ \text{ E}$ , which separates SAH from the LH. The westward flowing NEC is on the southern flank. A strong northward flow along  $55^\circ \text{ E}$  during January and February marks the western boundary. The SAH propagates westward as a Rossby wave between March and April. The arrival of SAH in the western boundary in April is accompanied by intensification of current along the coast of Somalia. In May, part of the SAH moved northward to form an anti-cyclonic eddy (with an apparent centre at  $13^\circ \text{ N}$ ,

53° E in the vicinity of the Gulf of Aden), namely the Gulf of Aden Eddy (GAE). The GAE extends horizontally about 600 km (along 13° N) and vertically down through the upper main thermocline to about 250 m.

### **Bay of Bengal Circulation:**

The circulation of waters in the Bay of Bengal is mainly influenced by the seasonal winds and fresh water discharge from major rivers opening out into the Bay. The surface circulation in the Bay of Bengal and Andaman Sea can be broadly divided into three gyres namely a) the northwestern gyre, which is clockwise during winter and anti-clockwise during summer, b) the large gyre in the southern Bay of Bengal, which is clockwise during both winter and summer and c) the Andaman gyre (Varkey et al., 1996).

The southwest monsoon winds directly produce an easterly drift in the open waters of the Bay together with a current setting northward and northeastward along the east coast of India. These winds indirectly drive the surface waters across the Bay and along the east coast of India to the head of the Bay leading to the piling up of water on the eastern side of the Bay. Since there is no escape for the piled up water a counter-clockwise circulation sets in over the head of the Bay, the flow of water being exactly in the opposite direction to the direct flow produced by the monsoon. This counter-clockwise circulation which sets in July extend southward and westward in the subsequent months, still remaining centered at the head of the Bay. In September it forms the predominant circulation of the whole Bay, west of the Andaman Islands (Reddy, 2001).

Murty et al. (1992<sub>a</sub>) studied the circulation of the Bay of Bengal during southwest monsoon and identified a large cyclonic gyre south of 15° N and anti-cyclonic eddies in the northern Bay and west of the Andaman Islands. This cyclonic gyre is driven by a positive curl field and is fed by the eastward flowing IMC in the southern Bay. While this current bends into the Bay from the southeast under the influence of a strong positive wind stress curl in the central Bay, it encounters less saline waters from the south Andaman Sea. At the centre of the gyre, cold waters resulting from the divergence (upwelling) of subsurface waters prevail along an axis oriented SW-NE. The circulation in the western Bay during the southwest monsoon is characterized by alternate cyclonic and anti-cyclonic eddies (Suryanarayana et al., 1992). A cold core subsurface cyclonic eddy is present in the northwestern Bay of Bengal during peak southwest monsoon (Babu et al., 1991).

During the transition period from spring to the southwest monsoon (May-June), a two gyre circulation system consisting of anti-cyclonic gyre (remnant of the spring season gyre) in the northwestern Bay of Bengal and cyclonic gyre (developing at the beginning of the southwest monsoon) west of the Andaman Islands is reported (Murty et al, 2000). In all the seasons the circulation is tight upto 100 m depth and weakens below 100 m, except at the centers of the eddies.

During the northeast monsoon, the circulation in the Bay of Bengal is influenced by the combined effect of the northeast winds and the winter cooling at the head of the Bay. From analysis of hydrographic data collected during early phase of northeast monsoon of 1983, Rao and Murty (1992) found a large cyclonic gyre between 18° and 12° N with southwest flow along the western boundary and northward flow in the east, west of the Andaman Islands. In the southern Bay the eastward flow is found to turn northward on the eastern side of the Bay. The circulation at 100 m depth is found similar to that at the sea surface with the centre of the cyclonic gyre shifting westward to 14° N, 83° E. At 500 m depth the cyclonic gyre is found to diffuse completely. Suryanarayana et al. (1992) concluded that during the northeast monsoon, the surface circulation is characterized by a large cyclonic cell between 19° N and 13° N in the offshore regions of the Bay, coupled with a strong southward coastal current along the central east coast of India. North of 19° N the circulation is found to be anti-cyclonic.

A prominent feature of the circulation in the Bay of Bengal is the seasonally reversing coastal currents. The coastal current along the east coast of India (EICC) flows poleward during February-May (in association with an anti-cyclonic gyre). During the summer season (July-September), the coastal current flows poleward in the south and equatorward in the north. During the post southwest monsoon season (October-November), an equatorward flowing western boundary current develops along the east coast of India due to the flow of heavy fresh water influx at the head of the Bay (Babu, 1992). Sanilkumar et al. (1997) found a strong poleward flow ( $> 90$  cm/s) in the northwestern Bay, north of  $15^\circ$  N during March 1993 (from a hydrographic survey) regarded as the western boundary current of the Bay of Bengal. Recent studies including modeling experiments suggest that the coastal circulation off the east coast of India is influenced by the remote forcing of winds over the equatorial Indian Ocean and the interior Ekman pumping besides along shore wind stress and river runoff.

### 3.4 WATER MASSES

In the Indian Ocean the information on the water mass structure has improved significantly due to the IIOE and subsequent oceanographic expeditions. The water masses of the north Indian Ocean (separated by a hydrological front near  $10^\circ$  S) are quite different from those in the north Atlantic and north Pacific, because of closure of the Indian Ocean on the northern side by the Asian landmass and monsoon climate and the associated changes in current pattern. A brief account of the characteristics of water masses in the upper 1000 m of the TIO is given below.

Three distinct saline water masses namely, the Arabian Sea High Salinity Water (ASHSW), the Persian Gulf Water (PGW) and the Red Sea Water (RSW) were documented first by Rochford (1964). The thermohaline characteristics and core depths of these high salinity waters in the Arabian Sea are given in the follow table (adapted from Prasanna Kumar and Prasad, 1999).

<b>Water mass</b>	<b>Temp. (C)</b>	<b>Salinity (psu)</b>	<b><math>s_t</math> (<math>\text{kg m}^{-3}</math>)</b>	<b>Depth (m)</b>
ASHSW	24-28	35.3-	22.8-	0-100
		36.7	24.5	
PGW	13-19	35.1-	26.2-	200-
		37.9	26.8	400
RSW	9-11	35.1-	27.0-	500-
		35.7	27.4	800

Sundararamam et al. (1968) studied water masses in the upper 500 m of the Arabian Sea using the hydrographic data collected during 1962 -1965. They traced PGW and Gulf of Oman Water in the upper 50 metres near the mouth of Persian Gulf and low saline Indus Water at 75-150 metres and RSW at 150-200 metres in the northern Arabian Sea. ASHSW shows salinity maximum at 75-150 metres in association with thermocline throughout the eastern Arabian Sea and spreads southward up to  $8^\circ$  N.

The ASHSW forms at the surface in the north Arabian Sea, where the evaporation exceeds precipitation. It builds up during May-July and stays more or less the same during August-October. It lies at the bottom of the Equatorial Surface Water (ESW), which forms due to high precipitation in the southern and eastern parts of the Arabian Sea (Darbyshire, 1967). Its coverage decreases during November-January and lowest during February-April. The depth of salinity maximum associated

with this water is shallowest (~ 20 m) in the northern Arabian Sea and is deepest (100 m) in the south (Shenoi et al. 1993) and generally increases from north to south and from west to east.

The evaporation at surface exceeds precipitation in the Persian Gulf (average depth 25 m) by about 2 m annually. This leads to formation of a warm saline water mass namely, the **PGW**, which flows into the Gulf of Oman at depths of 25 to 70 m through the straits of Hormuz. In the Gulf of Oman the water sinks to 200 – 250 m depth (Shetye et al. 1994) and this water spreads in the northern Arabian Sea and the associated salinity maximum is found between 200 m and 400 m with deeper depths in the south. The area covered by the PGW is maximum during November-January and minimum during May-July (Shenoi et al. 1993). Varma et al. (1980) reported the presence of PGW at about 300 m depth and ASHSW around 60 m depth in the eastern part of northern Arabian Sea during February-April from an analysis of STD data.

In the Red Sea too evaporation exceeds precipitation by over 2 m per year. The resulting **RSW** flows over the 110 m sill and enters the Gulf of Aden, and spreads in to the Arabian Sea. The northern extent of the salinity maximum associated with this water is approximately 18° N latitude and its depth increases from about 500 m in the north to about 800 m near the equator.

These three high salinity water masses merge in the central Arabian Sea within a thick layer extending from 150 – 900 m depth to be known as the North Indian High Salinity Intermediate Water, **NIHSIW** (Wyrтки, 1973<sub>b</sub>). High salinity water with salinity range 35.5 - 36.8 psu and temperature range 24 - 30° C is termed as Arabian Sea Water (**ASW**) by Emery and Meincke (1986).

The water mass between 100 m and 800 m in the western equatorial north Indian Ocean has been called the Indian Ocean Equatorial Water, **IEW** (Sverdrup et al., 1942). It is formed from mixture of the Indian Central Water (**ICW**) and the Australian Mediterranean Water, both of which form south of the equator. IEW and ICW have the same temperature range of 8.0 – 25.0° C but the Equatorial Water is some what less salty with a salinity range of 34.6 – 35.2 psu, while the Central Water goes up to 35.8 psu. IEW is a major subsurface water mass in the equatorial Indian Ocean and it extends from about 150-200 m depth to about 2000 m depth.

Waters at intermediate depths (500-1500 m) can be separated into those with a fresh water signature and those that are salty (Emery and Meincke, 1986). The salinity maximum associated with Red Sea – Persian Gulf Intermediate Water (**RSPGIW**) has a range of 34.8 - 35.4 psu and temperature range 5-14° C. The Antarctic Intermediate Water (**AIW**) with salinity range 33.8-34.8 psu and temperature range 2-10° C is present below the ICW in the south Indian Ocean.

LaFond (1958) grouped the surface waters of the western Bay of Bengal into three distinct classes, namely, the Northern Dilute Water (**NDW**), the transition water and the Southern Bay of Bengal Water (**SBBW**). NDW forms as a result of large quantities of fresh water influx from the Ganges and Brahmaputra rivers and has density less than  $19s_t$ . The transition water is a mixture of the NDW and the SBBW in the western Bay and has a density between  $19s_t$  and  $21s_t$ . The SBBW is the major source of surface water in the Bay with density between  $21s_t$  and  $22s_t$ . Varkey identified the low salinity surface water as the Bay of Bengal Low Salinity Water (**BBSW**), which appears in the northern Bay and Andaman Sea and is formed as a result of great dilution (Varkey et al. 1996). He assigned thermohaline indices for the BBSW as  $T=27^\circ\text{C}$ ,  $S=33\text{ psu}$  and  $s_t \sim 21.2$  in the northern Bay. The surface layer with freshwater component having salinity range from 35.0 down to 28.0 psu and temperature range 29-25° C is termed as Bay of Bengal Water (**BBW**) by Emery and Meincke (1986).

Rao and Jayaraman (1968<sub>b</sub>) have identified two water masses in the upper 100 m of the central and southern Bay of Bengal during the transition period between winter and summer namely,

(i) A low salinity water mass characterized by salinity  $< 33.0$  psu and  $s_t < 21.0$  in the upper 50 m of the eastern Bay and the Andaman Sea named as the Eastern Dilute Water of Indo-Pacific origin, considered to be formed by the admixture of the runoff from the Burmese coast with the less saline waters of Pacific region entering the southeastern Bay through the Straits of Malacca, (ii) Another water mass which resembles the SBBW with salinity range 33.0-34.0 psu and  $s_t$  range 21.0-22.0 in the upper 100 metres of the southern Bay and the western and middle parts of the central Bay. Below 100-150 m depth, they encountered the IEW as the major subsurface water mass in this region. The subsurface saline ( $> 35.0$  psu) layer was identified by Varkey as Intermediate High Salinity Water (**IHSW**) of the Bay of Bengal (Varkey et al. 1996), which represents the Indian Equatorial Intermediate Water (**IEIW**) identified by Gallagher (1966) to have been formed as a result of mixing between high salinity waters from the Arabian Sea present in the central and southern Bay at depths greater than 100-150 m up to 1000 metres with temperature range  $15-5^\circ$  C and salinity nearly constant (35.02 – 35.1 psu). ASHSW was identified at subsurface depths (50-100 m) in the southern Bay towards equator (Suryanarayana et al., 1993). The presence of PGW around 26.81  $s_t$ , RSW around 27.19  $s_t$  and ESW around 22.5  $s_t$  in the Bay of Bengal was reported by Varkey and Sastry (1992).

## 4. UPWELLING

Upwelling is an important oceanic process which affects the biological productivity and climate. It accounts for 80-90% of global ocean new production. In the north Indian Ocean, upwelling off the coasts of Somalia and Arabia is quite strong and well documented. However, upwelling observed off the west and east coasts of India are relatively weak. Upwelling describes the physical process of an ascending motion of water column for a minimum duration and extent by which water from subsurface layers of about 50 to 300 m is brought into the surface layers (this excludes the short term motions that are associated with vertical eddy mixing and overturning due to high frequency internal waves). The reverse is true in case of downwelling. Upwelling is largely a wind-driven process by which transfer of momentum from the prevailing wind fields to the surface ocean results in divergence, forcing cool, nutrient-rich subsurface waters up into the euphotic zone.

The upward motions associated with large-scale upper ocean upwellings are, only a few metres per day and thus cannot be measured directly. Upwelling velocities are usually deduced from indirect calculations. Upwelling systems are complex, demanding interdisciplinary study to enhance our understanding of how they work. Upwelling may take place anywhere in the ocean and can extend to hundreds of miles. One of the causative factors to induce upwelling is the horizontal divergence (Sharma, 1978). The differential absorption of solar radiation by the ocean results in horizontal density variation causing divergence and large-scale upwelling starts as a result. On the other hand convergence leads to downwelling. Wind can also cause convergence and divergence. Open ocean upwelling involves six times the volume of water upwelled in coastal upwelling systems and balance around 85% of the thermocline circulation (Summerhayes et al., 1995).

Upwelling systems can be classified into two major categories: wind driven and dynamical. Wind driven upwelling results from divergence in the Ekman layer of the ocean. Dynamical upwelling results from the divergence in the upper ocean or convergence deeper in the water column caused by large-scale oceanic current system. The upwelling is induced by the wind action under suitable conditions, although its occurrence in some areas does not appear to be due to the local wind. Upwelling/downwelling process can be broadly divided into three categories: (i) Coastal upwelling, (ii) Equatorial upwelling and (iii) Offshore or open ocean upwelling.

**Coastal Upwelling:** When wind blows in the Northern Hemisphere with the coast to the left, the Ekman transport being to the right of the wind, will carry surface water away from the coast (Fig.3). The same situation arises in the Southern Hemisphere if the wind blows with the coast on its right. In either case the continuity of flow is maintained by rising cool subsurface water from below the surface to replace the surface water, which is moving offshore. On the other hand, downwelling takes place if the wind blows in the opposite direction. According to Hidaka (1958), the most intense upwelling occurs when the wind makes an angle of  $21.5^\circ$  with the coastline in an offshore direction.

**Equatorial Upwelling:** Historically, even before the volume transport of currents could be estimated, the presence of open ocean upwelling near the equator had been inferred from the distribution of water masses and the meridional structure of isotherms. According to Brennecke (1921), the sinking of dense waters in convective areas had to be balanced by deep upwelling elsewhere. However, in the TIO, equatorial upwelling is not as prominent as it is in the Pacific and Atlantic.

**Offshore (open ocean) Upwelling:** As one goes away from the equator the Coriolis force becomes important, and the water in the offshore is deflected towards right in the Northern Hemisphere and towards left in the Southern Hemisphere. The wind stress curl can be regarded as a forcing function for oceanic motion. Positive wind stress curl is conducive to upwelling in the Northern Hemisphere and downwelling in the Southern Hemisphere. Negative wind stress curl is favorable to upwelling in the Southern Hemisphere and downwelling in the Northern Hemisphere. The largest values of vertical motion rotate this

water either in the cyclonic (anti-clock wise), or in the anti-cyclonic (clockwise) circulation (Hastenrath and Lamb, 1979). The cyclonic and anti-cyclonic circulations give rise to “upwelling” and “downwelling” at their centers respectively.

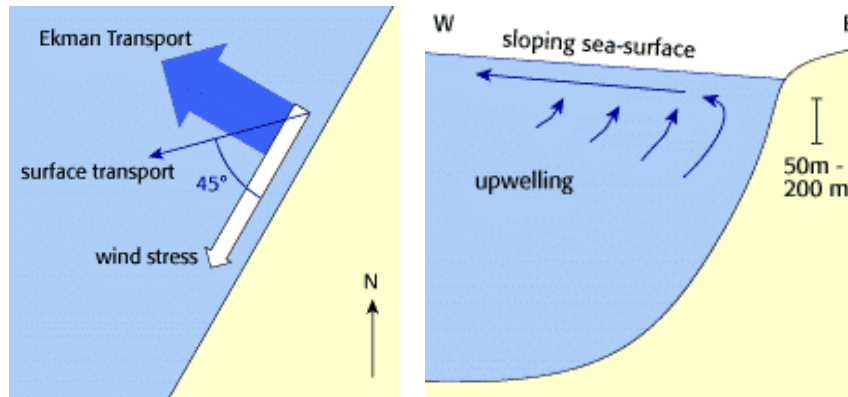


Fig. 3: Schematic diagram of Coastal Upwelling  
 (Downloaded from <http://seis.natsci.csulb.edu/rbehl/coastup.htm>)

### Upwelling in the Arabian Sea

Upwelling in the western Arabian Sea is a summer phenomenon and is intimately associated with the southwest monsoon circulation (Dietrich, 1973). The correlation between the upwelling off eastern Africa and Arabia and the monsoonal circulation has been described as the example of large-scale atmospheric forcing of the ocean.

#### *Upwelling along the Somalia coast:*

In the northwestern Indian Ocean during the summer monsoon, strong upwelling occurs over a large area along the Somali and Arabian Coasts. The commencing of upwelling is evident on both coasts in late April or early May, it is strong in July and August, and continues until early October. Swallow and Bruce (1966) found the coldest water (temperature  $<16^{\circ}\text{C}$ ) extended from about  $8^{\circ}30'$  N (where strong horizontal thermal gradients of  $0.6^{\circ}\text{C}/\text{km}$  were found) northeastward along the coast to  $10^{\circ}$  N, encompassing an area of  $8 \times 10^3 \text{ km}^2$  during 17-23 August 1964. They further reported that, about 10 days later (28 August - 5 September 1964) the cold water clearly had shifted, extending farther northward to the latitude of Ras Hafun, although the area of surface temperature  $<16^{\circ}\text{C}$  was still nearly the same. Warren et al. (1966) have noticed the presence of cold surface water with a temperature as low as  $14^{\circ}\text{C}$  near the Somalia coast during southwest monsoon season of 1964.

At low latitudes off the Somalia coast, upwelling is related to the turning offshore of the boundary current, which has reached that latitude partly as a result of overshoot from south of the equator (Anderson and Moore, 1979). At  $7^{\circ} - 10^{\circ}$  N, upwelling is initially due to offshore Ekman transport in response to the local southerly winds, but is quickly modified after the main monsoon onset by a strong clockwise eddy which propagates shore wards from the region of maximum clockwise wind stress curl (Schott and Quadfasel, 1982).

A sea surface temperature image of August 1995 revealed the coolest surface waters in the northwestern Arabian Sea at 10.5 ° N, 51.5° E on the Somali coast. Results from model studies of the northwest Indian Ocean circulation indicate that the local wind field and the gradient in wind stress curl are the primary determinants of the fate of upwelled waters (Hitchcock et al., 2000). Upwelling also occurs along the northern perimeter of the Great Whirl, at least to 53° E, in response to the vorticity balance as the 'stretching' term forces an uplift of the thermocline/pycnocline. Halpern and Woiceshyn (1999) reported from a study of satellite sensed wind and SST data, the occurrence of upwelling event north of the approximate position of the Somali Jet during June 1997. They also have reported the occurrence of the downwelling event south of the Somali Jet.

#### *Upwelling along the Arabian Coast:*

The southwest monsoon wind field causes upwelling along the Arabian coast, leading to observed persistent jets of cold upwelled water extending from the Oman coast, often reaching hundreds of kilometres into the interior (Brink et al., 1998). Gardner et al. (1999) reported strong upwelling during southwest monsoon near the Arabian Coast in 1995. The development of a broad swath of coastally upwelled water was evident in the June SST (1995) as the southeasterly winds driving coastal upwelling along Oman coast (Fischer et al., 2002). Off the southern coast of Arabia the boundary current is relatively weak, the upwelling region is broader and the process appears to go on more steadily. Besides the coastal upwelling due to Ekman transport of surface water offshore, in response to winds parallel to the coast, there is a region some 400 km wide in which open-sea upwelling occurs in response to positive wind stress curl (Swallow, 1984).

Wyrtki (1973<sub>a</sub>) noted that the Arabian upwelling differed from that of Somalia-specifically the Arabian upwelling is not associated with a strong boundary current, its nutrient enrichment is greater, and its volume transport may be higher. The Arabian upwelling is neither as cold (minimum 18° C) nor as fresh (minimum 35.7‰), as the upwelling off Somalia, which has a minimum temperature and salinity of < 14° C and 35.15‰, respectively.

#### *Upwelling along the Oman Coast:*

The Oman coast is also oriented in relation to the strong southwest winds similar to the Somalia coast. The wind-induced upwelling is limited to depth of 200-300 m and is more intense in the northern region of the Oman coast (Sastry and D'Souza, 1972). Remote sensing images of June 9, 1985 have shown regions of intense upwelling closer to the coast of Oman. This has been supported by the observations of summer 1987 which detected the coldest water on the downstream side of a headland and a diffuse patch of cold water near the Kuria Maria Island. There was at least a 5° C temperature difference between the regions of upwelled water and the ambient surface waters (Elliot and Savidge, 1990).

Upwelling off Salalah (Oman) starts generally between third week of May and the third week of June each year and lasts until the beginning of October. Upwelling velocities were averaged at the coast and for the adjacent near-shore area within a radius of 83 km around Salalah (Rixen et al, 2000). The mean coastal upwelling ( $2 \times 10^{-5}$  m/s) is roughly 10 times higher than the mean upwelling velocities in the near-shore area. Water welling up continuously for 4, 5 months with a velocity of  $2 \times 10^{-5}$  m/s could cover a distance of roughly 240 m. Assuming a 50 m thick euphotic zone, water from a depth of approximately 290 m could reach the surface during the upwelling season. This matches the observation made by Brock et al. (1992), who have suggested that coastal upwelling extends to water depths between 200 and 300 m. Three to seven weeks of enhanced wind stress seem to be necessary to establish upwelling along the coast during the starting/onset phase of the southwest monsoon.

Woodward et al. (1999) reported a sharp frontal zone off Oman, and related the same to the effect of the colder, nutrient rich upwelled water, resulting from the Ekman positive wind stress curl. Using AVHRR image, they have also shown that there is a decrease in surface temperature due to this upwelling effect.

#### *Upwelling along the west coast of India:*

The prevailing current system is to be regarded as the main reason for the upwelling off the southwest coast of India, and not the wind. As indicated, both by its geophysical position and by its large north south extent, this upwelling area bears some resemblance to the 'classical' upwelling region off the west coasts of the continents in low latitudes, i.e., at the eastern sides of the trade wind regions.

Off Bombay, from where upwelling is definitely known, the rising of the deep water on the left side of the coastal current may cause similar biological conditions near the sea-bed as off Cochin. This will not necessarily become reflected by changes in the very surface layers.

Upwelling off Cochin and farther south was found by Rama Sastry and Myrland (1959) during their first series of cruises in October 1957. The phenomenon extended to a mean distance of 60 miles from the shore, and it was stated that the upwelling water reaching the surface came from depths (Banse, 1959) between 50 and 75 m (Fig. 4). Off Calicut, upwelling is regularly found during the whole period of southwest monsoon, its effect is felt strongest in July and August and it lasts till October. According to the observations in 1957 and 1958, the upwelling extends southwards to Cape Comorin ( $8^{\circ}$  N). Towards north the upwelling certainly reaches  $15^{\circ}$ , and perhaps  $18^{\circ}$  N. Cold water is found off the southwest coast of India from June to September and even in October and is extending to about  $15^{\circ}$  N, south of Goa. The time of commencement of upwelling differs from depth to depth along the west coast of India. Off Cochin, the water at and below 100 m moves upright from February onwards while at 30 m depth upwelling starts in April. The upwelled water reaches the surface in late May and persist upto July/August. The downward movement sets in by the end of August at all depths and earlier in deeper layers (Sharma, 1966).

A study of the seasonal variation of oceanographic conditions of the southwest coast of India using the data collected during 1971-1975 under Pelagic Fishery Project (Johannessen et al., 1987) indicated that an uplift of water onto the shelf region begins in March or April. Associated with a south – flowing current, this upwelling lasts throughout the southwest monsoon period until September-October. The "rate" of upwelling can be qualitatively indicated by the rise of isolines for different parameters, which is of the order of 1.5 m/day for this region.

Hydrography and circulation off the west coast of India during the southwest monsoon of 1987 were studied by Shetye et al. (1990). The near-coast surface region off Trivandrum is marked by upsloping of isotherms and approximately 100 m deep and 150 km wide equatorward flow during June 1987. Below this lies a northward approximately 40 km wide undercurrent with its core (recognized by salinity maximum) at a depth of about 150 m. North of  $15^{\circ}$  N upwelling was hardly visible. Unnikrishnan and Antony (1992) identified a coastal front, associated with upwelling from the observed thermal field along the west coast of India during September, 1987. The front, which is seen very clearly upto a depth of about 75 m, has a horizontal gradient of temperature of about  $6^{\circ}$  C over a width varying between 45 and 70 km.

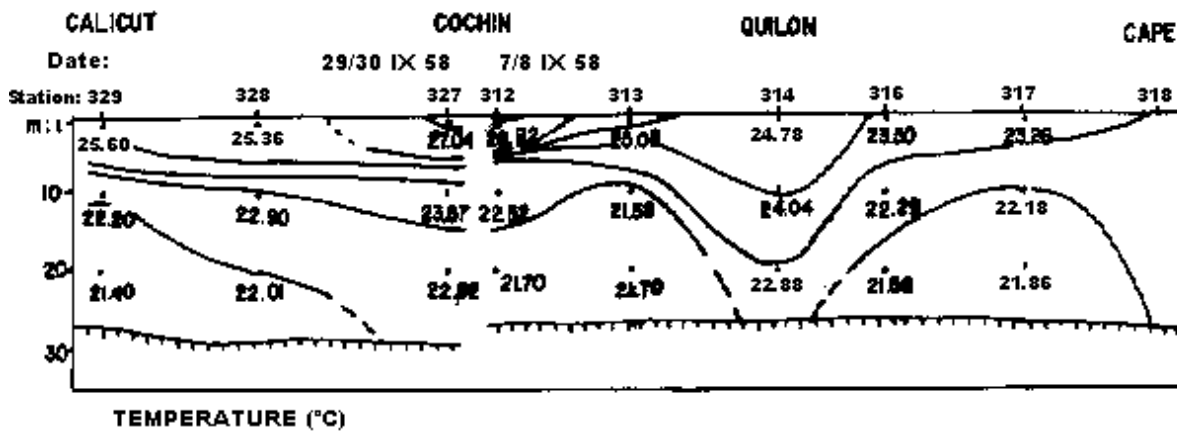


Figure 4: Vertical section of temperature along the southwest coast of India during September 1958. (Adapted from Banse, 1959).

The surface circulation along the west coast between 8° and 15° N closely follows the climatological wind pattern during the monsoon season and their influence is felt to a depth of 75 m, below which the current reverses, indicating the zone of poleward undercurrent at depth of 200 m (Muraleedharan et al., 1995). Muraleedharan and Prasannakumar (1996) inferred the upwelling favorable conditions from SST and MLD distributions along the southern shelf, which were less conspicuous towards north. They also have reported a remarkable shoaling of MLD from 100 metres at 11° N to 45 metres at 17° N, which was associated with active upwelling and downwelling on either side of the wind maxima. They have confirmed this with the SST distribution where cool water is found at the zone of maximum wind and warm water southward. The wind field along the southwest coast of India favored strong upwelling off Cochin, less strong off Mangalore and relatively weak off Goa.

Bhattathiri et al. (1996) observed highest primary production during the summer monsoon near the southwest coast of India. They related this to the upwelling contributing to high nitrate levels in the top layers which in turn supported high phytoplankton production and chlorophyll. During summer monsoon, primary production increases along the eastern Arabian Sea as a result of upwelling. Stramma et al. (1996) observed a typical eastern boundary upwelling region along the southwest coast of India during August 1993. A recent field experiment conducted by Sanilkumar et al. (2004b) during July 2003 off the southwest coast of India indicated intense upwelling with in upper 60 m water column all along the coast but the width of upwelling zone reduced significantly from south (>200 km) to north (~50 km).

#### *Open ocean upwelling in the Arabian Sea:*

In addition to the strong northward Somali current and upwelling off the coast of Somalia the southwest monsoon also drives open ocean Ekman pumping during the boreal summer (Ragu et al. 1999). Rao and Jayaraman (1966) reported upwelling in the Minicoy region during northeast monsoon. During November to January, the general set of current in the southern part of the Arabian Sea is westerly. Owing to the coastal conformation, north-northwesterly current develops off the west coast of India. These two currents diverge in the vicinity of Minicoy leading to upwelling in this region.

Upwelling appears to be the dominant factor in maintaining the heat balance of the Arabian Sea. Strong upwelling is limited to about one tenth of the total area, and only three months of the year, but the upwelling velocities are of the order of 30 times the required average, which could account for most of the required heat loss (Swallow, 1984). A striking feature of the upper ocean in the central northwestern Arabian Sea during both the SW and NE monsoon seasons is the deepening and cooling of the mixed layer (Rao et al., 1989). A number of studies (Bauer et al., 1991; McCreary et al., 1993) have emphasized the role

of Ekman pumping in setting the mixed layer depths structure across the Arabian Sea. Generally deeper mixed layers to the south and east of the Findlater Jet's wind axis and shallower mixed layers towards the Arabian Coast are found consistent with open-ocean Ekman upwelling and downwelling.

Bauer et al. (1991) observed seasonal occurrence of wind-induced upwelling in the northern Arabian Sea where there is a considerable shoaling of thermocline in the regions of strong winds. De Souza et al. (1996) noticed the occurrence of intense upwelling in the northwestern Arabian Sea during the southwest monsoon. The monsoon response of the upwelling is dominated by a combination of mixed-layer deepening and vertical motions associated with Ekman pumping. The Ekman dynamics, which depend more on the distribution of surface winds rather than solely on magnitude, induce latitudinal patterns in open-ocean upwelling and downwelling. In the southwest monsoon, however, Ekman pumping calculations indicate strong downwelling in the central Arabian Sea, and upwelling in the northern Arabian Sea (Bauer et al. 1991). Woodward et al. (1999) observed a marked upwelling towards the surface during September/October 1994 in the central Arabian Sea.

### **Upwelling in the Bay of Bengal**

The wind stress associated with southwest monsoon winds during summer and northeast monsoon winds during winter over the Bay of Bengal cause mass drift of oceanic waters leading to upwelling and downwelling along the east coast of India (Rao et al., 1993<sub>b</sub>).

#### *Upwelling off the east coast of India:*

Along the east coast of India the northeasterly current flows during January to July (which favours the development of upwelling along this coast), and the southwesterly current flows during August to December (which is conducive to sinking). Thus upwelling and sinking occur during different seasons along the east coast of India (Anonymous, 1953). This was determined from the vertical temperature section off Waltair coast and the seasonal temperature and salinity cycle of near shore surface water (Fig. 5). This upwelling was found to last from March to May. Repeated sections taken off the Andhra coast have determined the upwelling velocity to be 10-40 metres per month (LaFond, 1954). The effect of upwelling near the coast exists in June as well (LaFond, 1955). Studies based on the hydrographic data collected during March-May 1963 onboard R.V. Anton Bruun under IIOE (International Indian Ocean Exploration) indicated upwelling on the western side of the Bay, off Visakhapatnam and Madras (LaFond and LaFond, 1968).

Murty and Varadachari (1968) reported strong upwelling off the Waltair coast (with waters from depths greater than 100 m reaching surface) and weak upwelling (waters from 30 m depth reaching the surface) off Madras coast during summer monsoon of 1964. The difference in intensity of upwelling during this period was attributed by them to the relatively strong winds along the coast of Waltair.

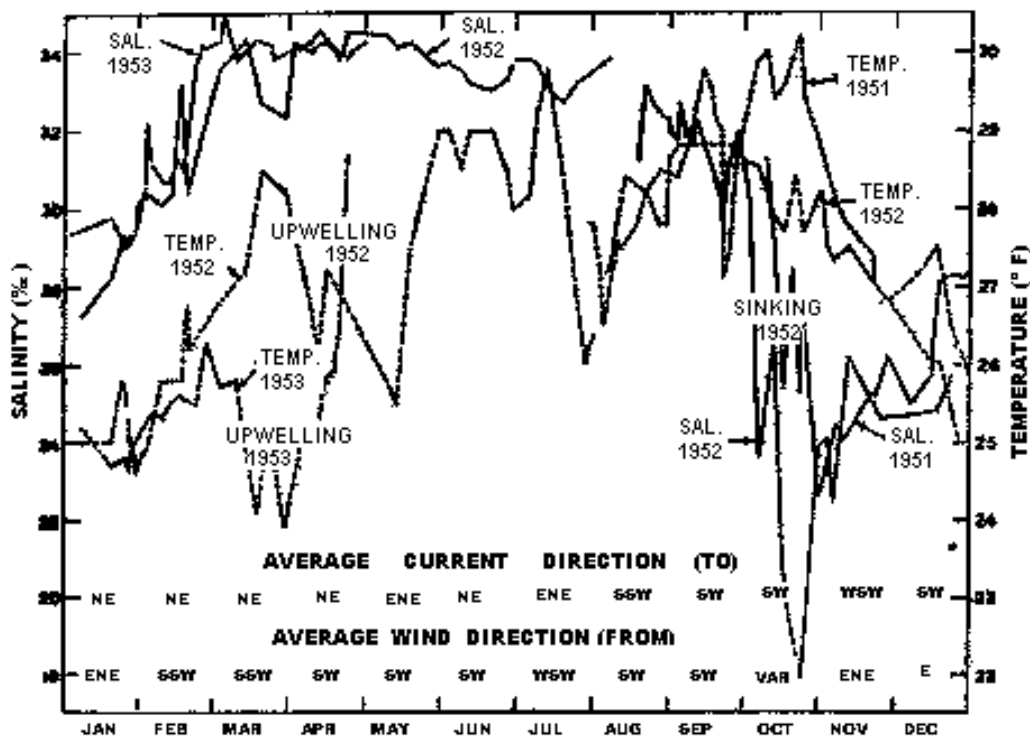


Figure 5: Seasonal cycles of surface temperature and salinity off Visakhapatnam showing periods of upwelling and sinking together with average monthly current and wind direction. (Adapted from LaFond, 1954).

Along the Visakhapatnam coast, winds become favourable for upwelling from the middle of February, when the northeast winds replace south-southwest winds. The observations reported by Rao et al. (1986) and Rao and Rao (1989) show a continued upwarping in the thermal structure and a steady growth in the magnitude of along shore velocity from February to May. An analysis of monthly data collected along a transect perpendicular to the Visakhapatnam coast during April 1979 - March 1980 showed that cold bottom waters upwelled from the middle of February when the northeast winds given place to southwest winds. The upwelling became vigorous during March and continued up to July and then decreased with the withdrawal of the southwest monsoon. With the onset of the northeast monsoon, when north-northeast winds prevailed, the wind stress has driven the offshore waters to the coast and sinking took place. The sinking was not as vigorous as that of upwelling since the wind stress during the northeast monsoon was weak. An estimation of the movement of the 22-24  $\sigma_t$  isopycnals reveal that upwelling speeds are  $9.6 \times 10^{-4}$  cm/sec during March to April and  $7.7 \times 10^{-4}$  cm/sec during May to July. From a similar estimation of the movement of the 18-19  $\sigma_t$  gave downwelling or sinking speed of  $5.77 \times 10^{-4}$  cm/sec for October and November. During March-May 1982, Rao and Rao (1989) reported upwelling off Visakhapatnam, in association with the northeastward along shore flow (20 to 50 cm/sec) and the relatively strong along shore velocity shear (0.008 to 0.016 /sec).

During southwest monsoon of 1984, between 16° and 14° N the influence of wind forcing was found upto the coast leading to the process of upwelling near the coast from about 80 m depth. South of 14° N the prevailing westerly winds in the nearshore region gave rise to southward Ekman transport which in turn led to the process of sinking along the coast (Suryanarayana et al, 1992).

Along the central east coast of India, winds were favourable for upwelling during April 1989 (Rao et al., 1995). In association with this, the hydrographic conditions across the continental shelf indicated a

horizontal gradient of temperature and salinity with the isotherms and isohalines sloping upward towards the coast depicting upwelling.

Based on the hydrographic data collected in the Bay of Bengal during the southwest monsoon (July-August 1989) Shetye et al. (1991) have shown that along most of the western boundary of Bay of Bengal, in an approximately 40 km wide band, isopycnals from depths up to about 70 m surfaced due to upwelling forced by local winds. Off Waltair, this upwelling band was a few metres wide in March and by May it covered half the width of the shelf.

Suryanarayana and Rao (1992) studied the Upwelling Index (magnitude of the offshore component of the Ekman transport) at eight coastal stations along the east coast of India (namely Balasore, Gopalpur, Visakhapatnam, Kakinada, Machilipatnam, Nellore, Chennai and Cuddalore) and noticed strong upwelling during the summer monsoon in the central part and downwelling during the winter monsoon in the northern part. Following the distribution pattern of Upwelling Index along the east coast, they divided the entire region into three zones, viz., northern, central and southern. In the northern zone (comprising stations at Balasore, Gopalpur and Visakhapatnam), the Upwelling Index is predominantly negative except at Visakhapatnam, where positive index is seen from July to September. In the central zone (Kakinada and Machilipatnam), the magnitudes of Upwelling Index are low compared to those at the other regions along the coast. In this zone, the intensity of positive and negative indices is found to be equally distributed. In the southern zone (Nellore, Chennai and Cuddalore) high values of Upwelling Index are noticed compared to other northerly zones with fluctuations in the Upwelling Index. These indices clearly showed predominant sinking in the northern zone in the course of an year. In the central zone, however, prevailing upwelling is well supported by the Upwelling Index.

Along the central east coast of India the upwelling is restricted to a coastal zone, whose width is of the order of Rossby radius of deformation. The upper thermocline region appears to be the source of upwelling water in the Bay of Bengal (Rao, 2002). Johns et al. (1992) have shown that the coastal upwelling off Visakhapatnam to be expected in the presence of the local application of southwesterly surface wind-stress forcing is suppressed by northern fresh water discharge and is, instead, replaced by local sinking. This supports the view of Gopalakrishna and Sastry (1985) that, even in the presence of upwelling favourable winds the discharge of fresh water from the Hugli and Mahanadi rivers during the monsoon seasons has an inhibiting effect on the occurrence of upwelling off Visakhapatnam. The circulation in the southwestern Bay of Bengal during northeast monsoon consists of a cyclonic gyre (Vinayachandran and Yamagata, 1998; Schott and McCreary, 2001) and this cyclonic gyre is forced primarily by upward Ekman pumping caused by positive (anti-clockwise) wind stress curl and the upwelling within this gyre cools the sea surface. The winds stress curl was found to be anti-clockwise resulting in the upward Ekman pumping during the northeast monsoon of 1996.

Srinivasa Rao et al. (2001) using IRS-P4 (OCM) and NOAA (AVHRR) data, observed cold waters in association with high chlorophyll concentration in the northwestern Bay of Bengal during the last week of April 2001 and April 2002 and there from inferred the presence of upwelling along the northeast coast of India.

#### *Upwelling off the Burmese coast and off the west coast of Thailand:*

LaFond and LaFond (1968) reported peripheral upwelling along the Burmese coast resulting from the prevailing northeast monsoon winds from March - May 1963. Ramesh Babu and Sastry (1976) inferred the presence of upwelling from the vertical sections of temperature, salinity and density off Irrawaddy River and off the west coast of Thailand in February-March 1963.

### *Upwelling in the Andaman Sea:*

During the northeast monsoon, under favourable wind conditions weak upwelling occurs along the eastern shore of the Andaman Sea (Wyrtki, 1973<sub>b</sub>). The distribution of temperature, salinity and vertical stability in the northern part of the Andaman Sea also indicate upwelling over the shelf (Varkey et al., 1996). In the southern part of the Andaman Sea the vertical distributions of hydrological parameters at the centre of the anti-cyclonic gyre exhibit a band of isohalines indicating sinking of the surface water (Maslennikov, 1973).

### **Upwelling off the east coast of Sri Lanka**

Climatological thermal structure along 85° E shows that a well developed dome is located east of Sri Lanka during July, and a second dome which is weaker than the first is seen further north during December (Vinayachandran and Yamagata, 1998). The genesis of the first dome coincides with the existence of a strong cyclonic curl in the wind field east of Sri Lanka, which peaks during May to September. The upward Ekman pumping induced by this cyclonic curl brings cooler water to the near-surface layers. During the May-July period the dominance of Ekman pumping is clearly seen. Therefore formation of the dome is certainly linked to the strong cyclonic curl in the wind stress over the dome. Though the wind stress curl remains positive through December, the downwelling due to the arrival of a warm Rossby wave from the east causes the decay of the dome. The role of gyres of the order of a few hundred kilometres in modifying the thermal structure of the upper ocean is significant; the Sri Lankan dome and the Bay of Bengal dome maintain waters cooler by 2-3° C than the surroundings, during their life span. In the case of Sri Lanka dome, although the local along shore winds may not be favourable for coastal upwelling, cooler nutrient rich water is brought to the surface by open-ocean upwelling within the dome.

### **Upwelling off the coasts of Java and Sumatra (Indonesia)**

Along the Java and Sumatra coasts annual upwelling is observed from June to October with cold SST and lower sea level. Upwelling along these coasts is a response to regional winds associated with the monsoon-climate (Susanto et al. 2001). During the southeast monsoon (June – September), southeasterly winds from Australia generate upwelling along the Java -Sumatra coasts. Conditions are reversed during the northwest monsoon (December – March). During the monsoon transition periods namely April-May and October-November, equatorial westerlies generate equatorial downwelling Kelvin waves propagating eastward and become coastally trapped waves along the Sumatra and Java Islands (Clarke and Liu, 1993; Sprintall et al., 2000). These waves play important role in the upwelling and downwelling processes along these coasts.

The upwelling centre with low sea surface temperature migrates westward and towards the equator during the southeast monsoon. Upwelling is eventually terminated due to the reversal of winds associated with the onset of the northwest monsoon and impingement of Indian Ocean equatorial Kelvin waves. Significant interannual variability of the Java-Sumatra upwelling is linked to ENSO through the Indonesian through flow and by anomalous easterly winds. During El Nino episodes, the Java-Sumatra upwelling extends in both time (into November) and space (close to the equator). During El Nino (La Nina) the Indonesian throughflow carries colder (warmer) water shallowing (deepening) thermocline depth and enhancing (reducing) upwelling strength.

### **Upwelling in the Equatorial Indian Ocean**

Over the Indian Ocean, the equatorial winds are weak in general throughout the year, and are maximum during the inter-monsoon periods (April and October) when they are westerlies. The southwest monsoon winds dominate the annual cycle, so that the annual-mean wind field has a structure much like that

in July. Because of this forcing, significant upwelling typically does not occur along the equator (Miyama et al., 2003). However, the rapid event-like onset of the westerlies generate a jet of surface current in the equatorial wave guide (O'Brien and Hurlburt, 1974; Wyrski, 1973<sub>a</sub>) and a reversal of undercurrent also takes place (Luyten, 1981). These changes are expected to be accompanied by marked vertical displacements of the thermocline, as shown by a non-linear numerical model (O'Brien and Hurlburt, 1974).

In the equatorial Indian Ocean the mixed layer deepening is seen after the onset of monsoon in the central and still more so in the eastern segments, where as, upwelling and mixed-layer shoaling is observed at the western end (Ali et al., 1987).

## 5. INTERNAL WAVES

Internal waves occur in the interior stratified region of strong temperature/density gradients (thermocline/pycnocline) in the sea. They can be either progressive or standing type of waves with periods varying from tidal period to 20 min or so. The amplitude and depth of internal waves also vary greatly. The speed of internal waves is generally less than that of the surface waves. Internal waves play a major role in the vertical mixing in the sea and affect the physical, chemical and biological parameters (Reddy, 2001).

When internal waves are near a boundary, their effect on vertical and horizontal motion is apparent from direct observations. Below the thermocline, there is a convergence of water ahead of the wave crest and divergence of water behind the crest. Above the thermocline, water particles diverge ahead of the crest and converge behind the crest. This leads to a series of slicks/smooth and ruffled/rough sea surface. Thus bands of slicks are indicative of convergence and sinking of surface water and if they move shoreward in shallow water they show the presence of internal waves (LaFond, 1962).

Internal waves may be caused due to several reasons. The tidal forces across the continental slope, varying winds in disturbed weather, surface waves and moving ship in harbor generate the internal waves in surface waters. The shears associated with currents in the water column, flows across rugged irregular sea bottom and submarine movements in the stratified waters generate internal waves in the subsurface waters (Murthy, 2002).

Internal waves were studied using time series BT/CTD measurements at fine resolutions (30 min to 3 hrs.) for periods up to three weeks from stationary ships, and with current metres from moored buoys or with thermister string from stationary ships. Isotherm Follower from instrumented Oceanographic Tower for recording shallow water internal waves and towed Thermister Chain or undulating CTD (Batfish) for deep water internal waves have been used. Internal waves were investigated through monitoring sea surface slicks by satellite sensors. A brief account of studies on the internal waves in the north Indian Ocean is given below.

Murthy (2002) reviewed the studies on internal waves in the seas around India. Perhaps the first investigation on internal waves in the Bay of Bengal was carried out in 1953 from repeated BT lowerings from a stationary ship (LaFond and Rao, 1954). Prominent internal tides of 15 m wave height occurring 4.5 hours behind tide were observed off the central east coast of India. A series of slicks/smooth and ruffled sea surface produced by internal waves were observed all along the eastern continental shelf of India. Internal waves were noticed more prominently up to 40 metres at different places in Bay of Bengal and Arabian Sea. High resolutions time series BT measurements showed high frequency internal waves (3 cph) at different places in Arabian Sea (Murthy, 2002). Antony et al. (1985) studied the subsurface temperature oscillations using time series data at 4 levels collected from current metres, suspended from a ship anchored at 25 m depth in the western Bay of Bengal off the mouth of Krishna River on 30 June 1982. They inferred the presence of internal waves propagating with a speed of about 13.3 cm/s and wave lengths between 0.8 and 1.3 km, generated as a result of flood current passing over a submarine obstacle in the presence of stratification. Charyulu et al. (1994) studied temperature oscillations in the upper thermocline region by thermister chain measurements from a stationary ship off Kalpeni Island in southern Arabian Sea in January 1989 and found that the internal waves of periods longer than 10 min had higher coherence below 88 m depth. LaFond and LaFond (1968) reported the presence of internal waves off Hooghly – Brahmaputra delta and in the eastern Andaman Sea during April 1963 from observations made from RV Anton Bruun. Internal waves of large amplitudes with a maximum height of 82 m were observed north of Sumatra by US research vessel Pioneer in June 1964 (Perry and Schimke, 1965).

In fair weather, high frequency internal waves manifest as slicks at the sea surface. The rough and smooth bands of slicks are separated by 300 to 500 m. The crest occurs below the rough band and troughs occur below the smooth band. Similar slicks were captured from satellite imageries off Goa (Spot, Landsat and ERS-SAR). Thus by monitoring slicks, the wave length, speed, direction and frequency of internal waves can be estimated (Murthy, 2002).

Apollo-Soyuz and Landsat photographs have shown the locations of internal wave packets in the Andaman Sea. Internal solitons with amplitudes up to 105 m have been observed in the southern Andaman Sea near the west coast of Thailand. These waves propagate beneath the free surface in density-stratified waters ranging from a few hundred metres to three kilometres in depth. The waves are generated by tidal interactions with bathymetric features near island chains to the west and southwest of the observed site. The solitons occur in packets of six to eight waves and propagate several hundred kilometres before encountering the coastline of Thailand. The leading wave in a packet has a typical crest length of 150 km. Bands of surface waves, called 'rips' accompany the internal waves. The bands are 600-1200 m wide, stretch tens to hundreds of kilometres across the sea surface and are seen easily in satellite photographs (Osborne and Burch, 1980). SIR-A imagery (of 14 November 1981) also has shown the presence of internal waves in the Andaman Sea.

Zheng et al. (1995) analysed and interpreted the visible images of deep ocean internal waves in the western equatorial Indian Ocean taken by a space shuttle Atlantis during mission STS 44 in 1991. They found internal waves in the form of a multisoliton packet in which there are about a dozen solitons. The average wave length of the soliton is  $1.8 \pm 0.5$  km ranging from 1.1- 2.6 km. The crest lines are mostly straight and reach as long as 100 km. The distance between two adjacent packets is about 66 km. The mean amplitude of the solution is 25 m, the nonlinear phase speed is 1.7 m/s and the average period is 18 min. The internal semidiurnal tides are the principal generating mechanism.

## 6. CONCLUDING REMARKS

Upper ocean physical processes in the TIO are unique and an understanding of their variability in different time and space scales is essential for predicting monsoon/climate variability and biological productivity. Surface heat fluxes, surface layer characteristics, circulation and currents, thermohaline structure, upwelling and internal waves are the most important features/processes to be understood.

During boreal winter, under the influence of dry and cold northeasterly winds the net surface heat flux cools the northern Indian Ocean, in greater measure in the northwestern Arabian Sea and northwestern Bay of Bengal. During summer monsoon season the net surface heat flux produces a dramatic cooling over the entire TIO with an exception of a band off Arabia where SST is cooler because of coastal upwelling. The cooling of the Arabian Sea during summer is mainly caused by the surface heat exchange processes and lateral and vertical advection. A combination of enhanced evaporation and the reduction in solar radiation (from October to January) results in significant decrease of SST and presence of cold surface waters ( $25^{\circ}\text{C}$ ) in the northern Arabian Sea during winter (January-February).

Mixed layer depth is highest ( $> 90\text{ m}$ ) in the central Arabian Sea during the peak summer monsoon (July-August) due to strong wind driven vertical mixing. It is lowest ( $< 20\text{ m}$ ) in the Bay of Bengal and Arabian Sea during northern spring (April).

The surface area covered by the Warm Pool ( $\text{SST} = 28^{\circ}\text{C}$ ) in the TIO is maximum during April and minimum during September. The Warm Pool persists in the Bay of Bengal from March through October. The maximum thickness of Warm Pool is about  $100\text{ m}$  during May-June. In the Arabian Sea, a mini Warm Pool develops off the west coast of India in the Lakshadweep Sea in March and by the end of May, the SST high becomes the core of the Warm Pool over the Arabian Sea and there by the warmest spot of the region. It helps in producing conditions favourable for the genesis of monsoon onset vortex.

A Barrier Layer (the layer between the halocline and the thermocline, which affects mixed layer heat budget) is present in the Bay of Bengal through most of the year due to advection of low salinity water diluted from monsoon river run off. A  $20\text{ m}$  thick BL is found in the southeastern Arabian Sea during March-April owing to a surface layer of low salinity water advected earlier during December-January from the Bay of Bengal.

Surface layer temperature inversion occurs in the southeastern Arabian Sea during winter. This is caused by surface advection of cold less saline Bay of Bengal water over the warm saline Arabian Sea water along the west coast of India. Spatially organized temperature inversion occurs in the coastal waters of the western and northeastern Bay during winter (November-January) adjacent to major fresh water inputs (from the Ganges, Brahmaputra, Irrawadi, Krishna and Godavari rivers).

The circulation in the southern Arabian Sea during winter is influenced by formation and propagation of mesoscale eddies. An anti-cyclonic eddy (Lakshadweep High, LH) is present in the southeastern Arabian Sea during early winter and a cyclonic eddy (Lakshadweep Low, LL) during early summer. The formation of LH and LL appear to be a consequence of westward propagating Rossby waves radiated by Kelvin waves propagating along the western margin of the Indian subcontinent. A large anti-cyclonic eddy, Southern Arabian Sea High (SAH) forms west of LH in the southern Arabian Sea during the northeast monsoon.

Somali current is one of the fastest currents found in the open ocean with surface velocities as high as  $3.5\text{ m/s}$  during July-August. It varies significantly with time. The EUC system in the TIO

exhibits pronounced seasonal variations forced by monsoon winds. The WICC flows poleward during November-March and equatorward during April-September. The EICC flows poleward during February-April and equatorward during November-December. During the southwest monsoon, a weak poleward flow develops in the south and an equatorward flow develops in the north. The coastal circulation off the east coast of India is influenced by the remote forcing of winds over the equatorial Indian Ocean and the interior Ekman pumping besides along shore wind stress and river run off.

Strong upwelling occurs over a large area along the Somalia and Arabia coasts during summer monsoon resulting in cold surface waters (SST < 14° C off Somalia and about 18° C off Arabia). The upwelling off Somalia is due to strong offshore Ekman transport in association with strong boundary current (Somali Current) and a complex two gyre system. The southwest monsoon wind field causes upwelling along the Arabian coast as well as the Oman coast. Off the southwest coast of India the prevailing current system is mainly responsible for upwelling (during June-August) aided by divergence and advection from wind field, besides the coastal configuration. In the Arabian Sea, under the influence of Findlater Jet, the axis of which is located around 17° N, the open ocean upwelling occurs towards the north. Along most of the western boundary of Bay of Bengal, upwelling forced by local winds occurs during southwest monsoon in about 40 km wide band. Off Waltair the width of this upwelling band increases from March-May. During the northeast monsoon a cyclonic gyre develops in the southwestern Bay of Bengal and the upwelling within this gyre due to Ekman pumping cools the sea surface. Upwelling occurs off the Burmese coast and off the west coast of Thailand due to northeast monsoon winds. Off the east coast of Sri Lanka upwelling occurs during May-July due to upward Ekman pumping induced by a strong cyclonic curl in the wind stress. During June-September southeasterly winds (from Australia) generate upwelling along the Java-Sumatra coast

Our knowledge of the upwelling phenomenon especially its mechanism, intensity, temporal and spatial variability off the west coast of India and off the east coast of India is limited, and needs to be studied through an integrated programme involving insitu measurements from ships and data buoys, remote sensing observations and modeling. Data on water transparency are sparse, and that on Chlorophyll-a and primary productivity are inadequate in the TIO for studying their seasonal variation. There were very few studies on internal waves in this region and specially designed programmes are necessary to understand their mechanism and role in the upper ocean dynamics. The equatorial current system in the TIO is quite complex and a comprehensive long term observation programme is necessary for improving our knowledge. Monitoring of upper ocean thermal structure through XBT network needs to be augmented to include salinity through using XCTDs for a better knowledge of the variability of upper ocean thermohaline structure. It is hoped that recent advances in satellite oceanography and availability of satellites with dedicated sensors for ocean parameters and two major long term programmes, namely Indian Climate Research Programme (ICRP)/ CLIVAR supported by DST and Ocean Observing System (OOS)/ Indian Ocean GOOS supported by DOD would contribute significantly for improving our knowledge on upper ocean physical processes in the TIO.

## REFERENCES

- Ali, M.M, Simon, B and Desai, P.S (1987): Inference of vertical motion in the equatorial Indian Ocean using satellite data, Proceedings International Symposium on Equatorial Vertical Motion, 6-10 May 1985, Paris, *Ocean. Acta*, pp. 71-75.
- Anderson D L T and Moore D W (1979): Cross-equatorial inertial jets with special relevance to very remote forcing of the Somali Current, *Deep-Sea Res.* Vol. 26, pp. 1-22.
- Anonymous (1953): *Bay of Bengal Pilot*, 8<sup>th</sup> edition (Dept. of Admiralty, London).
- Antony, M.K, Murthy, C.S., Reddy, G.V. and Rao, K.H. (1985): Sub-surface temperature oscillations and associated flow in the western Bay of Bengal, *Est. Coast. Shelf Sci.*, Vol. 21, pp. 823-834.
- Babu, M.T (1992): Equatorward western boundary current in the Bay of Bengal during November-December 1983, In: Physical Processes in the Indian Seas. (*Proceedings of the First Convention of the Indian Society of the Physical Sciences of the Ocean*), (Eds.) G.N. Swamy, M.K. Antony and V.Kesava Sas, Published by ISPSO, Goa, pp. 57-62.
- Babu, M.T, Prasanna Kumar, S and Rao, D.P (1991): A subsurface cyclonic eddy in the Bay of Bengal, *J Mar. Res.* Vol. 49, pp. 403-410.
- Banse, K (1959): On upwelling and bottom-trawling off the southwest coast of India, *J Marine Biol. Ass. India*, 1, pp. 33-49.
- Basil Mathew, Hareesh Kumar, P.V and Rao, R.R (2003): Mixed layer variability at selected locations in the Arabian Sea during pre and summer monsoon seasons: Observations and simulations, *Mausam*, Vol. 54, No. 4, pp. 917-928.
- Bauer, S, Hitchcock, G.L and Olson, D.B (1991): Influence of monsoonally-forced Ekman dynamics upon surface layer depth and plankton biomass distribution in the Arabian Sea, *Deep-Sea Res.* Vol. 38, pp. 531-553.
- Bauer, S, Hitchcock, G.L and Olson, D.B (1992): Response of the Arabian Sea surface layer to monsoon forcing. In: *Oceanography of the Indian Ocean* (ED) B.N. Desai (Oxford & IBH Publishing Col., New Delhi) pp. 659-672.
- Bhattathiri, P.M.A, Aditi Pant, Surekha, S, Gauns, M, Matondkar, S.G.P and Mohanraju, R (1996): Phytoplankton production and chlorophyll distribution in the eastern and central Arabian Sea in 1994-1995, *Curr. Sci.*, Special Section: JGOFS (India), Vol. 71, pp. 857-862.
- Brainerd, K.E and Gregg, M.C (1995): Surface mixed and mixing layer depths, *Deep-Sea Res.* Vol. 42A, pp. 1521-1543.
- Brennecke, W (1921): Die ozeanographischen Arbeiten der Deutschen Antarktischen Expedition 1911-1912 ("Deutschland"), *Aus dem Archiv der Deutschen Seewarte*, Vol. 39, pp. 87-101.
- Brink, K, Arnone, R, Coble, P, Flagg, C, Jones, B, Kindle, J, Lee, C, Phinney, D, Wood, M, Yentsch, C, and Young, D (1998): Monsoons boost biological productivity in Arabian Sea, EOS, Transactions, *Amer. Geophys. Unio.*, Vol. 27, pp. 168-169.
- Brock, J.C and McClain, C.R and Hay, W.W (1992): A southwest monsoon hydrographic climatology for the northwestern Arabian Sea, *J Geophys. Res.* Vol. 97, pp. 9455-9465.
- Bruce, J.G (1973): The equatorial undercurrent in the western Indian Ocean during the southwest monsoon, *J Geophys. Res.* Vol. 32, pp. 419-423.
- Bruce, J.G, Johnson, D.R and Kindle, J.C (1994): Evidence for eddy formation in the eastern Arabian Sea during the northeast monsoon, *J Geophys. Res.* Vol. 99, No. C4, pp. 7651-7664.
- Charyulu, R.J.K, Sarma, Y.V.B, Sarma, M.S.S and Rao, L.V.G (1994): Temperature oscillations in the upper thermocline region – A case study on internal waves off Kalpeni island in the southern Arabian Sea, *Ind. J Mar. Sci.* Vol. 23, pp. 14-17.
- Clarke, A.J and Liu, X (1993): Observations and dynamics of semiannual and annual sea levels near the eastern equatorial Indian Ocean boundary, *J Phys. Oceanogr.*, Vol. 23, pp. 386-399.
- Cutler, A.N and Swallow, J.C (1984): Surface currents of the Indian Ocean, Inst. Oceanogr. Sci., Wermley, U.K, Rep. No. 187, 42 p.
- Darbyshire, M (1967): The surface waters off the coast of Kerala, south-west India, *Deep-Sea Res.* Vol. 14, pp. 295-320.

- Defant, A (1961): Physical Oceanography, Vol. 1, Pergamon Press.
- De Souza, S.N, Dileep Kumar, M, Sardesai, S, Sarma, V.V.S.S and Shirodkar, P.V (1996): Seasonal variability in oxygen and nutrients in the central and eastern Arabian Sea, *Curr. Sci.* Vol. 70, pp. 847-851.
- Dietrich, G (1973): The unique situation in the environment of the Indian Ocean, in: *The Biology of the Indian Ocean*, B. Zeitzschel, ed., Springer-Verlag, New York, pp. 1-6.
- Duing, W (1970): The monsoon regime of the currents in the Indian Ocean. East-West Centre Press, Honolulu, 66 p.
- Duing, W and Leetma, A (1980): Arabian Sea cooling: A preliminary heat budget, *J Phys. Oceanogr.*, Vol. 10, pp. 307-312.
- Elliott, A.J and Savidge, G (1990): Some features of the upwelling off Oman, *J Mar. Res.* Vol. 48, pp. 319-333.
- Emery, W.J and Meincke, J (1986): Global water masses: summary and review, *Ocean. Acta*, Vol. 9, No. 4, pp. 383-391.
- Fischer, A.S, Weller, R.A, Rudnick, D.L, Eriksen, C.C, Lee, C.M, Brink, K.H, Fox, C.A, Leben, R.R (2002): Mesoscale eddies, coastal upwelling, and the upper-ocean heat budget in the Arabian Sea, *Deep-Sea Res. II*, Vol. 49, pp. 2231-2264.
- Gadgil, S, Joseph, P.V and Joshi, N.V (1984): Ocean-atmosphere coupling over monsoon regions, *Nature*, Vol. 31, pp. 141-143.
- Gallagher, J.F (1966): The variability of water masses in the Indian Ocean, Washington, DC: National Oceanographic Data Centre.
- Gardner, W.D, Gundersen, J.S, Richardson, M.J and Walsh, I.D (1999): The role of seasonal and diel changes in the mixed-layer depth on carbon and chlorophyll distribution in the Arabian Sea, *Deep-Sea Res II*, Vol. 46, pp. 1833-1858.
- Gnanaseelan, G, Mishra, A.K, Thompson, B and Salvekar, P.S (2003): Thermodynamics and dynamics of the upper ocean mixed layer in the central and eastern Arabian Sea, Research Report No. RR-098, ISSN 0252-1075, Indian Institute of Tropical Meteorology, Pune, India, 44 p.
- Gopala Krishna, V.V and Sastry, J.S (1985): Surface circulation over the shelf off the east coast of India during the southwest monsoon, *Ind. J Mar. Sci.* Vol. 14, pp. 62-65.
- Halpern, D, Freilich, M.H and Weller, R.A (1998): Arabian Sea surface winds and ocean transports determined from ERS-1 Scatterometer, *J Geophys. Res.* Vol. 103, pp. 7799-7805.
- Halpern, D and Woiceshyn, P.M (1999): Onset of the Somali Jet in the Arabian Sea during June 1997, *J Geophys. Res.* Vol. 104, pp. 18041-18046.
- Hareesh Kumar, P.V and Basil Mathew (1997): Salinity distribution in the Arabian Sea, *Ind. J Mar. Sci.* Vol. 26, pp 271-277.
- Hastenrath, S and Lamb, P.J (1979): *Climatic Atlas of the Indian Ocean* (University of Wisconsin Press, Madison, Wisconsin), 97 p.
- Hidaka, K (1958): Computation of the wind stresses over the oceans, *Rec. Oceanogr. Wks. Japan*, Vol. 4, pp. 77-123.
- Hitchcock, G.L, Key, E. L and Masters, J (2000): The fate of upwelled waters in the Great Whirl, August 1995, *Deep-Sea Res. II*, 47, pp. 1605-1621.
- Johannessen, O.M, Subbaraju, G and Blindheim, J (1987): Seasonal variations of the oceanographic conditions off the southwest coast of India during 1971-1975, *Fisk. Dir. Skr. Ser. Hav Unders.*, Vol. 18, pp. 247-261.
- Johns, B, Rao, A.D and Rao, G.S (1992): On the occurrence of upwelling along the east coast of India, *Est. Coast. Shelf Sci.*, Vol. 35, pp. 75-90.
- Joseph, M.G, Hareesh Kumar, P.V and Madhusoodanan, P (1996): Upper ocean responses in the central western equatorial Indian Ocean during southwest monsoon season, *Mausam*, Vol. 47, No. 1, pp. 21-30.
- Joseph, P.V (1990): Warm Pool over the Indian Ocean and Monsoon Onset, TOGA newsletter, No. 53, pp. 1-5
- Josey, S.A, Kent, E.C, Oakley, D and Taylor, P.K. (1996): The SOC air-sea flux climatology: A new global air-sea heat and momentum flux climatology.

- Kalnay, E, Kanamitsu, M, Kistler, R, Collins, W, Deaven, D, Gandin, L, Iredell, M, Saha, S, White, G, Woollen, J, Zhu, Y, Chelliah, M, Ebisuzaki, W, Higgins, W, Janowiak, J, Mo, K. C, Ropelewski, C, Wang, J, Leetmaa, A, Reynolds, R, Roy Jenne and Dennis Joseph (1996): The NMC/NCAR 40-Year Reanalysis Project. *Bull. Amer. Meteor. Soc.*, Vol. 77, pp. 437-471.
- Knox, R.A (1974): Reconnaissance of the Indian Ocean Equatorial Undercurrent near Addu Atoll, *Deep-Sea Res.* Vol. 21, pp. 123-129.
- LaFond, E.C (1954): On upwelling and sinking off the East Coast of India, *Andhra Univ. Memoirs in Oceanography.*, Vol. 1, pp. 117-121.
- LaFond, E.C (1955): On upwelling and fisheries, *Curr. Sci.*, Vol. 24, pp. 258-259.
- LaFond, E.C (1958): On the circulation of the surface layers on the east coast of India, *Andhra Univ. Memoirs in Oceanography*, Vol. 2, pp. 1-11.
- LaFond, E.C and LaFond, K.G (1968): Studies of oceanic circulation in the Bay of Bengal, *Bull. Natl. Inst. Sci. India*, Vol. 38, pp. 164-183.
- LaFond, E.C and Lee, O.S (1962): Internal waves in the Ocean, *Navigation*, Vol. 9, No. 3, pp. 231-236.
- LaFond, K.G and Rao, C.P (1954): Vertical oscillations of tidal periods in the temperature structure of the sea, *Andhra Univ. Memoirs*, Vol. 1, pp. 109-116.
- Luis, A.J and H. Kawamura (2002): Mechanism for sea surface cooling in the Gulf of Oman during winter, *Geophys. Res. Lett.*, Vol. 29, No. 11, 10.1029/2001GL014148.
- Luis, A.J and Kawamura, H (2003): Seasonal SST patterns along the West India shelf inferred from AVHRR, *Rem. Sen. Environ.*, Vol. 86, pp. 206-215.
- Luis, A.J and Kawamura, H (2004): Air-Sea interaction, coastal circulation and primary production in the eastern Arabian Sea: A review, *J Oceanogr.*, Vol. 60, pp. 205-218.
- Luyten, J.R (1981): Recent observations in equatorial Indian Ocean, in: *Monsoon dynamics*, edited by J. Lighthill and R. Pearce, (Cambridge Univ. Press), pp. 465-480.
- Madhupratap, M and Parulekar, A.H (1993): Biological processes of the Northern Indian Ocean, In: *Monsoon Biogeochemistry*, Ed. V. Ittekkot and R.R. Nair, Mitt. Geol.-Palaont. Inst. Univ. Hamburg.
- Madhupratap, M, Prasanna Kumar, S, Bhattathiri, P.M.A, Dileep Kumar, M, Raghukumar, S, Nari, K.K.C and Ramaiah, N (1996): Mechanism of the biological response to winter cooling in the northeastern Arabian Sea, *Natur*, Vol. 384, pp. 549-552.
- Maslennikov, V.V (1973): Oceanographic investigations in the Andaman Sea and the northern part of the Bay of Bengal, In: *Soviet fisheries investigations in the Indian Ocean*, edited by A.S. Bogdanov, (Programme for Scientific Translation (English Translation), Jerusalem, Israel, pp. 42-51.
- McCreary Jr J P, Kundu P, and Molinari R L (1993): A numerical investigation of dynamics, thermodynamics, and mixed-layer processes in the Indian Ocean, *Progr. Oceanogr.*, Vol. 31, pp. 181-244.
- Miyama, T, McCreary, Jr.J.P, Jensen, T.G, Loschinger, J, Godfrey, S and Ishida, A (2003): Structure and dynamics of the Indian-Ocean cross-equatorial cell, *Deep-Sea Res. II*, Vol. 50, pp. 2023-2047.
- Molinari, R.L., Olson, D and Reverdin, G (1990): Surface circulation distributions in the tropical Indian Ocean derived from compilations of surface buoys trajectories, *J Geophys. Res.* Vol. 95, pp. 7217-7238.
- Morrison, J.M and D.B. Olson (1992): Seasonal basin wide extremes in T-S characteristics in the near surface waters of the Arabian Sea and Somali basin. In: *Oceanography of the Indian Ocean* (Ed.) B.N. Desai, Oxford & IBH Publication, New Delhi, pp 605-616.
- Muraleedharan, P.M and Prasanna Kumar, S (1996): Arabian Sea upwelling: A comparison between coastal and open ocean regimes, *Curr. Sci.*, Vol. 70, pp. 842-846.
- Muraleedharan, P.M, Ramesh Kumar, M.R and Rao, L.V.G (1995): A note on poleward undercurrent along the southwest coast of India, *Cont. Shelf Res.* Vol. 15, pp. 165-184.
- Murty, C.S and Murty, V.S.N (2001): Physical Oceanography, In: *The Indian Ocean A Perspective*, Vol. 1 (Ed. R. Sen Gupta and E. Desa), Vol. 1, pp 1-54.
- Murthy, P.G.K (2002): An insight into internal waves in the seas around India, *Proceedings of ICONS 2002, International Conference on Sonar – Sensors and Systems*, pp. 525-532.
- Murty, V.S.N, Sarma, Y.V.B, Rao D.P and Murty, C.S (1992<sub>a</sub>): Water characteristics, mixing and circulation in the Bay of Bengal during southwest monsoon, *J Mar. Res.* Vol. 50, pp 207-228.

- Murty, V.S.N, Sarma, Y.V.B, Babu, M.T and Rao, D.P (1992<sub>b</sub>): Hydrography and circulation in the northwestern Bay of Bengal during the retreat of southwest monsoon, *Proc. Ind. Acad. Sci. (Earth and Planetary Sciences)*, Vol. 101, pp. 67-75.
- Murty, V.S.N, Sarma, M.S.S, Lambata, B.P, Gopala Krishna, V.V, Pednekar, S.M, Suryachandra Rao, A, Luis, A.J, Kaka, A.R and Rao, L.V.G (2000): Seasonal variability of upper-layer geostrophic transport in the tropical Indian Ocean during 1992-1996 along TOGA-I XBT tracklines, *Deep-Sea Res.-I*, Vol. 47, pp. 1569-1582.
- Murty, V.S.N, Sarma, Y.V.B and Rao, D.P (1996): Variability of the oceanic boundary layer characteristics in the northern Bay of Bengal during MONTBLEX-90, *Earth Planet Sci.* Vol. 105, pp. 41-61.
- Murty, V.S.N, Subrahmanyam, B, Rao, L.V.G and Reddy, G.V (1998): Seasonal variation of sea surface temperature in the Bay of Bengal during 1992 as derived from NOAA-AVHRR SST data, *Int. J. Rem. Sen.* Vol. 19, No. 12, pp. 2361-2372.
- Murty C S, and Varadachari, V.V.R (1968): Upwelling along the east coast of India, *Bull. Nat. Inst. Sci. India*, Vol. 36, pp. 80-86.
- Namita, A.J and Rao, L.V.G and Panigrahi, R.C (2000): Pigment patterns in the Arabian Sea: Spatio-temporal variability as observed by ADEOS, *PORSEC Proceedings*, Vol. 1, pp. 50-54.
- O'Brien, J.J and Hurlburt, H.E (1974): Equatorial jet in the Indian Ocean: theory, *Science*, Vol. 184, pp. 1075-1077.
- Osborne, A.R and Burch, T.L (1980): Internal solitons in the Andaman Sea, *Science*, Vol. 208, pp. 451-460.
- Pankajakshan, T and Gosh, A.K (1992): Surface layer temperature inversion in the Arabian Sea during winter, *J Ocean.* Vol. 48, pp. 293-304.
- Pankajakshan, T, Gopala Krishna, V.V, Murleedharan, P.M, Reddy, G.V, Araligidat, N, Shenoy, S (2002): Surface layer temperature inversion in the Bay of Bengal, *Deep-Sea Res.I*, Vol. 49, pp. 1801-1818.
- Perry, R.B and Schimke, G.R (1965): Large-amplitude internal waves observed off the northwest coast of Sumatra, *J Geophys. Res.* Vol. 70, No. 10, pp. 2319-2324.
- Prasad, T.G and Bahulayan, N (1996): Mixed layer depth and thermocline climatology of the Arabian Sea and western equatorial Indian Ocean, *Ind. J Mar. Sci.* Vol. 25, pp. 182-194.
- Prasad, T.G and Ikeda, M (2001): Spring evolution of Arabian Sea High in the Indian Ocean, *J Geophys. Res.* Vol. 106, No. C11, pp. 31085-31098.
- Prasanna Kumar, S, Madhupratap, M, Dileepkumar, M, Muraleedharan, P.M, de Souza, S.N, Mangesh Gauns and Sarma, V.V.S.S (2001): High biological productivity in the central Arabian Sea during the summer monsoon driven by Ekman pumping and lateral advection, *Curr. Sci.* Vol. 81, pp. 1633-1638.
- Prasanna Kumar, S, Madhupratap, M, Dileepkumar, M, Gauns, M, Muraleedharan, P.M, Sarma, V.V.S.S and De Souza, S.N (2000): Physical control of primary productivity on a seasonal scale in central and eastern Arabian Sea, *Proc. Ind. Acad. Sci. (Earth Planet. Sci.)*, Vol. 109, pp. 433-441.
- Prasanna Kumar, S and Prasad, T.G (1996): Winter cooling in the northern Arabian Sea, *Curr. Sci.* Vol. 71, No. 11, Special Section: JGOFS (India), pp. 834-841.
- Prasanna Kumar, S and Prasad, T.G (1999): Formation and spreading of Arabian Sea high-salinity water mass, *J Geophys. Res.* Vol. 104, No. C1, pp. 1455-1464.
- Qasim, S.Z (1977): Biological Productivity of the Indian Ocean, *Ind. J Mar. Sci.* Vol. 6, pp. 122-137.
- Qasim, S.Z (1978): Distribution of Chlorophyll a in the Indian Ocean, *Ind. J Mar. Sci.* Vol. 7, pp. 258-262.
- Radhakrishna, K.G, Basil Mathew, Hareesh Kumar, P.V and Mohan Kumar, N (1997): Thermocline climatology of the Arabian Sea – a review, *Mar. Freshwater Res.* Vol. 48, pp. 465-472.
- Rama Sastry, A.A and Myrland, P (1959): Distribution of Temperature, Salinity and Density in the Arabian Sea along the south Malabar coast (South India) during the post-monsoon season, *Ind. J. Fish.* Vol. 6, pp. 223-255.
- Ragu, G.M, Sergio, S.R, Signorini, R, Christian, J.R, Busalacchi, A.J, McClain, C.R and Picaut, J (1999): Ocean color variability of the tropical Indo-Pacific basin observed by SeaWiFS during 1997-1998, *J Geophys. Res.* Vol. 104, pp. 18351-18366.
- Rama Sastry, A.A (1961): Exploration of the Indian Ocean-Physical Oceanography, *Indian J. Meteorol. Geophys.* Vol. 12, No. 2, pp. 182-188.

- Ramesh Babu, V, Rao, L.V.G, Varkey, M.J and Udaya Varma, P (1976): Temperature distribution in the upper layers of the northern and eastern Arabian Sea during Indo-Soviet monsoon experiment, *Indian J Met. Hydrol. Geophys.*, Vol. 27, No. 3, pp. 291-293.
- Ramesh Babu, V and Sastry, J.S (1976): Hydrography of the Andaman Sea during late winter, *Ind J Mar. Sci.*, Vol. 5, pp. 179-189.
- Ramesh Babu, V, Suryanarayana, A and Murty, V.S.N (2001): Thermohaline circulation in the central Indian basin (CIB) during austral summer and winter periods of 1997, *Deep-Sea Res. II*, Vol. 48, pp. 3327-3342.
- Rao, T.S.S (1957): Studies on the penetration of light in the Bay of Bengal, Part 1. Transparency of the waters on the east coast of Indian and its significance, *Proc. Nat. Inst. Sci. India*, 23B, 165-170.
- Rao, T.V.N (2002): Spatial distribution of upwelling off the central east coast of India, *Est. Coast. Shelf Sci.* Vol. 54, pp. 141-156.
- Rao, T.V.N and Rao, B.P (1989): Alongshore velocity field off Visakhapatnam, east coast of India during pre-monsoon season; *Ind. J Mar. Sci.* Vol. 18, pp. 46-49.
- Rao, T.V.N, Rao, B.P, Rao, V.S and Sadhuram, Y (1995): Variability of the flow field in the inner shelf along the central east coast of India during April, 1989, *Cont. Shelf Res.* Vol. 15, pp. 241-253.
- Rao, T.V.N, Rao, D.P, Rao, B.P and Raju, V.S.R (1986): Upwelling and sinking along Visakhapatnam coast, *Ind. J Mar. Sci.* Vol. 15, pp. 84-87.
- Rao, L.V.G and Jayaraman, R (1966): Upwelling in the Minicoy region of the Arabian Sea, *Curr. Sci.* Vol. 35, pp. 378-380.
- Rao, L.V.G and Jayaraman, R (1968<sub>a</sub>): Vertical distribution of temperature, salinity and density in the upper 500 metres of the north equatorial Indian Ocean during the northeast monsoon period, *Bul. Nat. Inst. of Sci. of India*, No. 38, pp. 123-148.
- Rao, L.V.G and Jayaraman, R (1968<sub>b</sub>): Hydrographical features of the southern and central Bay of Bengal during the transition period between winter and summer, *Bul. Nat. Inst. of Sci. of India*, No. 38, pp. 184-205.
- Rao, R.R, Molinari, R.L and Festa, J.F (1989): Evolution of the climatological near-surface thermal structure of the tropical Indian Ocean. 1. Description of mean monthly mixed-layer depth, and sea surface temperature, surface current, and surface meteorological fields, *J Geophys. Res.* Vol. 94, pp. 10801-10815.
- Rao, D.P and Murty, V.S.N (1992): Circulation and geostrophic transport in the Bay of Bengal, Physical processes in the Indian Seas (*Proc. First Convention, ISPSO, 1990*), pp. 79-85.
- Rao, R.R, Basil Mathew and Hareesh Kumar, P.V (1993<sub>a</sub>): A summary of results on thermohaline variability in the upper layers of the east central Arabian Sea and Bay of Bengal during summer monsoon experiments, *Deep-Sea Res. I*, Vol. 40, No. 8, pp. 1647-1672.
- Rao, A.D, Sinha, P.C, Dube, S.K and Charmorathi, S (1993<sub>b</sub>): Numerical simulation of upwelling off Visakhapatnam on east coast of India during pre-monsoon months, *Proc. Ind. Acad. Sci. (Earth Planet. Sci.)*, Vol. 102, pp. 465-486.
- Rao, R.R and Sivakumar, R (1999): On the possible mechanisms of the evolution of a mini-warm pool during the presummer monsoon season and the genesis of onset vortex in the southeastern Arabian Sea, *Q J R Meteorol. Soc.* Vol. 125, pp. 787-809.
- Rao, R.R and Sivakumar, R (2000): Seasonal variability of near-surface thermal structure and heat budget of the mixed layer of the tropical Indian Ocean from a new global ocean temperature climatology, *J Geophys. Res.* Vol. 105, No. C1, pp. 995-1015.
- Reddy, M.P.M (2001): Descriptive Physical Oceanography, Oxford & IBH Publishing Co. Pvt. Ltd., New Delhi, 440 p.
- Reynolds, R.W, Rayner, N.A, Smith, T.M, Stokes, D.C and Want, W (2002): An improved insitu and satellite SST Analysis for climate, *J Clim.* Vol. 15, pp. 1609-1625.
- Rixen, T, Haake, B and Ittekkot, V (2000): Sedimentation in the western Arabian Sea the role of coastal and open-ocean upwelling, *Deep-Sea Res. II*, Vol. 47, pp. 2155-2178.
- Rochford, D.J (1964): Salinity maxima in the upper 1000 metres of the north Indian Ocean, *Austr. J Mar. Freshw. Res.* Vol. 15, pp. 1-24.

- Sanilkumar, K.V, Kuruvilla, T.V, Jogendranath, D and Rao, R.R (1997): Observation of the western boundary current of the Bay of Bengal from a hydrographic survey during March 1993, *Deep-Sea Res.I* Vol. 44, pp. 135-145.
- Sanilkumar, K.V, Hareesh Kumar, P.V, Joseph, J and Panigrahi, J.K (2004<sub>a</sub>): Arabian Sea mini warm pool during May 2000, *Curr. Sci.*, Vol. 86, No. 1, pp. 180-184.
- Sanilkumar K V, Unni, V.K and James, V.V (2004<sub>b</sub>): Upwelling characteristics off the southwest coast of India during 2003, METOC – 2004, *Proceedings of National Symposium on Emerging Trends in the fields of Meteorology & Oceanography*, 5 – 6 Feb. Kochi, pp. 137-143.
- Sarma, Y.V.B, Rama Rao, E.P, Saji, P.K and Sarma, V.V.S.S (1999): Hydrography and Circulation of the Bay of Bengal during withdrawal phase of the southwest Monsoon, *Ocean. Acta*, Vol. 22, No. 5, pp. 453-471.
- Sarma, Y.V.B, Sarma, M.S.S and Rao, L.V.G (1993): Thermal structure of the western Indian Ocean during the southwest monsoon, 1983, *Ocean. Acta*, Vol. 16, No. 1, pp 45-52.
- Sarupriya, J.S and Bhargava, R.M.S (1998): Seasonal distribution of Chlorophyll-a in the exclusive economic zone (EEZ) of India, *Ind. J Mar. Sci.* Vol. 27, pp. 292-297.
- Sastry, J.S and D'souza, R.S (1972): Upwelling and upward mixing in the Arabian Sea, *Ind. J Mar. Sci.*, Vol. 1, pp. 17-27.
- Sastry, J.S and Ramesh Babu, V (1985): Summer cooling of the Arabian Sea – a review, *Proc. Indian Acad. Sci. (Earth Planet. Sci.)*, Vol. 94, No. 2, pp. 117-128.
- Sastry, J.S, Rao, D.P, Murty, V.S.N, Sarma, Y.V.B, Suryanarayana, A. and Babu, M.T (1985): Watermass structure in the Bay of Bengal, *Mahasagar – Bull. Nat. Inst. of Oceanography*, Vol. 18, pp. 153-162.
- Schott, F (1983): Monsoon response of the Somali current and associated upwelling, *J Phys. Oceanogr.*, Vol. 12, pp. 357-382.
- Schott, F and McCreary, J.P (2001): The monsoon circulation of the Indian Ocean, *Progr. Oceanogr.*, Vol. 51, pp. 1-123
- Schott, F and Quadfasel, D.R (1982): Variability of the Somali Current system during the onset of the southwest monsoon of 1979, *J Phys. Oceanogr.*, Vol. 12, pp. 1343-1357.
- Sharma, G.S (1966): Thermocline as an indicator of upwelling, *J Mar. Biol. Ass. India*, VIII, pp. 8-19.
- Sharma, G.S (1978): Upwelling off the southwest coast of India, *Indian J Mar. Sci.*, Vol. 7, pp. 209-218.
- Shankar, D, Gopalakrishna, V.V, Shenoi, S.S.C, Durand, F, Shetye, S.R, Rajan, C.K, Johnson, Z, Aralingidad, N and Michael, G.S (2004): Observational evidence for westward propagation of temperature inversion in the southeastern Arabian Sea, *Geophys. Res. Lett.* Vol. 31, L08305.
- Shankar, D and Shetye, S.R (1997): On the dynamics of the Lakshadweep high and low in the southeastern Arabian Sea, *J Geophys. Res.* Vol. 102, No. C6, pp. 12,551-12,562,
- Shenoi, S.S.C, Saji, P.K and Almeida, A.M (1999<sub>a</sub>): Near-surface circulation and kinetic energy in the tropical Indian Ocean derived from Lagrangian drifters, *J Mar. Res.* Vol. 57, pp. 885-907.
- Shenoi, S.S.C, Shankar, D and Shetye, S.R (1999<sub>b</sub>): On the sea surface temperature high in the Lakshadweep Sea before the onset of the southwest monsoon, *J Geophys. Res.* Vol. 104, No. C7, pp. 15,703-15,712.
- Shenoi, S.S.C, Shankar, D and Shetye, S.R (2004): Remote forcing annihilates barrier layer in southeastern Arabian Sea, *Geophys. Res. Lett.*, Vol. 31, L05307, doi:10.1029/2003GL019270, 2004.
- Shenoi, S.S.C, Shetye, S.R, Gouveia, A.D and Michael, G.S (1993): Salinity Extrema in the Arabian Sea, In: *Monsoon Biogeochemistry* (Ed. Ittekkot and Nair) pp. 37-49.
- Shenoi, S.S.C, Gouveia, A.D, Shetye, S.R and Rao, L.V.G (1992): Satellite observations of the northeast monsoon coastal current, Proceedings of the PORSEC-'92, in Okinawa, Conference for Pacific Ocean Environments & Probing, 25-31 August, 1992, Vol. 2, Okinawa, Japan, pp. 796-801
- Shetye, S.R and Gouveia, A.D (1998): Coastal circulation in the north Indian Ocean coastal segment (14-S-W), *The Sea*, Volume 11, (Ed. A.R. Robinson and K.H. Brink) John Wiley & Sons, Inc. pp. 523-556.
- Shetye S.R, Gouveia, A.D and Shenoi, S.S.C (1994): Circulation and water masses of the Arabian Sea, *Proc. Ind. Accad. Sci. (Earth Planet. Sci.)*, Vol. 103, No. 2, pp. 107-123.

- Shetye, S.R, Gouveia, A.D, Shenoi, S.S.C, Sundar, D, Michael, G.S, Almeida, A.M and Santanam, K (1990): Hydrography and circulation off the west coast of India during the southwest monsoon 1987, *J Mar. Res.* Vol. 48, pp. 359-378.
- Shetye, S.R, Gouveia, A.D and Shenoi, S.S.C (1994): Circulation and water masses of the Arabian Sea, *Proc. Ind. Acad. Sci. (Earth Planet. Sci.)*, Vol. 103, No. 2, pp. 107-123.
- Shetye, S.R and Shenoi, S.S.C (1988): Seasonal cycle of surface circulation in the coastal North Indian ocean, *Proc. Indian Acad. Sci. (Earth planet. Sci.)*, Vol. 97, pp. 53-62.
- Shetye, S.R, Shenoi, S.S.C, Gouveia, A.D, Michael, G.S, Sundar, D and Nampoothiri, G (1991): Wind driven coastal upwelling along the western boundary of the Bay of Bengal during the southwest monsoon, *Cont. Shelf Res.* Vol. 11, pp. 1397-1408.
- Sprintall, J, Gordon, A.L, Murtugudde, R and Susanto, R.D (2000): A semi-annual Indian Ocean forced Kelvin waves observed in the Indonesian Seas, May 1997, *J Geophys. Res.* Vol. 105, pp. 17,217-17,230.
- Sprintall, J and Tomczak, M (1992): Evidence of the Barrier Layer in the Surface Layer of the Tropics, *J Geophys. Res.* Vol. 97, No. C5, pp. 7305-7316.
- Srinivasa Rao, N, Rao, K.H, Ramana, I.V and Dash, S.K (2001): Study of oceanic features using multi sensor data in the north Indian Ocean, In: Biological and Physical Oceanographic process from Satellite data, 34<sup>th</sup> assembly of COSPAR, 10-19 October, 2001, Houston, Texas, USA.
- Stramma, L, Fischer, J, and Schott, F (1996): The flow field off southwest India at 8N during the southwest monsoon of August 1993, *J Mar. Res.* Vol. 54, pp. 55-72.
- Subrahmanyam, B, Ramesh Babu, V, Murty, V.S.N and Rao, L.V.G (1996): Surface circulation off Somalia and western equatorial Indian Ocean during summer monsoon of 1988 from Geosat altimeter data, *Int. J Rem. Sen.* Vol. 17, No. 4, pp. 761-770.
- Sundararamam, K.V, Balakrishna Kurup, C.K and Sreerama Murty, K.V (1968): Water masses of the Arabian Sea in the upper 500 metres, *Bull. Natl. Inst. Sci. India*. Part I, No. 38, pp. 240-253.
- Summerhayes, C.P, Emeis, K.-C, Angel, M.V, Smith, R.L and Zeitzschel, B (1995): Upwelling in the Ocean: Modern process and ancient records, Dahlem Workshop Reports (Environmental Sciences research report; ES 18), (John Wiley & Sons Ltd., England), 422 p.
- Suryanarayana, A, Murty, V.S.N, Sarma, Y.V.B, Babu, M.T, Rao, D.P and Sastry, J.S (1992): Hydrographic features of the western Bay of Bengal in the upper 500 m under the influence of NE and SW monsoons, In: *Oceanography of the Indian Ocean*, edited by B.N. Desai (Oxford & IBH Publishing Co. Pvt. Ltd., New Delhi), pp. 595-604.
- Suryanarayana, A, Murty, V.S.N and Rao, D.P (1993): Hydrography and circulation of the Bay of Bengal during early winter, 1983, *Deep-Sea Res.* Vol. 40, pp. 205-217.
- Suryanarayana, A and Rao, D.P (1992): Coastal circulation and upwelling index along the east coast of India, In: *Physical processes in the Indian Seas, Proceedings of the first convention of the Indian Society for Physical Sciences of the Ocean* (13-15 December, 1989), Goa, Ed. by G. N. Swamy, V.K. Das and M.K. Antony, December pp. 125-129.
- Suryanarayana, A, Reddy, G.V and Pankajakshan, T (1987): Watermass structure and current system in the Equatorial western Indian Ocean during August, 1985, *Dt. Hydrogr. Z.* 40, H.4. *Mitteilungen*, pp. 181-190.
- Susanto, R.D, Gordon, A.L and Zheng, Q (2001): Upwelling along the coasts of Java and Sumatra and its relation to ENSO, *Geophys. Res. Lett.* Vol. 28, pp. 1599-1602.
- Sverdrup, H.U, Johnson, M.W and Fleming, R.H (1942): The Oceans: their physics, chemistry and general biology, Prentice-Hall Inc., 1087 p.
- Swallow, J.C (1967): The equatorial undercurrent in the western Indian Ocean in 1964, *Studies in Tropical Oceanography*, Miami, No. 5, pp 15-36.
- Swallow, J.C (1984): Some aspects of the Physical Oceanography of the Indian Ocean, *Deep-Sea Res.* Vol. 31, pp. 639-650.
- Swallow, J.C and Bruce, J.G (1966): Current measurements off the Somali coast during the southwest monsoon of 1964, *Deep Sea Res.* Vol. 13, pp. 861-888.
- Taft, B.A and Knauss, J.A (1967): The equatorial undercurrent of the Indian Ocean as observed by the Lusiad Expedition, *Bull. Scripps Inst. Oceanogr.* Vol. 9, pp. 163.

- Tchernia, P (1980): Descriptive Regional Oceanography, Pergamon Press, New York, 253 p.
- Thomson, R.E and Fine, I.V (2003): Estimating Mixed Layer Depth from Oceanic Profile Data, *J Atm. Ocean. Tech.* Vol. 20, pp. 319-329.
- Tomczak, M and J.S. Godfrey (1994): Regional Oceanography, An introduction, Pergamon Publishers, London, 422 p.
- Unnikrishnan, A.S and Antony, M.K (1992): On the upwelling front along the west coast of India during later part of southwest monsoon, Physical Processes in the Indian Seas, Proceedings of First convention, ISPSO-1990, pp. 131-135.
- Varadachari, V.V.R and Sharma, G.S (1967): Circulation of the surface waters in the North Indian Ocean, *J Ind. Geophys. Uni.* Vol. 4(2), pp 61-73.
- Varkey, M.J and Kesavadas, V (1976): Light transmission characteristics of the northern Arabian Sea during December-May, *Ind. J Mar. Sci.* Vol. 5, pp. 147-151.
- Varkey, M.J, Murty, V.S.N and Sur yanarayana, A (1996): Physical oceanography of the Bay of Bengal, In: *Oceanography and Marine Biology: an Annual Review*, edited by A.D. Ansell, R.N. Gibson and M. Barnes, No. 34 pp. 1-70.
- Varkey, M.J and. Sastry, J.S (1992): Characteristic Mixing Triangles in the Bay of Bengal, In: *Physical Processes in the Indian Seas* (Proc. First Convention, ISPSO, 1990), pp. 47-50.
- Verlecar, X.N and Parulaker, A.H (2001): Primary Productivity, In: *The Indian Ocean A perspective*, Vol. 2, (Ed. R. Sen Gupta and E. Desa), pp. 397-415.
- Varma, K.K, Kesava Das, V and Gouveia, A.D (1980): Thermohaline Structure & Watermasses in the Northern Arabian Sea during February-April. *Ind. J Mar. Sci.*, Vol. 9, pp. 148-155.
- Vinayachandran, P.N, Murty, V.S.N and Ramesh Babu, V (2002): Observations of barrier layer formation in the Bay of Bengal during summer monsoon, *J Geophys. Res.* Vol. 107, No. C12, 8018, doi: 10.1029/2001JC000831, 2002.
- Vinayachandran, P.N and Shetye, S.R (1991): The warm pool in the Indian Ocean, *Proc. Ind. Acad. Sci. (Earth Planet. Sci.)*, Vol. 100, pp 165-175.
- Vinayachandran, P.N and Yamagata, T (1998): Monsoon response of the Sea around Sri Lanka: Generation of thermal domes and anticyclonic vortices, *J Phys. Oceanogr.*, Vol. 28, pp. 1946-1960.
- Warren B, Stomme, H and Swallow, J.C (1966): Water masses and patterns of flow in the Somali Basin during the southwest monsoon of 1964, *Deep-Sea Res.* Vol. 13, pp. 825-860.
- Woodward, E.M.S, Rees, A.P and Stephens, J.A (1999): The influence of the south-west monsoon upon the nutrient biogeochemistry of the Arabian Sea, *Deep-Sea Res. II*, Vol. 46, pp. 571-591.
- Wooster, W.S, Schaefer, M.B and Robinson, M.K (1967): Atlas of the Arabian Sea for fishery oceanography, (Institute of Marine Resources, La Jolla, California, USA).
- Wijesekera, R.W and Gregg, M.C (1996): Surface layer response to weak winds, westerly bursts, and rain squalls in the western Pacific warm pool, *J Geophys. Res.* Vol. 101, pp. 977-997.
- Wyrtki, K (1971): Oceanographic Atlas of the International Indian Ocean Expedition, National Science Foundation, Washington, D.C., 531 p.
- Wyrtki, K (1973<sub>a</sub>): An equatorial jet in the Indian Ocean, *Science*, Vol. 181, pp. 262-264.
- Wyrtki, K (1973<sub>b</sub>): Physical oceanography of the Indian Ocean, In: *The Biology of the Indian Ocean, Ecological Studies-Analyses and Synthesis*, Vol. 3, Ed. by B. Zeitzschel and S.A. Gerlach (Springer-Verlag, Berlin) pp. 18-36.
- Zheng, Q, Klemas, V. and Yan, X.-H (1995): Dynamic interpretation of space shuttle photographs: deepwater internal waves in the western equatorial Indian Ocean, *J Geophys. Res.* Vol. 100, No. C2, pp. 2579-2589.

**OCEANOGRAPHIC ATLAS OF THE TROPICAL INDIAN OCEAN**

**by**

**L.V. Gangadhara Rao and P. Shree Ram**  
**National Institute of Oceanography**  
**Regional Centre, Visakhapatnam**

**April 2005**

This atlas consists of two parts. Part A contains descriptions of surface parameters/fields, namely mean monthly surface winds, SST, surface currents (from Ekman drifts and drifting buoys), surface heat fluxes, and seasonal and annual distributions of Chlorophyll concentration in the Tropical Indian Ocean. Part B contains descriptions of upper ocean thermohaline fields, namely mean monthly distributions of temperature, salinity, density ( $\sigma_t$ ), mixed layer depth, mixed layer heat content, depth of 20° C isotherm and geostrophic currents.

Mean monthly data of sea surface winds for the global oceans over  $2.5^\circ \times 2.5^\circ$  grid (Kalnay, et al. 1996) available for the period 1948-2003 were downloaded from the NCEP/NCAR web site (<ftp://ftp.cdc.noaa.gov/Datasets/ncep.reanalysis.derived/surface>) and the data for the TIO ( $30^\circ\text{S}$ - $30^\circ\text{N}$  &  $30^\circ$ - $120^\circ\text{E}$ ) were extracted, and distribution maps were generated and shown in Figs. A01-A03. Mean monthly sea surface temperature data for the global oceans over  $1^\circ \times 1^\circ$  grid (Reynolds et al. 2002) available for the period 1982-2003 were downloaded from the NOAA web site ([ftp://ftp.ncep.noaa.gov/pub/cmb/sst/oimonth\\_v2/](ftp://ftp.ncep.noaa.gov/pub/cmb/sst/oimonth_v2/)) and data for the TIO were extracted, and distribution maps were prepared and shown in Figs. A04-A06. Using the above wind data, mean monthly surface Ekman drifts were calculated and the maps of currents were presented in Figs. A07-A09. Using the mean monthly surface current vectors derived from drifting buoys data for the period 1976-2002 on a  $2^\circ \times 2^\circ$  square (provided by Dr. S.S.C. Shenoi, NIO, Goa), maps of near surface currents were generated and presented in Figs. A10-A12. Mean monthly latent heat flux, sensible heat flux and net heat flux data over  $1^\circ \times 1^\circ$  grid are available for global oceans in SOC air-sea flux climatology (Josey et al. 1996). From this, the data for the TIO were extracted and the distribution maps were generated and presented in Figs. A13-A15, A16-A18 and A19-A21 respectively. Surface Chlorophyll-a data for the TIO were extracted from NIO BIO data base (2002) and average values were computed over  $5^\circ \times 5^\circ$  grid for the three seasons, namely monsoon (June-September), post-monsoon (October-January) and pre-monsoon (February-May), and seasonal and annual distribution maps were presented in Fig. A22. Distribution of surface Chlorophyll-a derived from SeaWiFS data (1998-2001) for the above seasons and the annual average were presented in Fig. A23.

Mean monthly values of temperature and salinity for the TIO on  $1^\circ \times 1^\circ$  grid upto 1000 m depth were extracted from the World Ocean Atlas (2001): Objectively analysed temperature and salinity data (available at [www.nodc.noaa.gov/0c5/WOA01/woa01dat.html](http://www.nodc.noaa.gov/0c5/WOA01/woa01dat.html)) and density ( $\sigma_t$ ) values were computed.

Mean monthly temperature distribution at 9 depth levels (surface, 50m, 100m, 150m, 200m, 300m, 500m, 700m, 1000m) were presented in Figs. B001-B027. Mean monthly temperature distribution upto 1000 m depth along 10 latitudes ( $20^\circ\text{N}$ ,  $15^\circ\text{N}$ ,  $10^\circ\text{N}$ ,  $5^\circ\text{N}$ ,  $0^\circ$ ,  $5^\circ\text{S}$ ,  $10^\circ\text{S}$ ,  $15^\circ\text{S}$ ,  $20^\circ\text{S}$ ,  $25^\circ\text{S}$ ) and along 11 longitudes ( $50^\circ$ ,  $55^\circ$ ,  $60^\circ$ ,  $65^\circ$ ,  $70^\circ$ ,  $75^\circ$ ,  $80^\circ$ ,  $85^\circ$ ,  $90^\circ$ ,  $95^\circ$ ,  $100^\circ\text{E}$ ) were prepared and presented in Figs. B028-B087 and Figs. B088-B153 respectively.

Mean monthly salinity distribution at 9 depth levels (surface, 50m, 100m, 150m, 200m, 300m, 500m, 700m, 1000m) were presented in Figs. B154-B180. Mean monthly salinity distribution upto 1000 m depth along 10 latitudes ( $20^\circ\text{N}$ ,  $15^\circ\text{N}$ ,  $10^\circ\text{N}$ ,  $5^\circ\text{N}$ ,  $0^\circ$ ,  $5^\circ\text{S}$ ,  $10^\circ\text{S}$ ,  $15^\circ\text{S}$ ,  $20^\circ\text{S}$ ,  $25^\circ\text{S}$ ) and along 11 longitudes ( $50^\circ$ ,  $55^\circ$ ,  $60^\circ$ ,  $65^\circ$ ,  $70^\circ$ ,  $75^\circ$ ,  $80^\circ$ ,  $85^\circ$ ,  $90^\circ$ ,  $95^\circ$ ,  $100^\circ\text{E}$ ) were prepared and presented in Figs. B181-B240 and Figs. B241-B306 respectively.

Mean monthly density ( $\sigma_t$ ) distribution at 9 depth levels (surface, 50m, 100m, 150m, 200m, 300m, 500m, 700m, 1000m) were presented in Figs. B307-B333. Mean monthly density ( $\sigma_t$ ) distribution upto 1000 m depth along 10 latitudes ( $20^\circ\text{N}$ ,  $15^\circ\text{N}$ ,  $10^\circ\text{N}$ ,  $5^\circ\text{N}$ ,  $0^\circ$ ,  $5^\circ\text{S}$ ,  $10^\circ\text{S}$ ,  $15^\circ\text{S}$ ,  $20^\circ\text{S}$ ,  $25^\circ\text{S}$ ) and along 11 longitudes ( $50^\circ$ ,  $55^\circ$ ,  $60^\circ$ ,  $65^\circ$ ,  $70^\circ$ ,  $75^\circ$ ,  $80^\circ$ ,  $85^\circ$ ,  $90^\circ$ ,  $95^\circ$ ,  $100^\circ\text{E}$ ) were prepared and presented in Figs. B334-B393 and Figs. B394-B459 respectively.

From the above density profiles data, values of mixed layer depth (depth at which sigma-t is more than 0.2 kg/m<sup>3</sup> from the surface value) were calculated and mean monthly distribution of MLD is presented in Figs. B460-B462. Mixed layer heat content (MLHC) was computed from the equation:

$$MLHC = \rho C_p \int_0^D \bar{T} dz$$

where  $\rho$  is density of sea water (taken as 1.02),

$C_p$  is specific heat of sea water at constant pressure (taken as 0.954),

$T$  is the mean temperature of the layer thickness,  $dz$

$D$  is the depth upto which integration is carried out (i.e., MLD).

and the mean monthly MLHC is presented in Figs. B463-B465.

The depth of 20° C isotherm (whose topography has strong relation to circulation in the upper thermocline region) was obtained from the temperature profiles and the mean monthly distribution charts are presented in Figs. B466-B468.

Using the above temperature and salinity data, dynamic height and geostrophic currents with reference to 1000 m depth were calculated for 8 depth levels (surface, 50m, 100m, 150m, 200m, 300m, 500m, 700m). The mean monthly dynamic topography and geostrophic current vectors for different levels are presented in Figs. B469-B492.

For generating the distribution maps GMT software was used extensively. FERRET was used for computation of dynamic height and geostrophic currents, and GMT was used for generating these maps.

## LIST OF FIGURES

### (A) Surface parameters/fields

- Fig. A01: Mean monthly sea surface wind vectors from January through April
- Fig. A02: Mean monthly sea surface wind vectors from May through August
- Fig. A03: Mean monthly sea surface wind vectors from September through December
- Fig. A04: Mean monthly sea surface temperature from January through April
- Fig. A05: Mean monthly sea surface temperature from May through August
- Fig. A06: Mean monthly sea surface temperature from September through December
- Fig. A07: Mean monthly surface Ekman currents from January through April
- Fig. A08: Mean monthly surface Ekman currents from May through August
- Fig. A09: Mean monthly surface Ekman currents from September through December
- Fig. A10: Mean monthly surface current vectors from January through April
- Fig. A11: Mean monthly surface current vectors from May through August
- Fig. A12: Mean monthly surface current vectors from September through December
- Fig. A13: Mean monthly latent heat flux from January through April
- Fig. A14: Mean monthly latent heat flux from May through August
- Fig. A15: Mean monthly latent heat flux from September through December
- Fig. A16: Mean monthly sensible heat flux from January through April
- Fig. A17: Mean monthly sensible heat flux from May through August
- Fig. A18: Mean monthly sensible heat flux from September through December
- Fig. A19: Mean monthly net surface heat flux from January through April
- Fig. A20: Mean monthly net surface heat flux from May through August
- Fig. A21: Mean monthly net surface heat flux from September through December
- Fig. A22: Seasonal and annual surface chlorophyll-a (from NIO-BIO data base)
- Fig. A23: Seasonal and annual surface chlorophyll-a (from SeaWiFS)

### (B) Upper ocean thermohaline fields from WOA 2001

- Fig. B001: Mean monthly sea surface temperature from January through April
- Fig. B002: Mean monthly sea surface temperature from May through August
- Fig. B003: Mean monthly sea surface temperature from September through December
- Fig. B004: Mean monthly temperature at 50 m depth from January through April
- Fig. B005: Mean monthly temperature at 50 m depth from May through August
- Fig. B006: Mean monthly temperature at 50 m depth from September through December
- Fig. B007: Mean monthly temperature at 100 m depth from January through April
- Fig. B008: Mean monthly temperature at 100 m depth from May through August
- Fig. B009: Mean monthly temperature at 100 m depth from September through December
- Fig. B010: Mean monthly temperature at 150 m depth from January through April
- Fig. B011: Mean monthly temperature at 150 m depth from May through August
- Fig. B012: Mean monthly temperature at 150 m depth from September through December
- Fig. B013: Mean monthly temperature at 200 m depth from January through April
- Fig. B014: Mean monthly temperature at 200 m depth from May through August
- Fig. B015: Mean monthly temperature at 200 m depth from September through December
- Fig. B016: Mean monthly temperature at 300 m depth from January through April
- Fig. B017: Mean monthly temperature at 300 m depth from May through August
- Fig. B018: Mean monthly temperature at 300 m depth from September through December
- Fig. B019: Mean monthly temperature at 500 m depth from January through April
- Fig. B020: Mean monthly temperature at 500 m depth from May through August
- Fig. B021: Mean monthly temperature at 500 m depth from September through December
- Fig. B022: Mean monthly temperature at 700 m depth from January through April

Fig. B023: Mean monthly temperature at 700 m depth from May through August  
Fig. B024: Mean monthly temperature at 700 m depth from September through December  
Fig. B025: Mean monthly temperature at 1000 m depth from January through April  
Fig. B026: Mean monthly temperature at 1000 m depth from May through August  
Fig. B027: Mean monthly temperature at 1000 m depth from September through December  
Fig. B028: Mean monthly temperature section along 19.5° N for January and February  
Fig. B029: Mean monthly temperature section along 19.5° N for March and April  
Fig. B030: Mean monthly temperature section along 19.5° N for May and June  
Fig. B031: Mean monthly temperature section along 19.5° N for July and August  
Fig. B032: Mean monthly temperature section along 19.5° N for September and October  
Fig. B033: Mean monthly temperature section along 19.5° N for November and December  
Fig. B034: Mean monthly temperature section along 14.5° N for January and February  
Fig. B035: Mean monthly temperature section along 14.5° N for March and April  
Fig. B036: Mean monthly temperature section along 14.5° N for May and June  
Fig. B037: Mean monthly temperature section along 14.5° N for July and August  
Fig. B038: Mean monthly temperature section along 14.5° N for September and October  
Fig. B039: Mean monthly temperature section along 14.5° N for November and December  
Fig. B040: Mean monthly temperature section along 9.5° N for January and February  
Fig. B041: Mean monthly temperature section along 9.5° N for March and April  
Fig. B042: Mean monthly temperature section along 9.5° N for May and June  
Fig. B043: Mean monthly temperature section along 9.5° N for July and August  
Fig. B044: Mean monthly temperature section along 9.5° N for September and October  
Fig. B045: Mean monthly temperature section along 9.5° N for November and December  
Fig. B046: Mean monthly temperature section along 4.5° N for January and February  
Fig. B047: Mean monthly temperature section along 4.5° N for March and April  
Fig. B048: Mean monthly temperature section along 4.5° N for May and June  
Fig. B049: Mean monthly temperature section along 4.5° N for July and August  
Fig. B050: Mean monthly temperature section along 4.5° N for September and October  
Fig. B051: Mean monthly temperature section along 4.5° N for November and December  
Fig. B052: Mean monthly temperature section along 0.5° S for January and February  
Fig. B053: Mean monthly temperature section along 0.5° S for March and April  
Fig. B054: Mean monthly temperature section along 0.5° S for May and June  
Fig. B055: Mean monthly temperature section along 0.5° S for July and August  
Fig. B056: Mean monthly temperature section along 0.5° S for September and October  
Fig. B057: Mean monthly temperature section along 0.5° S for November and December  
Fig. B058: Mean monthly temperature section along 5.5° N for January and February  
Fig. B059: Mean monthly temperature section along 5.5° N for March and April  
Fig. B060: Mean monthly temperature section along 5.5° N for May and June  
Fig. B061: Mean monthly temperature section along 5.5° N for July and August  
Fig. B062: Mean monthly temperature section along 5.5° N for September and October  
Fig. B063: Mean monthly temperature section along 5.5° N for November and December  
Fig. B064: Mean monthly temperature section along 10.5° N for January and February  
Fig. B065: Mean monthly temperature section along 10.5° N for March and April  
Fig. B066: Mean monthly temperature section along 10.5° N for May and June  
Fig. B067: Mean monthly temperature section along 10.5° N for July and August  
Fig. B068: Mean monthly temperature section along 10.5° N for September and October  
Fig. B069: Mean monthly temperature section along 10.5° N for November and December  
Fig. B070: Mean monthly temperature section along 15.5° N for January and February  
Fig. B071: Mean monthly temperature section along 15.5° N for March and April  
Fig. B072: Mean monthly temperature section along 15.5° N for May and June  
Fig. B073: Mean monthly temperature section along 15.5° N for July and August  
Fig. B074: Mean monthly temperature section along 15.5° N for September and October

Fig. B075: Mean monthly temperature section along 15.5° N for November and December  
Fig. B076: Mean monthly temperature section along 20.5° N for January and February  
Fig. B077: Mean monthly temperature section along 20.5° N for March and April  
Fig. B078: Mean monthly temperature section along 20.5° N for May and June  
Fig. B079: Mean monthly temperature section along 20.5° N for July and August  
Fig. B080: Mean monthly temperature section along 20.5° N for September and October  
Fig. B081: Mean monthly temperature section along 20.5° N for November and December  
Fig. B082: Mean monthly temperature section along 25.5° N for January and February  
Fig. B083: Mean monthly temperature section along 25.5° N for March and April  
Fig. B084: Mean monthly temperature section along 25.5° N for May and June  
Fig. B085: Mean monthly temperature section along 25.5° N for July and August  
Fig. B086: Mean monthly temperature section along 25.5° N for September and October  
Fig. B087: Mean monthly temperature section along 25.5° N for November and December  
Fig. B088: Mean monthly temperature section along 50.5° E for January and February  
Fig. B089: Mean monthly temperature section along 50.5° E for March and April  
Fig. B090: Mean monthly temperature section along 50.5° E for May and June  
Fig. B091: Mean monthly temperature section along 50.5° E for July and August  
Fig. B092: Mean monthly temperature section along 50.5° E for September and October  
Fig. B093: Mean monthly temperature section along 50.5° E for November and December  
Fig. B094: Mean monthly temperature section along 55.5° E for January and February  
Fig. B095: Mean monthly temperature section along 55.5° E for March and April  
Fig. B096: Mean monthly temperature section along 55.5° E for May and June  
Fig. B097: Mean monthly temperature section along 55.5° E for July and August  
Fig. B098: Mean monthly temperature section along 55.5° E for September and October  
Fig. B099: Mean monthly temperature section along 55.5° E for November and December  
Fig. B100: Mean monthly temperature section along 60.5° E for January and February  
Fig. B101: Mean monthly temperature section along 60.5° E for March and April  
Fig. B102: Mean monthly temperature section along 60.5° E for May and June  
Fig. B103: Mean monthly temperature section along 60.5° E for July and August  
Fig. B104: Mean monthly temperature section along 60.5° E for September and October  
Fig. B105: Mean monthly temperature section along 60.5° E for November and December  
Fig. B106: Mean monthly temperature section along 65.5° E for January and February  
Fig. B107: Mean monthly temperature section along 65.5° E for March and April  
Fig. B108: Mean monthly temperature section along 65.5° E for May and June  
Fig. B109: Mean monthly temperature section along 65.5° E for July and August  
Fig. B110: Mean monthly temperature section along 65.5° E for September and October  
Fig. B111: Mean monthly temperature section along 65.5° E for November and December  
Fig. B112: Mean monthly temperature section along 70.5° E for January and February  
Fig. B113: Mean monthly temperature section along 70.5° E for March and April  
Fig. B114: Mean monthly temperature section along 70.5° E for May and June  
Fig. B115: Mean monthly temperature section along 70.5° E for July and August  
Fig. B116: Mean monthly temperature section along 70.5° E for September and October  
Fig. B117: Mean monthly temperature section along 70.5° E for November and December  
Fig. B118: Mean monthly temperature section along 75.5° E for January and February  
Fig. B119: Mean monthly temperature section along 75.5° E for March and April  
Fig. B120: Mean monthly temperature section along 75.5° E for May and June  
Fig. B121: Mean monthly temperature section along 75.5° E for July and August  
Fig. B122: Mean monthly temperature section along 75.5° E for September and October  
Fig. B123: Mean monthly temperature section along 75.5° E for November and December  
Fig. B124: Mean monthly temperature section along 80.5° E for January and February  
Fig. B125: Mean monthly temperature section along 80.5° E for March and April  
Fig. B126: Mean monthly temperature section along 80.5° E for May and June

Fig. B127: Mean monthly temperature section along 80.5° E for July and August  
Fig. B128: Mean monthly temperature section along 80.5° E for September and October  
Fig. B129: Mean monthly temperature section along 80.5° E for November and December  
Fig. B130: Mean monthly temperature section along 85.5° E for January and February  
Fig. B131: Mean monthly temperature section along 85.5° E for March and April  
Fig. B132: Mean monthly temperature section along 85.5° E for May and June  
Fig. B133: Mean monthly temperature section along 85.5° E for July and August  
Fig. B134: Mean monthly temperature section along 85.5° E for September and October  
Fig. B135: Mean monthly temperature section along 85.5° E for November and December  
Fig. B136: Mean monthly temperature section along 90.5° E for January and February  
Fig. B137: Mean monthly temperature section along 90.5° E for March and April  
Fig. B138: Mean monthly temperature section along 90.5° E for May and June  
Fig. B139: Mean monthly temperature section along 90.5° E for July and August  
Fig. B140: Mean monthly temperature section along 90.5° E for September and October  
Fig. B141: Mean monthly temperature section along 90.5° E for November and December  
Fig. B142: Mean monthly temperature section along 95.5° E for January and February  
Fig. B143: Mean monthly temperature section along 95.5° E for March and April  
Fig. B144: Mean monthly temperature section along 95.5° E for May and June  
Fig. B145: Mean monthly temperature section along 95.5° E for July and August  
Fig. B146: Mean monthly temperature section along 95.5° E for September and October  
Fig. B147: Mean monthly temperature section along 95.5° E for November and December  
Fig. B148: Mean monthly temperature section along 100.5° E for January and February  
Fig. B149: Mean monthly temperature section along 100.5° E for March and April  
Fig. B150: Mean monthly temperature section along 100.5° E for May and June  
Fig. B151: Mean monthly temperature section along 100.5° E for July and August  
Fig. B152: Mean monthly temperature section along 100.5° E for September and October  
Fig. B153: Mean monthly temperature section along 100.5° E for November and December

Fig. B154: Mean monthly sea surface salinity from January through April  
Fig. B155: Mean monthly sea surface salinity from May through August  
Fig. B156: Mean monthly sea surface salinity from September through December  
Fig. B157: Mean monthly salinity at 50 m depth from January through April  
Fig. B158: Mean monthly salinity at 50 m depth from May through August  
Fig. B159: Mean monthly salinity at 50 m depth from September through December  
Fig. B160: Mean monthly salinity at 100 m depth from January through April  
Fig. B161: Mean monthly salinity at 100 m depth from May through August  
Fig. B162: Mean monthly salinity at 100 m depth from September through December  
Fig. B163: Mean monthly salinity at 150 m depth from January through April  
Fig. B164: Mean monthly salinity at 150 m depth from May through August  
Fig. B165: Mean monthly salinity at 150 m depth from September through December  
Fig. B166: Mean monthly salinity at 200 m depth from January through April  
Fig. B167: Mean monthly salinity at 200 m depth from May through August  
Fig. B168: Mean monthly salinity at 200 m depth from September through December  
Fig. B169: Mean monthly salinity at 300 m depth from January through April  
Fig. B170: Mean monthly salinity at 300 m depth from May through August  
Fig. B171: Mean monthly salinity at 300 m depth from September through December  
Fig. B172: Mean monthly salinity at 500 m depth from January through April  
Fig. B173: Mean monthly salinity at 500 m depth from May through August  
Fig. B174: Mean monthly salinity at 500 m depth from September through December  
Fig. B175: Mean monthly salinity at 700 m depth from January through April  
Fig. B176: Mean monthly salinity at 700 m depth from May through August  
Fig. B177: Mean monthly salinity at 700 m depth from September through December

Fig. B178: Mean monthly salinity at 1000 m depth from January through April  
Fig. B179: Mean monthly salinity at 1000 m depth from May through August  
Fig. B180: Mean monthly salinity at 1000 m depth from September through December  
Fig. B181: Mean monthly salinity section along 19.5° N for January and February  
Fig. B182: Mean monthly salinity section along 19.5° N for March and April  
Fig. B183: Mean monthly salinity section along 19.5° N for May and June  
Fig. B184: Mean monthly salinity section along 19.5° N for July and August  
Fig. B185: Mean monthly salinity section along 19.5° N for September and October  
Fig. B186: Mean monthly salinity section along 19.5° N for November and December  
Fig. B187: Mean monthly salinity section along 14.5° N for January and February  
Fig. B188: Mean monthly salinity section along 14.5° N for March and April  
Fig. B189: Mean monthly salinity section along 14.5° N for May and June  
Fig. B190: Mean monthly salinity section along 14.5° N for July and August  
Fig. B191: Mean monthly salinity section along 14.5° N for September and October  
Fig. B192: Mean monthly salinity section along 14.5° N for November and December  
Fig. B193: Mean monthly salinity section along 9.5° N for January and February  
Fig. B194: Mean monthly salinity section along 9.5° N for March and April  
Fig. B195: Mean monthly salinity section along 9.5° N for May and June  
Fig. B196: Mean monthly salinity section along 9.5° N for July and August  
Fig. B197: Mean monthly salinity section along 9.5° N for September and October  
Fig. B198: Mean monthly salinity section along 9.5° N for November and December  
Fig. B199: Mean monthly salinity section along 4.5° N for January and February  
Fig. B200: Mean monthly salinity section along 4.5° N for March and April  
Fig. B201: Mean monthly salinity section along 4.5° N for May and June  
Fig. B202: Mean monthly salinity section along 4.5° N for July and August  
Fig. B203: Mean monthly salinity section along 4.5° N for September and October  
Fig. B204: Mean monthly salinity section along 4.5° N for November and December  
Fig. B205: Mean monthly salinity section along 0.5° S for January and February  
Fig. B206: Mean monthly salinity section along 0.5° S for March and April  
Fig. B207: Mean monthly salinity section along 0.5° S for May and June  
Fig. B208: Mean monthly salinity section along 0.5° S for July and August  
Fig. B209: Mean monthly salinity section along 0.5° S for September and October  
Fig. B210: Mean monthly salinity section along 0.5° S for November and December  
Fig. B211: Mean monthly salinity section along 5.5° N for January and February  
Fig. B212: Mean monthly salinity section along 5.5° N for March and April  
Fig. B213: Mean monthly salinity section along 5.5° N for May and June  
Fig. B214: Mean monthly salinity section along 5.5° N for July and August  
Fig. B215: Mean monthly salinity section along 5.5° N for September and October  
Fig. B216: Mean monthly salinity section along 5.5° N for November and December  
Fig. B217: Mean monthly salinity section along 10.5° N for January and February  
Fig. B218: Mean monthly salinity section along 10.5° N for March and April  
Fig. B219: Mean monthly salinity section along 10.5° N for May and June  
Fig. B220: Mean monthly salinity section along 10.5° N for July and August  
Fig. B221: Mean monthly salinity section along 10.5° N for September and October  
Fig. B222: Mean monthly salinity section along 10.5° N for November and December  
Fig. B223: Mean monthly salinity section along 15.5° N for January and February  
Fig. B224: Mean monthly salinity section along 15.5° N for March and April  
Fig. B225: Mean monthly salinity section along 15.5° N for May and June  
Fig. B226: Mean monthly salinity section along 15.5° N for July and August  
Fig. B227: Mean monthly salinity section along 15.5° N for September and October  
Fig. B228: Mean monthly salinity section along 15.5° N for November and December  
Fig. B229: Mean monthly salinity section along 20.5° N for January and February

Fig. B230: Mean monthly salinity section along 20.5° N for March and April  
 Fig. B231: Mean monthly salinity section along 20.5° N for May and June  
 Fig. B232: Mean monthly salinity section along 20.5° N for July and August  
 Fig. B233: Mean monthly salinity section along 20.5° N for September and October  
 Fig. B234: Mean monthly salinity section along 20.5° N for November and December  
 Fig. B235: Mean monthly salinity section along 25.5° N for January and February  
 Fig. B236: Mean monthly salinity section along 25.5° N for March and April  
 Fig. B237: Mean monthly salinity section along 25.5° N for May and June  
 Fig. B238: Mean monthly salinity section along 25.5° N for July and August  
 Fig. B239: Mean monthly salinity section along 25.5° N for September and October  
 Fig. B240: Mean monthly salinity section along 25.5° N for November and December  
 Fig. B241: Mean monthly salinity section along 50.5° E for January and February  
 Fig. B242: Mean monthly salinity section along 50.5° E for March and April  
 Fig. B243: Mean monthly salinity section along 50.5° E for May and June  
 Fig. B244: Mean monthly salinity section along 50.5° E for July and August  
 Fig. B245: Mean monthly salinity section along 50.5° E for September and October  
 Fig. B246: Mean monthly salinity section along 50.5° E for November and December  
 Fig. B247: Mean monthly salinity section along 55.5° E for January and February  
 Fig. B248: Mean monthly salinity section along 55.5° E for March and April  
 Fig. B249: Mean monthly salinity section along 55.5° E for May and June  
 Fig. B250: Mean monthly salinity section along 55.5° E for July and August  
 Fig. B251: Mean monthly salinity section along 55.5° E for September and October  
 Fig. B252: Mean monthly salinity section along 55.5° E for November and December  
 Fig. B253: Mean monthly salinity section along 60.5° E for January and February  
 Fig. B254: Mean monthly salinity section along 60.5° E for March and April  
 Fig. B255: Mean monthly salinity section along 60.5° E for May and June  
 Fig. B256: Mean monthly salinity section along 60.5° E for July and August  
 Fig. B257: Mean monthly salinity section along 60.5° E for September and October  
 Fig. B258: Mean monthly salinity section along 60.5° E for November and December  
 Fig. B259: Mean monthly salinity section along 65.5° E for January and February  
 Fig. B260: Mean monthly salinity section along 65.5° E for March and April  
 Fig. B261: Mean monthly salinity section along 65.5° E for May and June  
 Fig. B262: Mean monthly salinity section along 65.5° E for July and August  
 Fig. B263: Mean monthly salinity section along 65.5° E for September and October  
 Fig. B264: Mean monthly salinity section along 65.5° E for November and December  
 Fig. B265: Mean monthly salinity section along 70.5° E for January and February  
 Fig. B266: Mean monthly salinity section along 70.5° E for March and April  
 Fig. B267: Mean monthly salinity section along 70.5° E for May and June  
 Fig. B268: Mean monthly salinity section along 70.5° E for July and August  
 Fig. B269: Mean monthly salinity section along 70.5° E for September and October  
 Fig. B270: Mean monthly salinity section along 70.5° E for November and December  
 Fig. B271: Mean monthly salinity section along 75.5° E for January and February  
 Fig. B272: Mean monthly salinity section along 75.5° E for March and April  
 Fig. B273: Mean monthly salinity section along 75.5° E for May and June  
 Fig. B274: Mean monthly salinity section along 75.5° E for July and August  
 Fig. B275: Mean monthly salinity section along 75.5° E for September and October  
 Fig. B276: Mean monthly salinity section along 75.5° E for November and December  
 Fig. B277: Mean monthly salinity section along 80.5° E for January and February  
 Fig. B278: Mean monthly salinity section along 80.5° E for March and April  
 Fig. B279: Mean monthly salinity section along 80.5° E for May and June  
 Fig. B280: Mean monthly salinity section along 80.5° E for July and August  
 Fig. B281: Mean monthly salinity section along 80.5° E for September and October

Fig. B282: Mean monthly salinity section along 80.5° E for November and December  
 Fig. B283: Mean monthly salinity section along 85.5° E for January and February  
 Fig. B284: Mean monthly salinity section along 85.5° E for March and April  
 Fig. B285: Mean monthly salinity section along 85.5° E for May and June  
 Fig. B286: Mean monthly salinity section along 85.5° E for July and August  
 Fig. B287: Mean monthly salinity section along 85.5° E for September and October  
 Fig. B288: Mean monthly salinity section along 85.5° E for November and December  
 Fig. B289: Mean monthly salinity section along 90.5° E for January and February  
 Fig. B290: Mean monthly salinity section along 90.5° E for March and April  
 Fig. B291: Mean monthly salinity section along 90.5° E for May and June  
 Fig. B292: Mean monthly salinity section along 90.5° E for July and August  
 Fig. B293: Mean monthly salinity section along 90.5° E for September and October  
 Fig. B294: Mean monthly salinity section along 90.5° E for November and December  
 Fig. B295: Mean monthly salinity section along 95.5° E for January and February  
 Fig. B296: Mean monthly salinity section along 95.5° E for March and April  
 Fig. B297: Mean monthly salinity section along 95.5° E for May and June  
 Fig. B298: Mean monthly salinity section along 95.5° E for July and August  
 Fig. B299: Mean monthly salinity section along 95.5° E for September and October  
 Fig. B300: Mean monthly salinity section along 95.5° E for November and December  
 Fig. B301: Mean monthly salinity section along 100.5° E for January and February  
 Fig. B302: Mean monthly salinity section along 100.5° E for March and April  
 Fig. B303: Mean monthly salinity section along 100.5° E for May and June  
 Fig. B304: Mean monthly salinity section along 100.5° E for July and August  
 Fig. B305: Mean monthly salinity section along 100.5° E for September and October  
 Fig. B306: Mean monthly salinity section along 100.5° E for November and December

Fig. B307: Mean monthly sea surface density (sigma-t) from January through April  
 Fig. B308: Mean monthly sea surface density (sigma-t) from May through August  
 Fig. B309: Mean monthly sea surface density (sigma-t) from September through December  
 Fig. B310: Mean monthly density (sigma-t) at 50 m depth from January through April  
 Fig. B311: Mean monthly density (sigma-t) at 50 m depth from May through August  
 Fig. B312: Mean monthly density (sigma-t) at 50 m depth from September through December  
 Fig. B313: Mean monthly density (sigma-t) at 100 m depth from January through April  
 Fig. B314: Mean monthly density (sigma-t) at 100 m depth from May through August  
 Fig. B315: Mean monthly density (sigma-t) at 100 m depth from September through December  
 Fig. B316: Mean monthly density (sigma-t) at 150 m depth from January through April  
 Fig. B317: Mean monthly density (sigma-t) at 150 m depth from May through August  
 Fig. B318: Mean monthly density (sigma-t) at 150 m depth from September through December  
 Fig. B319: Mean monthly density (sigma-t) at 200 m depth from January through April  
 Fig. B320: Mean monthly density (sigma-t) at 200 m depth from May through August  
 Fig. B321: Mean monthly density (sigma-t) at 200 m depth from September through December  
 Fig. B322: Mean monthly density (sigma-t) at 300 m depth from January through April  
 Fig. B323: Mean monthly density (sigma-t) at 300 m depth from May through August  
 Fig. B324: Mean monthly density (sigma-t) at 300 m depth from September through December  
 Fig. B325: Mean monthly density (sigma-t) at 500 m depth from January through April  
 Fig. B326: Mean monthly density (sigma-t) at 500 m depth from May through August  
 Fig. B327: Mean monthly density (sigma-t) at 500 m depth from September through December  
 Fig. B328: Mean monthly density (sigma-t) at 700 m depth from January through April  
 Fig. B329: Mean monthly density (sigma-t) at 700 m depth from May through August  
 Fig. B330: Mean monthly density (sigma-t) at 700 m depth from September through December  
 Fig. B331: Mean monthly density (sigma-t) at 1000 m depth from January through April  
 Fig. B332: Mean monthly density (sigma-t) at 1000 m depth from May through August

Fig. B333: Mean monthly density (sigma-t) at 1000 m depth from September through December  
 Fig. B334: Mean monthly density (sigma-t) section along 19.5° N for January and February  
 Fig. B335: Mean monthly density (sigma-t) section along 19.5° N for March and April  
 Fig. B336: Mean monthly density (sigma-t) section along 19.5° N for May and June  
 Fig. B337: Mean monthly density (sigma-t) section along 19.5° N for July and August  
 Fig. B338: Mean monthly density (sigma-t) section along 19.5° N for September and October  
 Fig. B339: Mean monthly density (sigma-t) section along 19.5° N for November and December  
 Fig. B340: Mean monthly density (sigma-t) section along 14.5° N for January and February  
 Fig. B341: Mean monthly density (sigma-t) section along 14.5° N for March and April  
 Fig. B342: Mean monthly density (sigma-t) section along 14.5° N for May and June  
 Fig. B343: Mean monthly density (sigma-t) section along 14.5° N for July and August  
 Fig. B344: Mean monthly density (sigma-t) section along 14.5° N for September and October  
 Fig. B345: Mean monthly density (sigma-t) section along 14.5° N for November and December  
 Fig. B346: Mean monthly density (sigma-t) section along 9.5° N for January and February  
 Fig. B347: Mean monthly density (sigma-t) section along 9.5° N for March and April  
 Fig. B348: Mean monthly density (sigma-t) section along 9.5° N for May and June  
 Fig. B349: Mean monthly density (sigma-t) section along 9.5° N for July and August  
 Fig. B350: Mean monthly density (sigma-t) section along 9.5° N for September and October  
 Fig. B351: Mean monthly density (sigma-t) section along 9.5° N for November and December  
 Fig. B352: Mean monthly density (sigma-t) section along 4.5° N for January and February  
 Fig. B353: Mean monthly density (sigma-t) section along 4.5° N for March and April  
 Fig. B354: Mean monthly density (sigma-t) section along 4.5° N for May and June  
 Fig. B355: Mean monthly density (sigma-t) section along 4.5° N for July and August  
 Fig. B356: Mean monthly density (sigma-t) section along 4.5° N for September and October  
 Fig. B357: Mean monthly density (sigma-t) section along 4.5° N for November and December  
 Fig. B358: Mean monthly density (sigma-t) section along 0.5° S for January and February  
 Fig. B359: Mean monthly density (sigma-t) section along 0.5° S for March and April  
 Fig. B360: Mean monthly density (sigma-t) section along 0.5° S for May and June  
 Fig. B361: Mean monthly density (sigma-t) section along 0.5° S for July and August  
 Fig. B362: Mean monthly density (sigma-t) section along 0.5° S for September and October  
 Fig. B363: Mean monthly density (sigma-t) section along 0.5° S for November and December  
 Fig. B364: Mean monthly density (sigma-t) section along 5.5° N for January and February  
 Fig. B365: Mean monthly density (sigma-t) section along 5.5° N for March and April  
 Fig. B366: Mean monthly density (sigma-t) section along 5.5° N for May and June  
 Fig. B367: Mean monthly density (sigma-t) section along 5.5° N for July and August  
 Fig. B368: Mean monthly density (sigma-t) section along 5.5° N for September and October  
 Fig. B369: Mean monthly density (sigma-t) section along 5.5° N for November and December  
 Fig. B370: Mean monthly density (sigma-t) section along 10.5° N for January and February  
 Fig. B371: Mean monthly density (sigma-t) section along 10.5° N for March and April  
 Fig. B372: Mean monthly density (sigma-t) section along 10.5° N for May and June  
 Fig. B373: Mean monthly density (sigma-t) section along 10.5° N for July and August  
 Fig. B374: Mean monthly density (sigma-t) section along 10.5° N for September and October  
 Fig. B375: Mean monthly density (sigma-t) section along 10.5° N for November and December  
 Fig. B376: Mean monthly density (sigma-t) section along 15.5° N for January and February  
 Fig. B377: Mean monthly density (sigma-t) section along 15.5° N for March and April  
 Fig. B378: Mean monthly density (sigma-t) section along 15.5° N for May and June  
 Fig. B379: Mean monthly density (sigma-t) section along 15.5° N for July and August  
 Fig. B380: Mean monthly density (sigma-t) section along 15.5° N for September and October  
 Fig. B381: Mean monthly density (sigma-t) section along 15.5° N for November and December  
 Fig. B382: Mean monthly density (sigma-t) section along 20.5° N for January and February  
 Fig. B383: Mean monthly density (sigma-t) section along 20.5° N for March and April  
 Fig. B384: Mean monthly density (sigma-t) section along 20.5° N for May and June



Fig. B437: Mean monthly density (sigma-t) section along 85.5° E for March and April  
Fig. B438: Mean monthly density (sigma-t) section along 85.5° E for May and June  
Fig. B439: Mean monthly density (sigma-t) section along 85.5° E for July and August  
Fig. B440: Mean monthly density (sigma-t) section along 85.5° E for September and October  
Fig. B441: Mean monthly density (sigma-t) section along 85.5° E for November and December  
Fig. B442: Mean monthly density (sigma-t) section along 90.5° E for January and February  
Fig. B443: Mean monthly density (sigma-t) section along 90.5° E for March and April  
Fig. B444: Mean monthly density (sigma-t) section along 90.5° E for May and June  
Fig. B445: Mean monthly density (sigma-t) section along 90.5° E for July and August  
Fig. B446: Mean monthly density (sigma-t) section along 90.5° E for September and October  
Fig. B447: Mean monthly density (sigma-t) section along 90.5° E for November and December  
Fig. B448: Mean monthly density (sigma-t) section along 95.5° E for January and February  
Fig. B449: Mean monthly density (sigma-t) section along 95.5° E for March and April  
Fig. B450: Mean monthly density (sigma-t) section along 95.5° E for May and June  
Fig. B451: Mean monthly density (sigma-t) section along 95.5° E for July and August  
Fig. B452: Mean monthly density (sigma-t) section along 95.5° E for September and October  
Fig. B453: Mean monthly density (sigma-t) section along 95.5° E for November and December  
Fig. B454: Mean monthly density (sigma-t) section along 100.5° E for January and February  
Fig. B455: Mean monthly density (sigma-t) section along 100.5° E for March and April  
Fig. B456: Mean monthly density (sigma-t) section along 100.5° E for May and June  
Fig. B457: Mean monthly density (sigma-t) section along 100.5° E for July and August  
Fig. B458: Mean monthly density (sigma-t) section along 100.5° E for September and October  
Fig. B459: Mean monthly density (sigma-t) section along 100.5° E for November and December

Fig. B460: Mean monthly mixed layer depth from January through April  
Fig. B461: Mean monthly mixed layer depth from May through August  
Fig. B462: Mean monthly mixed layer depth from September through December

Fig. B463: Mean monthly mixed layer heat content from January through April  
Fig. B464: Mean monthly mixed layer heat content from May through August  
Fig. B465: Mean monthly mixed layer heat content from September through December

Fig. B466: Mean monthly isotherm depth of 20° C from January through April  
Fig. B467: Mean monthly isotherm depth of 20° C from May through August  
Fig. B468: Mean monthly isotherm depth of 20° C from September through December

Fig. B469: Mean monthly dynamic topography & geostrophic currents at surface with reference to 1000 m from January through April  
Fig. B470: Mean monthly dynamic topography & geostrophic currents at surface with reference to 1000 m from May through August  
Fig. B471: Mean monthly dynamic topography & geostrophic currents at surface with reference to 1000 m from Sept. through December  
Fig. B472: Mean monthly dynamic topography & geostrophic currents at 50 m with reference to 1000 m from January through April  
Fig. B473: Mean monthly dynamic topography & geostrophic currents at 50 m with reference to 1000 m from May through August  
Fig. B474: Mean monthly dynamic topography & geostrophic currents at 50 m with reference to 1000 m from September through December  
Fig. B475: Mean monthly dynamic topography & geostrophic currents at 100 m with reference to 1000 m from January through April  
Fig. B476: Mean monthly dynamic topography & geostrophic currents at 100 m with reference to 1000 m from May through August

Fig. B477: Mean monthly dynamic topography & geostrophic currents at 100 m with reference to 1000 m from September through December

Fig. B478: Mean monthly dynamic topography & geostrophic currents at 150 m with reference to 1000 m from January through April

Fig. B479: Mean monthly dynamic topography & geostrophic currents at 150 m with reference to 1000 m from May through August

Fig. B480: Mean monthly dynamic topography & geostrophic currents at 150 m with reference to 1000 m from September through December

Fig. B481: Mean monthly dynamic topography & geostrophic currents at 200 m with reference to 1000 m from January through April

Fig. B482: Mean monthly dynamic topography & geostrophic currents at 200 m with reference to 1000 m from May through August

Fig. B483: Mean monthly dynamic topography & geostrophic currents at 200 m with reference to 1000 m from September through December

Fig. B484: Mean monthly dynamic topography & geostrophic currents at 300 m with reference to 1000 m from January through April

Fig. B485: Mean monthly dynamic topography & geostrophic currents at 300 m with reference to 1000 m from May through August

Fig. B486: Mean monthly dynamic topography & geostrophic currents at 300 m with reference to 1000 m from September through December

Fig. B487: Mean monthly dynamic topography & geostrophic currents at 500 m with reference to 1000 m from January through April

Fig. B488: Mean monthly dynamic topography & geostrophic currents at 500 m with reference to 1000 m from May through August

Fig. B489: Mean monthly dynamic topography & geostrophic currents at 500 m with reference to 1000 m from September through December

Fig. B490: Mean monthly dynamic topography & geostrophic currents at 700 m with reference to 1000 m from January through April

Fig. B491: Mean monthly dynamic topography & geostrophic currents at 700 m with reference to 1000 m from May through August

Fig. B492: Mean monthly dynamic topography & geostrophic currents at 700 m with reference to 1000 m from September through December